Convention on Long-range Transboundary Air Pollution

emep

Co-operative programme for monitoring and evaluation of the long-range transmission of air pollutants in Europe

STATUS REPORT 2/2018 July 2018

Assessment of heavy metal transboundary pollution on global, regional and national scales

Status Report 2/2018

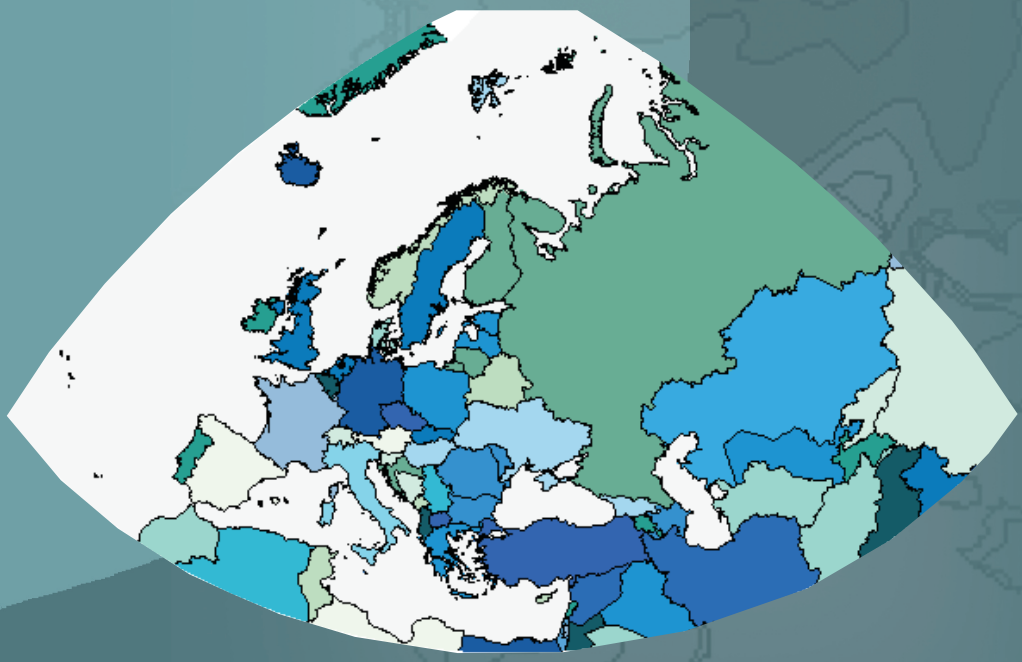

msc-e & ccc

EMEP Status Report 2/2018

July 2018

Assessment of heavy metal transboundary pollution on global, regional and national scales

METEOROLOGICAL SYNTHESIZING CENTRE - EAST

I.Ilyin, O.Rozovskaya, O.Travnikov

CHEMICAL CO-ORDINATING CENTRE

W. Aas, K.A. Pfaffhuber

MCS-E

Meteorological Synthesizing Centre - East

2nd Roshchinsky proezd, 8/5
115419 Moscow
Russia
Phone.: +7 926 906 91 78
Fax: +7 495 956 19 44
E-mail: msce@msceast.org
Internet: www.msceast.org

CCC

Norwegian Institute for Air Research (NILU)

P.O. Box 100NO-2027 Kjeller
Norway
Phone: +47 63 89 80 00
Fax: +47 63 89 80 50
E-mail: kjetil.torseth@nilu.no
Internet: www.nilu.no

EXECUTIVE SUMMARY

Heavy metals including lead (Pb), cadmium (Cd) and mercury (Hg) are known as toxic pollutants of the environment. Despite a rapid decrease of emissions of heavy metals in the past decades, long-term risks continue to exist for human health and biota. Therefore, as it is stated in the updates and revisions to the long-term strategy for the Convention [*ECE/EB.AIR/WG.5/2018/3*], *"… the Convention should pursue mitigation activities on heavy metals within the ECE region and consider acting as a centre of expertise … on reducing heavy metals, focusing on sharing its technical knowledge in terms of best available techniques, emission inventories, modelling and monitoring*". Variety of information related to transboundary pollution by heavy metals is collected and analysed by research centres of the Co-operative Programme for Monitoring and Evaluation of Long-range Transmission of Air Pollutants in Europe (EMEP).

The current Status Report overviews research activities of the EMEP Centres in the field of heavy metal pollution performed in accordance with the bi-annual workplan of the Convention for 2018-2019 [*ECE/EB.AIR/GE.1/2017/20-ECE/EB.AIR/WG.1/2017/13*]. The report covers various aspects of heavy metal pollution assessment based both on monitoring and modelling, research and development aimed at improvement of the modelling approaches, co-operation with national experts within the framework of country-scale case studies as well as collaboration with Subsidiary Bodies to the Convention and other international programmes.

Various input information used in the model assessment is prepared by the EMEP Centres. It includes gridded sector-specific emissions of heavy metals is prepared by the Centre of Emission Inventories and Projections (CEIP), measurements of heavy metals at the EMEP monitoring network collected by the Chemical Coordinating Centre (CCC), variety of other input data for modelling (meteorology, additional emission parameters, wind re-suspension, boundary conditions etc.) prepared by the Meteorological Synthesizing Centre – East (MSC-E).

Assessment of heavy metal pollution of the EMEP region is based on both measurement data and modelling results. Measurements of Cd and Pb in the EMEP region were available at 66 stations located in 21 countries, whereas Hg was measured at 29 sites. Most of the stations are located in the central, western, northern and south-western parts of Europe, while in the vast areas of eastern and southern-eastern Europe and Central Asia measurements of heavy metals are scarce. The lowest heavy metal concentrations in air and precipitation are generally found in Scandinavia, whereas the highest levels are in the Benelux region, Central and Eastern Europe. Strong seasonality in the concentrations of Hg in air is observed at several of the EMEP sites, with higher concentrations in winter, whereas low concentrations are observed in summer. This seasonal variation has been recently explained by vegetation uptake of atmospheric Hg. The new findings can have significant implications for the global Hg cycle and interpretation of long-term trends.

Model assessment of heavy metal pollution in the EMEP countries for 2016 was performed over the new EMEP grid based on the most recent dataset of heavy metal emissions for 2015 available at the moment of the study[1]. The highest levels of heavy metal pollution are noted for the central part of

[1] *Update of the modelling results based on the new emission data for 2016 is available at the MSC-E web site [www.msceast.org].*

Europe, northern Italy, Benelux and Balkans regions. Deposition levels differ significantly among different land cover categories with larger fluxes to vegetated surfaces and lower ones to barren lands and inland waters. Heavy metal deposition in the EMEP countries is originated from the EMEP anthropogenic sources, secondary emissions, and contribution of non-EMEP sources. Contribution of anthropogenic sources to total deposition in the EMEP countries varies within 6-63% and 8-74% for Pb and Cd, respectively. For Hg the anthropogenic contribution is lower (4-19%) due to significant effect of intercontinental transport (non-EMEP sources). Contribution of transboundary transport to anthropogenic deposition of Pb, Cd, and Hg exceeded deposition from national sources in 38, 38, and 40 of 51 EMEP countries, respectively. Moreover, proportion of various emission sectors in the transboundary transport vary markedly among the countries. In most of the EMEP countries more than 60% of emitted heavy metals were transported beyond the national borders.

Assessment of Hg pollution is among priority tasks within the Convention. Significant efforts of MSC-E during the past year were focused on collaborative work with the scientific community for evaluation of Hg pollution on global and regional scales as a part of the UN Environment Global Mercury Assessment 2018. The Centre co-ordinated a multi-model study of Hg dispersion on a global scale. Results of the analysis showed the relative share of direct anthropogenic emissions varies within 21-50% and decrease from industrial regions to remote regions. Both domestic and foreign anthropogenic sources contribute almost equally to the total anthropogenic Hg deposition in Europe. The largest foreign contributors are ranked in the order of East Asia (18%), Africa (8%), CIS countries (6%), and South Asia (5%). Mercury deposition in Europe and Central Asia are dominated by contributions from power generation and industrial emission sectors. The assessment provides valuable information for evaluation of Hg pollution levels in the EMEP countries and improves co-operation with the UN Environment and with the Minamata Convention.

The work on refinement of the Hg chemical scheme applied in the Global EMEP Multi-media Modelling System (GLEMOS) was further continued. For this purpose, the chemical mechanism of Hg oxidation by Br was incorporated into the model and evaluated in test runs and comparison with measurements. Further steps of implementation of the Br oxidation chemistry for the EMEP operational modelling will include evaluation of possible Hg reduction mechanisms in the atmosphere. Update and refinement of the model Hg chemical scheme should improve quality of assessment of Hg pollution of the EMEP countries.

The Centre co-operates with Parties to the Convention in the framework of heavy metal pollution assessment on a country scale. This year a case study for Poland has been completed. Polish national experts was provided with detailed model assessment of Cd pollution including source-receptor relationships for the country as a whole and for various provinces of the country, contribution of emission source categories and large point sources to Cd pollution levels. The study demonstrated that available emission data could contain significant uncertainties, which affected results of pollution assessment. The dispersion modelling supplemented by monitoring data can be used as an independent tool for evaluation of reported emissions. However, this activity requires close cooperation between monitoring, modelling and emissions communities. Results of the study were published in a special Technical Report [*Ilyin et al*., 2018]. In addition, major findings of the country-scale studies gained during the whole period of the project were summarised in [*Travnikov et al*., 2018].

A special attention of the country-scale study for Poland was paid to assessment of heavy metal pollution of cities. The source-receptor modelling with fine spatial resolution was applied to distinguish contribution of external sources and city emissions (urban increment) to pollution in selected cities of the country. Besides, seasonal variability of the urban increment was investigated. The suggested method of direct fine resolution modelling allowed matching modelled and observed Cd air concentrations in cities with sufficient quality. Comparison of the urban increments calculated in the current study with results of other studies, based on modelling or observations, revealed reasonable agreement of the applied methods for large cities. Thorough testing and evaluation of the applied approach will be continued for other countries and pollutants.

Collaboration with subsidiary bodies to the Convention and other international organisations is an important part of MSC-E activities. Main results and plans of future activities were presented at annual TFMM meeting. The Centre also contributed to the Task Force on Emission Inventories and Projections (TFEIP) with discussion on possible application of transport models for evaluation of reported emissions. Ecosystem-specific deposition maps of Pb, Cd and Hg were prepared by MSC-E on the new EMEP grid to support effect-based activity of the Working Group on Effects (WGE). Besides, the Centre performed a combined analysis of heavy metal pollution using both model estimates and data from the recent moss measurement survey.

MSC-E continued co-operation with the United Nations Environment Programme (UN Environment). The Centre took part in the new Global Mercury Assessment 2018 (GMA 2018) coordinating work of an international group of experts focused on modelling of mercury pollution on global and regional scales. In addition, MSC-E participated in the first meeting of the Conference of the Parties to the Minamata Convention on Mercury (COP1) presenting the experience and approaches used within CLRTAP. Besides, MSC-E performs regular model assessment of the Baltic Sea pollution by various pollutants including heavy metals. This work is carried out in accordance with the Memorandum of Understanding between CLRTAP and the Baltic Marine Environment Protection Commission (HELCOM).

Future directions of MSC-E activities will be aimed at quality improvement of heavy metal pollution assessment in the EMEP region. Further development and evaluation of the GLEMOS model will include further testing of the Br oxidation mechanism, evaluation of possible reduction pathways and further development of the multi-media approach for Hg simulations. The country-scale case studies will be continued for a number of countries (e.g. Germany, the UK, Norway) with particular focus on Hg pollution and the link with adverse effects on human health and biota. Besides, evaluation of the direct fine resolution modelling for assessment of city pollution will be continued for other countries and pollutants. Finally, MSC-E will continue co-operation with subsidiary bodies of the Convention (WGE, TFMM, TFEIP, TF HTAP), international organizations (UN Environment, AMAP, HELCOM etc.) and national experts.

CONTENTS

Introduction

Heavy metals are toxic pollutants, which are within the scope of the UNECE Convention on Long-range Transboundary Air Pollution (hereafter, CLRTAP or the Convention) for a long period. Despite a rapid decrease of emissions of heavy metals in the past decades, long-term risks continue to exist for human health and biota. Therefore, as it is stated in the updates and revisions to the long-term strategy for the Convention [*ECE/EB.AIR/WG.5/2018/3*], *"… the Convention should pursue mitigation activities on heavy metals within the ECE region and consider acting as a centre of expertise … on reducing heavy metals, focusing on sharing its technical knowledge in terms of best available techniques, emission inventories, modelling and monitoring*".

Variety of information related to transboundary pollution by heavy metals, including lead (Pb), cadmium (Cd) and mercury (Hg), is collected and analysed by research centres of the Co-operative Programme for Monitoring and Evaluation of Long-range Transmission of Air Pollutants in Europe (EMEP) – the Centre of Emission Inventories and Projections (CEIP), the Chemical Coordinating Centre (CCC), the Meteorological Synthesizing Centre – East (MSC-E) and the Centre for Integrated Assessment Modelling (CIAM). More detailed information on operational activities of EMEP and its research centres is available at the EMEP website [*www.emep.int*].

The current Status Report overviews research activities of the EMEP Centres in the field of heavy metal pollution performed in accordance with the bi-annual workplan of the Convention for 2018-2019 [*ECE/EB.AIR/GE.1/2017/20-ECE/EB.AIR/WG.1/2017/13*]. The report covers various aspects of heavy metal pollution assessment based both on monitoring and modelling, research and development aimed at improvement of the modelling approaches, co-operation with national experts within the framework of country-scale case studies as well as collaboration with Subsidiary Bodies to the Convention and other international programmes.

Assessment of heavy metal pollution in the EMEP countries is based on a synergy of research efforts of the EMEP Centres. CCC contributes information on measurements of heavy metals in air and precipitation at the EMEP monitoring network. Information on gridded sector-specific emissions of heavy metals is prepared by CEIP based on reported data and expert estimates. MSC-E prepares variety of input information required for modelling (*Chapter 1*) and performs model assessment of heavy metal pollution. The assessment results include modelled patterns of air concentration and deposition of Pb, Cd, and Hg within the EMEP region in 2016, source-receptor relationships, contribution of various emission sectors, and estimates of ecosystem-specific deposition for evaluation of adverse effects (*Chapter 2*). In addition, information on heavy metal pollution of the Arctic sector of the EMEP region is also presented.

Assessment of Hg pollution is among priority tasks within the Convention. Significant efforts of MSC-E during the past year were focused on collaborative work with the scientific community for evaluation of Hg pollution on global and regional scales as a part of the UN Environment Global Mercury Assessment 2018. The Centre co-ordinated a multi-model study of Hg dispersion on a global scale (*Chapter 3*). Results of the analysis contain information on spatial patterns, source apportionment and sectoral composition of Hg deposition in various terrestrial and aquatic regions, and are relevant for both better understanding of Hg atmospheric cycle and improvement of

pollution assessment for the EMEP countries. In addition, the work on refinement of the Hg chemical scheme applied in the Global EMEP Multi-media Modelling System (GLEMOS) was further continued. For this purpose, the chemical mechanism of Hg oxidation by Br was incorporated into the model and evaluated in test runs and comparison with measurements. Further steps of the chemical scheme development were formulated.

The Centre co-operates with Parties to the Convention in the framework of heavy metal pollution assessment on a country scale. This year a case study for Poland has been completed (*Chapter 4*). The analysis of heavy metal pollution of the country includes model assessment of Cd air concentration and deposition levels with fine spatial resolution, evaluation of national anthropogenic emissions, source apportionment of Cd deposition to various provinces of the country including contribution of different emission sectors. A special attention is paid to assessment of Cd pollution of cities. The source-receptor approach was applied to distinguish contribution of internal and external sources to pollution in selected cities of Poland. The results of the study were published in a special Technical Report [*Ilyin et al*., 2018]. In addition, major findings of the country-scale studies gained during the whole period of the project were summarised in [*Travnikov et al*., 2018].

Collaboration with subsidiary bodies to the Convention and other international organisations is also an important part of MSC-E activities (*Chapter 5*). Results of MSC-E research and development activities as well as plans for future research were presented and discussed at the Task Force on Measurements and Modelling (TFMM). The Centre also contributed to the Task Force on Emission Inventories and Projections (TFEIP) with discussion on possible application of transport models for evaluation of reported emissions. Besides, new results of combined analysis of heavy metal pollution using both model estimates and measurements in mosses were presented to the Working Group on Effects (WGE). Moreover, the Centre continued co-operation with other international organizations and programmes (the United Nations Environmental Programme, the Arctic Monitoring and Assessment Programme, Helsinki Commission etc.) to broaden dissemination of the scientific and policy oriented information generated within EMEP.

Detailed information on transboundary pollution by heavy metals of the EMEP region and individual EMEP countries is available at the MSC-E website [*www.msceast.org*]. Additionally, information on heavy metal pollution of the countries of Eastern Europe, Caucasus and Central Asia (EECCA) and the Russian Federation is given in Russian [*www.ru.msceast.org*].

Chapter 1. INPUT INFORMATION FOR MODEL ASSESSMENT

1.1. Meteorology

Meteorological information is very important for modelling of atmospheric transport and deposition of heavy metals and POPs. In particular, wind patterns and atmospheric stability affect dispersion of the pollutants in the atmosphere. Atmospheric precipitation is responsible for wet scavenging of the pollutants. Rates of chemical reactions affecting POPs and Hg transformations depend on air temperature.

Meteorological information for modelling is generated by the WRF meteorological pre-processor (version 3.7.1) [*Skamarok et al*., 2008]. Data of atmospheric analyses at pressure levels obtained from ECMWF were used as input information. For generation of gridded meteorological parameters over the EMEP domain a nesting approach was used. Cloud microphysics is calculated using the WSM3 scheme [*Hong and Lim*, 2006]. Boundary layer parameterization is based on Mellor-Yamada-Janjic approach, which original version is described in [*Mellor and Yamada*, 1982]. The convection scheme is based on modified version of the Kain-Fritsch approach [*Kain*, 2004].

Atmospheric conditions observed in 2016 compared to the climatic levels are characterized by wide range of peculiarities and anomalies occurred in different parts of the EMEP region. In the European region this year was warmer by 0.58 °C compared to the mean value over the period from 1991 to 2010 [*WMO*, 2018]. The highest anomalies (3-6 °C) of near-surface air temperatures occurred in the Arctic region (Fig. 1.1). Over the northern part of Scandinavia the anomaly is 2-3 °C. The lowest anomalies took place in France and Ireland, north of the United Kingdom, some parts of Spain and Portugal. It is interesting to note that all annual mean anomalies over the considered region were positive.

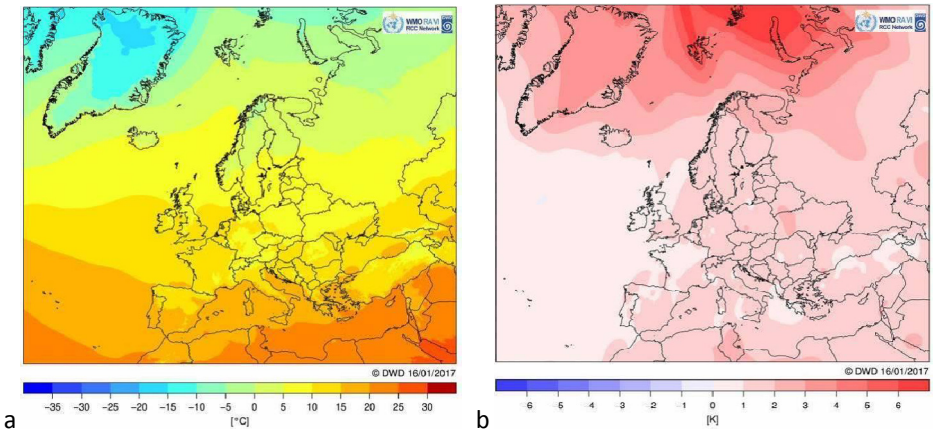

a b

Fig. 1.1. *Mean annual temperature in °C (a) and anomalies (b) for 2016. (reference period 1961-1990, source: http://www.dwd.de/rcc-cm).*

Over most of the EMEP region annual sums of atmospheric precipitation were close to climatic mean values both in absolute (Fig 1.2a) and relative terms (Fig. 1.2b). Positive anomalies around 10-30 mm/month (from +25% to +67%) were noted for the north of Scandinavian Peninsula, the eastern part of Europe, some Balkan (Romania, Serbia, Albania) and central European countries (Hungary, Slovakia, Austria). Stronger relative anomaly (up to +150%) took place in the near-Caspian region.

Conditions drier than normal occurred in the northern part of Spain, southern regions of France and some regions of Italy, Germany and Scandinavia.

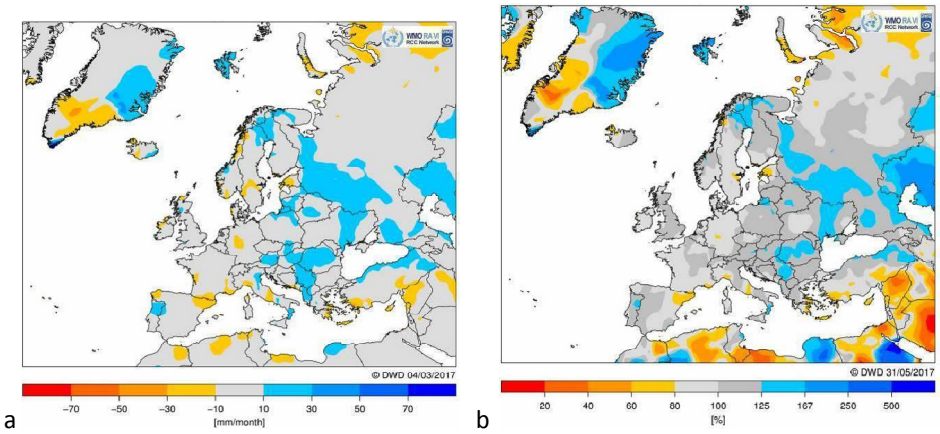

a b

Fig. 1.2. *Absolute (a, mm/month) and relative (b, %) anomaly of annual precipitation sums in 2016 relative to climatic mean value for the period from 1961 to 1990. Source: http://www.dwd.de/rcc-cm*

Annual sums of precipitation over the EMEP region in 2016 vary considerably. Over most part of land area of the EMEP region precipitation sums range from 500 to 1000 mm/year (Fig. 1.3). In mountainous regions and along the western coasts of the temperate zone the annual sums increase up to 2000 mm/year and in some regions even exceed this value. In the northern part of the Central Asia the precipitation sums amount to 200-400 mm/year, and in the southern part, characterized by arid climate, they lie below 200 mm/year.

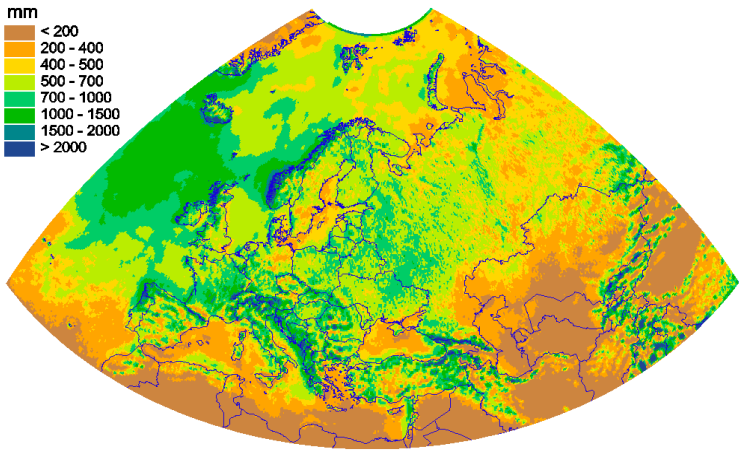

Fig. 1.3. *Annual sums of atmospheric precipitation in 2016*

Strength and direction of winds depends on spatial gradient of atmospheric pressure. In 2016 spatial distribution of annual mean sea level pressure in the European region is presented by Icelandic low extended from southern Greenland to Iceland and Azores high spreading across southern and central Europe to European Russia. Anomalies of the atmospheric pressure in 2016 are relatively low (±2 hPa) over most part of the region. Intensity of zonal component of atmospheric circulation in the middle troposphere is close to normal over most of the year, and it is somewhat lower than normal in the autumn [*HMCR*, 2018]. The meridianal component of the circulation is close to normal throughout the year.

1.2. Anthropogenic emissions

Model assessment of heavy metal pollution in the EMEP countries for 2016 has been performed for the first time over the new EMEP grid. It is based on the most recent dataset of heavy metal emissions available at the moment of the study, which was prepared by CEIP on the new EMEP grid for 2015 [*http://www.ceip.at*][2]. Detailed information on heavy metal emissions in each country, as well as the gap-filling methods that have been used for the 2015 GNFR inventory can be found in the CEIP Technical Report 01/2017 [*Tista et al.*, 2017]. The total values of heavy metal anthropogenic emissions in the EMEP countries are estimated for 2015 at 3704 t/y for Pb, 200 t/y for Cd, and 142 t/y for Hg. More detailed analysis of emission changes in the EMEP countries due to national recalculations can be found in [*Ilyin et al.,* 2017]. Spatial distributions of gridded anthropogenic emissions of Pb, Cd, and Hg are shown in Fig. 1.4. According to available data, elevated emissions of heavy metals are characteristics of Central and Southern Europe, as well as in some regions of Central Asia. Significant emissions also take place from individual large point sources located in other parts of the EMEP region.

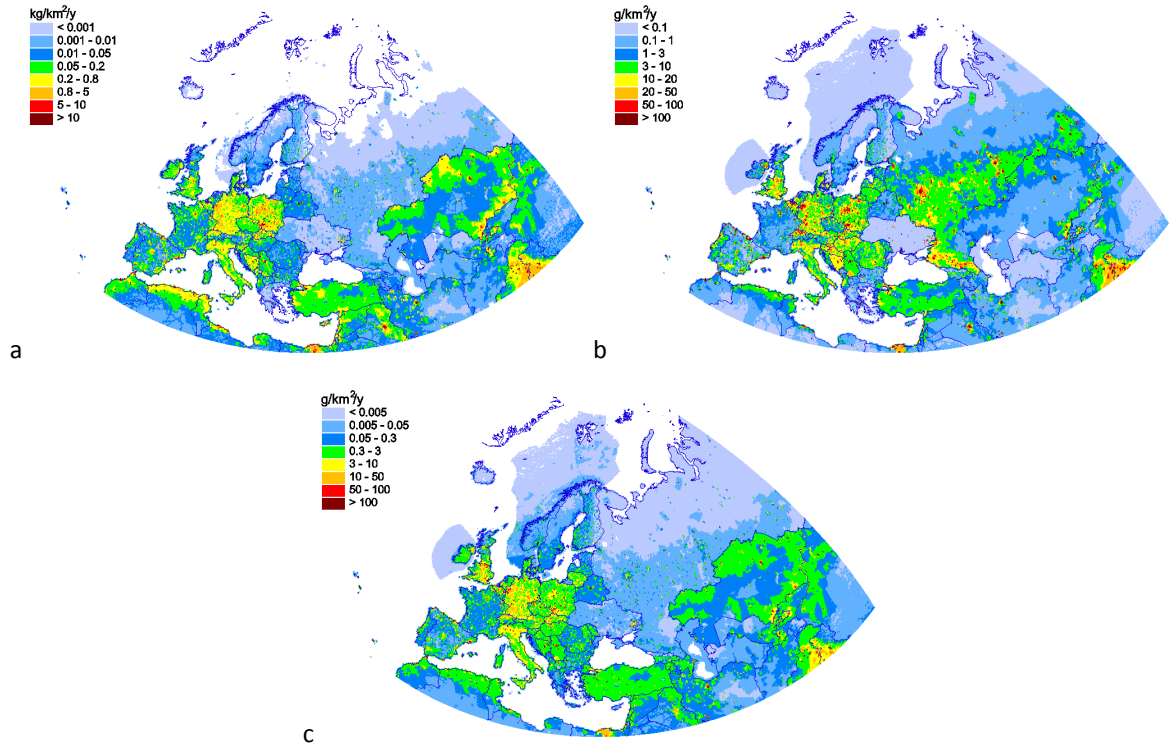

Fig. 1.4. *Spatial distributions of Pb (a), Cd (b), and Hg (c) anthropogenic emissions in 2015*

Additional emission parameters required for heavy metal modelling were prepared by MSC-E. They include seasonal variation, vertical distribution of emissions of all three metals as well as chemical speciation of Hg emissions. Seasonal variation of emissions was estimated using parameterization developed by *van der Gon et al.* [2011]. For implementation of the parameterization into the model gridded annual emissions of heavy metals from individual sectors were multiplied by sector-specific scaling factors (Fig. 1.5). The 'Public power' and 'Residential combustion' sectors are characterised by

[2] *Update of the modelling results based on the new emission data for 2016 is available at the MSC-E web site [www.msceast.org].*

maximum emissions in the cold season and minimum emissions during the warm one (Fig. 1.5a). Seasonality of industrial and transport emissions is relatively small (Fig. 1.5b). Considerable seasonal variation is characteristics of the sector 'Field burning in agriculture' with maximum during the spring cultivation period (Fig. 1.5c) but its contribution to total emissions of heavy metals in the EMEP countries is insignificant (Fig. 1.5d). Seasonal variation of emissions from other sectors was neglected.

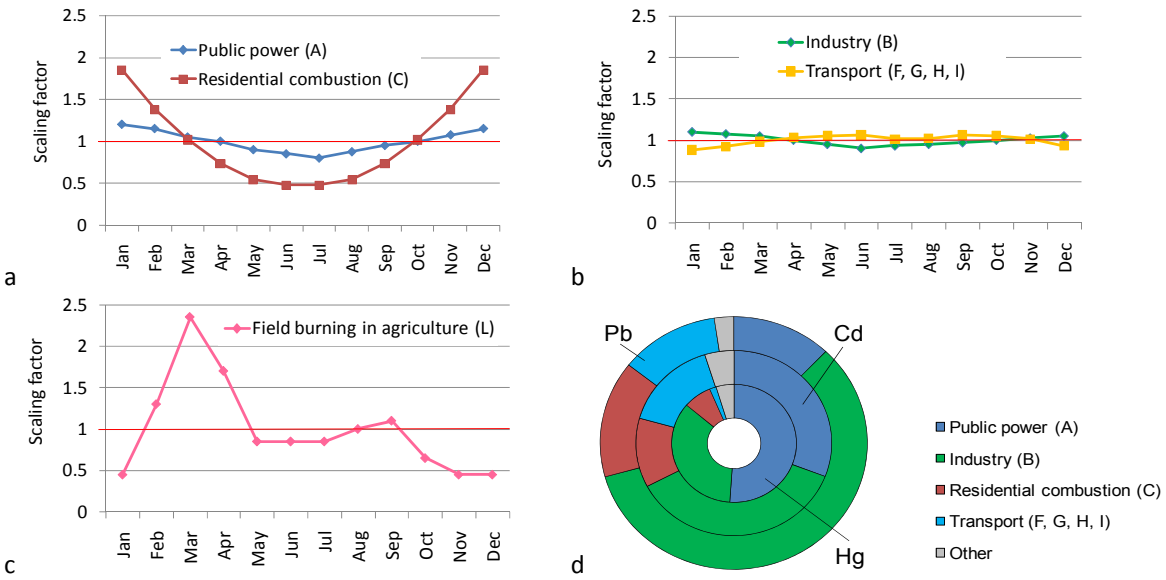

Fig. 1.5. *Seasonal variation of major sectors of heavy metal emissions (a-c) and contribution of the sectors to total emissions of Pb, Cd, and Hg in the EMEP countries in 2015 (d)*

A new scheme of emissions distribution with height was applied in the current model assessment. It is based on parameterisation suggested by *Bieser et al*. [2011] and consists of application of sector-specific vertical profiles (Fig. 1.6) derived by averaging of emission heights for various meteorological conditions and various pollutants. According to the applied approach emissions from the 'Public power' sector take place mostly at heights 300-500 m. The 'Industry' sector share emissions between 50 and 150 m. The 'Waste incineration' mostly emits heavy metals at 150-250 m. It is assumed that heavy metal emissions from other sectors occur near the ground.

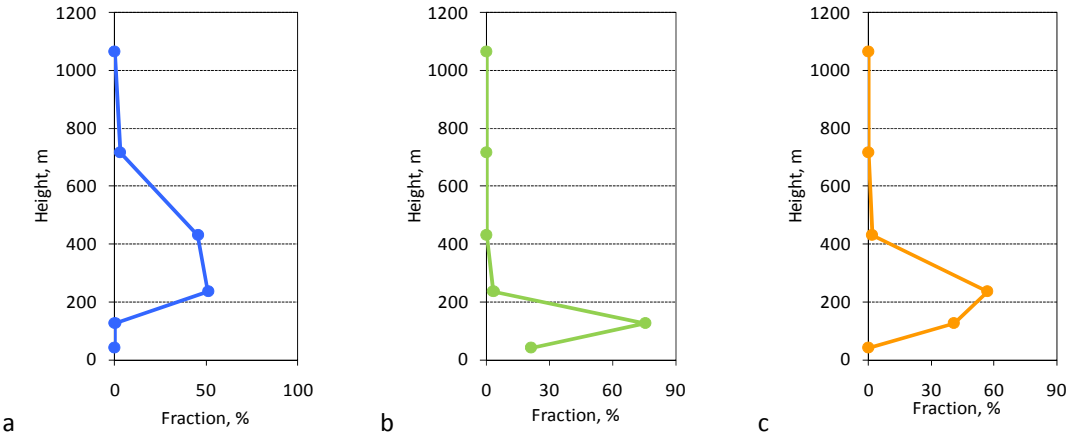

Fig. 1.6. *Vertical distribution of heavy metal emissions for selected emission sectors: (a) – Public power; (b) – Industry; (c) – Waste incineration.*

Mercury is emitted to the atmosphere in various chemical forms: elemental (Hg^0), gaseous oxidized ($HgII_{gas}$) and particulate ($HgII_{part}$). Atmospheric behaviour of Hg strongly depends on its form. The speciation of Hg emissions is not included in the information reported by the Parties to the Convention. Therefore, expert estimates of Hg emission speciation have been derived by MSC-from a global emission dataset [*AMAP/UNEP*, 2013]. According to these data about 70% (52-90%) of Hg is emitted in the EMEP countries in the elemental form. The contributions of the oxidized forms are 24% (7-38%) and 6% (0-10%) for the gaseous oxidized and the particulate forms, respectively (Fig. 1.7).

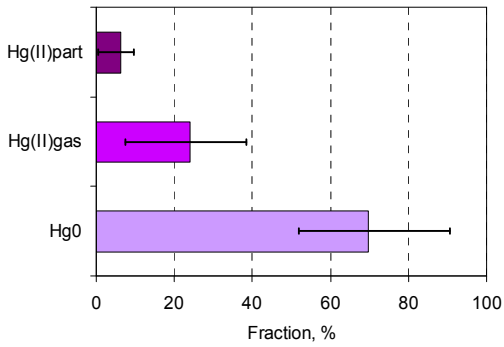

Fig. 1.7. *Chemical speciation of Hg emissions in the EMEP countries based on [AMAP/UNEP, 2013]. Bars present average values; whiskers show variation of the values among the countries.*

1.3. Secondary emissions (wind re-suspension)

Wind re-suspension is important contributor to atmospheric emissions of heavy metals in the EMEP region. It represents suspension of dust particles or sea salt aerosol from the underlying surface by action of wind. The suspended dust particles contain heavy metals (Pb and Cd) which can have natural origin or can came from the accumulation over long-term period of deposition from anthropogenic sources. Parameterization of this process used in the model is described in [*Gusev et al.*, 2006; 2007]. It is assumed that re-suspension occurs from water surface, arable lands in spring and autumn, from lands not covered by vegetation (e.g., deserts) and from urban territories. Total annual re-suspension of Pb from territories of the EMEP countries is 3700 tonnes, and Cd – 72 tonnes. On one hand, these values are comparable with the anthropogenic emissions in the EMEP countries (3704 and 200 tonnes, respectively). On the other hand, uncertainty of these estimates is high.

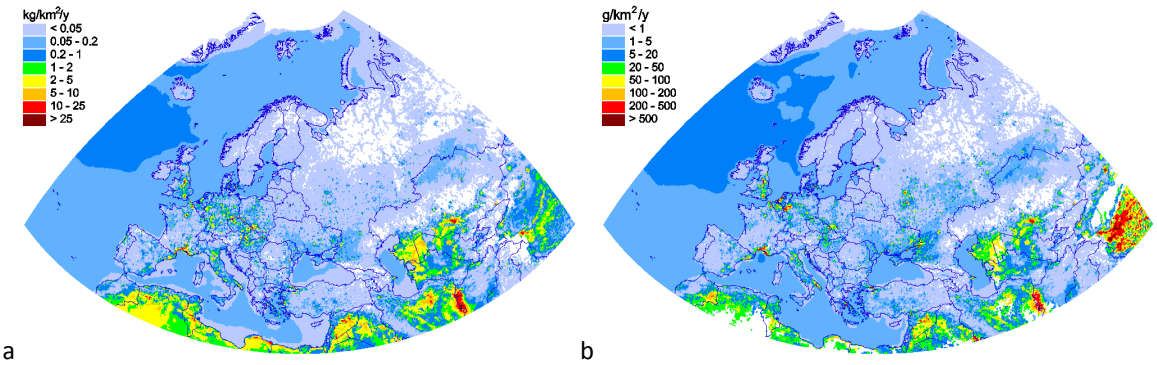

Fig. 1.8. *Wind re-suspension flux of Pb (a) and Cd (b) in the EMEP region in 2016.*

Re-suspension flux depends not only on land-cover characteristics, but also on meteorological conditions, in particular, on soil wetness and near-surface wind velocity. Therefore, this flux is highly

variable in space and time. The highest re-suspension fluxes of Pb (Fig 1.8a) and Cd (Fig. 1.8b) occur in the southern and south-eastern parts of the EMEP domain because of large areas of deserts. Besides, high levels are seen in the central part of Europe and near large cities. It is explained by assumed accumulation of the metals in soils over recent decades and by large fraction of urban territories. The lowest re-suspension fluxes take place in the northern part of the EMEP domain.

1.4. Boundary conditions for regional modelling

Lead and Cd emitted in the neighbouring regions of the EMEP domain can reach the EMEP countries. In case of Hg contribution of intercontinental transport can even exceed the contribution of the EMEP sources (see section 2.2). In order to establish concentrations of the considered metals at the EMEP boundaries global scale calculations are carried out using GLEMOS calculations on a global scale.

Global scale concentrations of Pb and Cd are the highest in the south-eastern part of Asia, mainly because of emissions in China (Fig. 1.9a and 1.9b). Besides, comparatively high levels are noted for the south-western part of Asia, Middle East and the northern part of Africa. It is explained by significant dust suspension in these regions and, hence, contribution of secondary emission sources to atmospheric concentrations. The lowest levels occur over the North Atlantic and the Arctic.

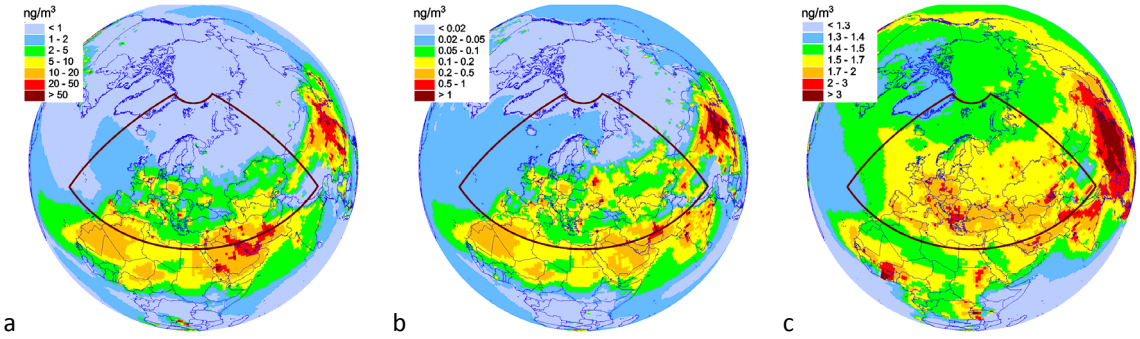

a b c

Fig. 1.9. *Global annual mean concentrations of Pb (a), Cd (b) and elemental Hg (c) in 2016. Dark frame denotes boundaries of the EMEP region.*

China, Indonesia (Asia) and Ghana (Africa) are characterized by the highest concentrations of elemental Hg mostly because of large anthropogenic emissions (Fig. 1.9c). Over other parts of the Northern Hemisphere the concentrations are distributed relatively homogeneously. Somewhat higher levels are seen at the southern and eastern boundaries of the EMEP region due to influence of anthropogenic emission sources, and partly because of natural emissions in the southern part of Europe. The lowest concentrations are noted in the Arctic.

Model concentrations of Pb, Cd and Hg at boundaries of the EMEP region strongly depend on global-scale emission data. However, present-time gridded emission data of Pb and Cd over the global scale are not available. Assumptions used to estimate these emissions give rise to uncertainties of the modelling results over the global scale, and further, in the EMEP countries. ***In order to improve quality of model assessment of concentrations and deposition in the EMEP region contemporary gridded global-scale heavy metal emissions are needed.***

Chapter 2. HEAVY METAL POLLUTION OF THE EMEP REGION IN 2016

Assessment of heavy metal pollution of the EMEP region is based on both measurement data and modelling results and includes evaluation of spatial patterns and transboundary transport of the pollution as well as contribution of various emission sectors and ecosystem-specific deposition fluxes.

2.1. Measurements of heavy metals at the EMEP monitoring network

Measurement network

In 2016, there were 36 sites measuring heavy metals (Cd or Pb) in both aerosols and precipitation, and altogether there were 66 measurement sites. Twenty nine sites were measuring Hg in either air and precipitation, 13 of these with co-current measurements in air and precipitation In total, 21 Parties to the Convention reports heavy metal data to EMEP, 7 of these fulfil their monitoring obligations as defined in the EMEP monitoring strategy [*UNECE*, 2009] with at least one site of level 2 with both air and precipitation measurements of heavy metals in air and precipitation. A number of countries have been reporting heavy metals within the EMEP area in connection with different national and international programmers such as HELCOM, AMAP and OSPAR. Detailed information about the sites and the measurement methods are found in EMEP/CCC's data report on heavy metals and POPs [*Aas et al.*, 2018]. This report includes also other elements like Zn, Ni, As, Cu, Co, Cr, Mn, V, Fe, Al and more. All the data are available from the EBAS database [*http://ebas.nilu.no/*].

In the last year report (EMEP Status report 2/2017), we discussed the new reporting guidelines of Hg for a consistent definition of component names. Besides, additional metadata have been included to give important information on methodology and quality. There are few Parties that have yet taken the new guidelines into account. Thus, there is a need to follow up on this to improve the reporting as well as clean up historical data in the database so they are harmonised with the new guidelines especially on component names.

Observed concentration levels of Pb, Cd in 2016

Annual averages of Pb and Cd concentrations in precipitation and in air in 2016 are presented in Fig. 2.1-2.4. The lowest concentrations for all elements are generally found in Scandinavia, and the highest in Central and Eastern Europe. Some of the high concentrations are due to too high detection limit of the method, i.e. Cd in aerosols in Portugal.

For Pb, the highest concentration in aerosols is observed in Hungary followed by sites in Estonia, and in the Benelux. In precipitation, the highest volume weighted annual mean is observed in Denmark followed by Slovakia, Spain and the Benelux. For Cd, the highest concentration in aerosols in observed in Estonia followed by sites in Hungary and Belgium, if not considering the Portuguese sites with high detection limit. In precipitation, the highest level is seen in Slovakia followed by sites in France, Spain and Sweden.

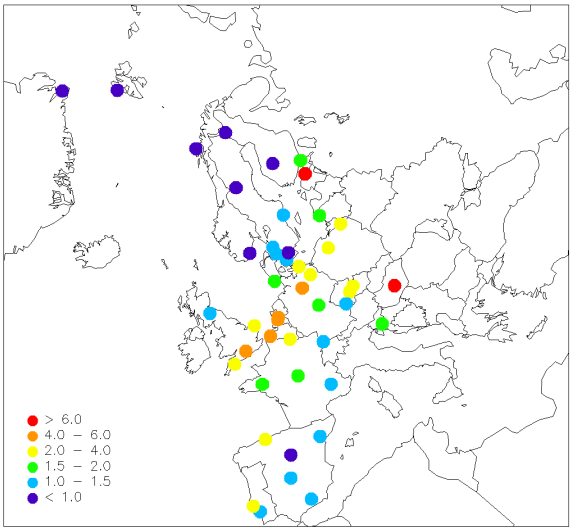

Fig. 2.1. *Pb in aerosol, ng/m^3*

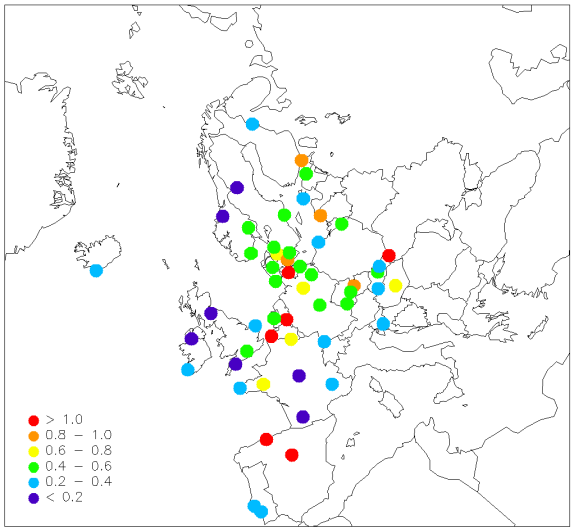

Fig. 2.2. *Pb in precipitation, µg/L*

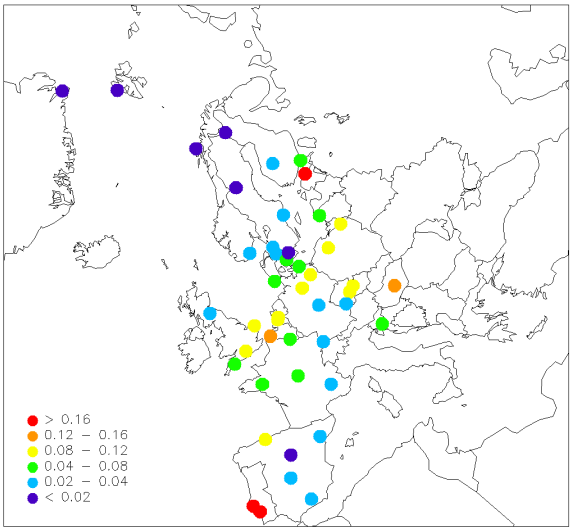

Fig. 2.3*. Cd in aerosol, ng/m^3*

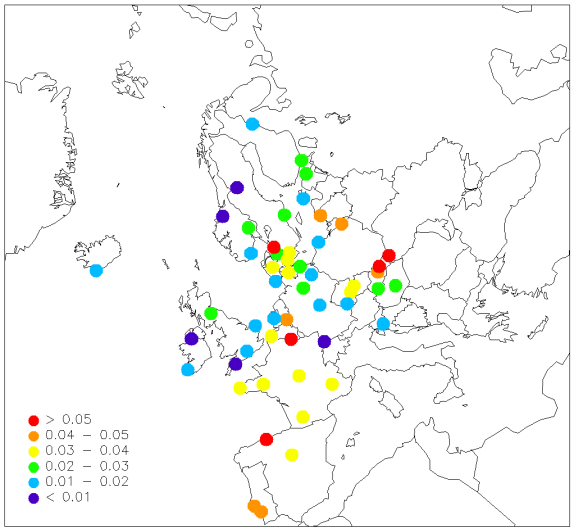

Fig. 2.4. *Cd in precipitation, µg/L*

Observed concentration levels of Hg in 2016

For total gaseous and elemental Hg the highest concentration is seen in Poland followed by Germany and one site in the UK reflecting the source regions of Hg in Europe. In precipitation, the highest levels are seen in Latvia and Germany followed by sites in Sweden, t he Netherlands and Spain, if excluding the sites with high detection limits in Portugal and Ireland. Lowest concentrations are seen in Finland and Great Britain.

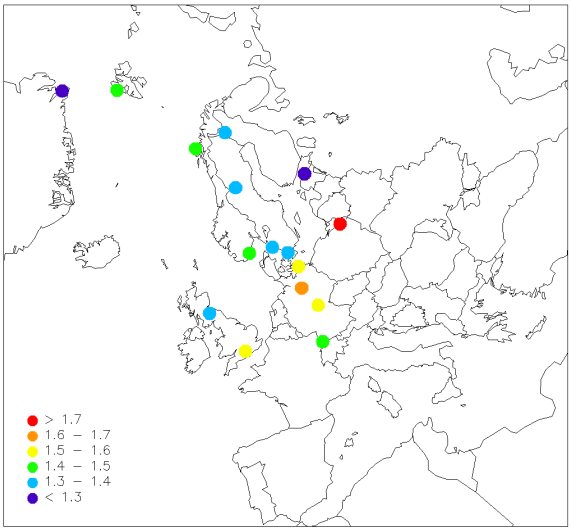

Fig. 2.5. *Hg (g) in air, ng/m^3*

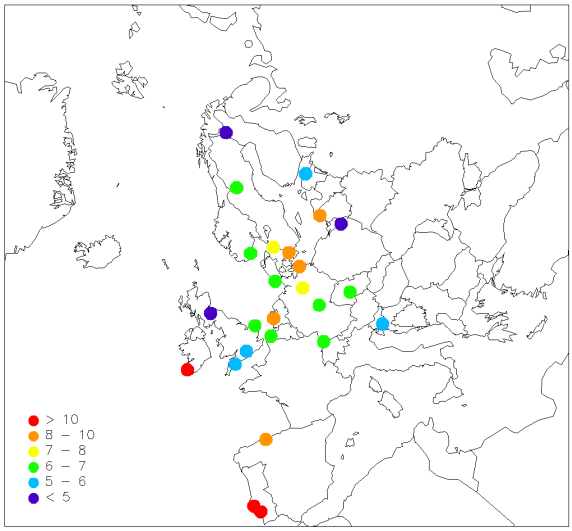

Fig. 2.6. *Hg in precipitation, ng/L*

Strong seasonality in the concentrations of Hg in air is observed at several EMEP sites, with higher concentrations in winter whereas low concentrations are observed in summer. This strong seasonality is described for most temperate sites in the Northern Hemisphere [*Temme et al.,* 2007*; Sprovieri et al.*, 2016] and is generally explained by peaking primary anthropogenic Hg emissions in winter due to high energy demand [*Temme et al.,* 2007] and faster atmospheric oxidation rates and subsequent deposition in summer [*Holmes et al*., 2010]. However, global Hg models have not yet been able to reproduce the wintertime high concentrations as current anthropogenic Hg emission inventories have no seasonal resolution and are kept constant through the year. Secondly, no seasonal oscillation is observed in the Southern Hemisphere [*Slemr et al*., 2015], questioning the dominant role of the atmospheric oxidation. Therefore a new study by *Jisrka et al*. [2018] proposed an alternative hypothesis; uptake of atmospheric Hg by vegetation, and that vegetation sequester as much as approximately 50% of primary anthropogenic emissions. They found that Hg correlates with CO_2, a tracer for gas exchange by vegetation, implying that Hg uptake by vegetation is controlled by gas exchange similar to CO_2. Further, they found a strong correlation between the normalized difference vegetation index (NDVI) and Hg that also points to uptake of Hg by vegetation. The correlation was stronger for inland terrestrial sites compared to coastal sites, supporting the theory that vegetation uptake is responsible for Hg depletion in summer when the vegetation activity is the highest. In Figure 2.7, we compare a monthly mean concentrations averaged for the last five years to avoid annual variations, at selected EMEP sites for different environment. There is a clear difference in seasonality for terrestrial and arctic sites.

This new hypothesis have large implications for the global Hg cycle and the forecasting and interpretations of long term trends, also suggesting that the decreasing atmospheric Hg concentration is not due to decreasing emissions but vegetation uptake and increased primary production. The effect of Hg uptake in vegetation related to climate change and land-use change must be considered in mitigation strategies to reduce human Hg exposure. The importance of Hg uptake as a deposition pathway demands revised Hg deposition monitoring strategies by environmental agencies [*Jiskra et al*., 2018].

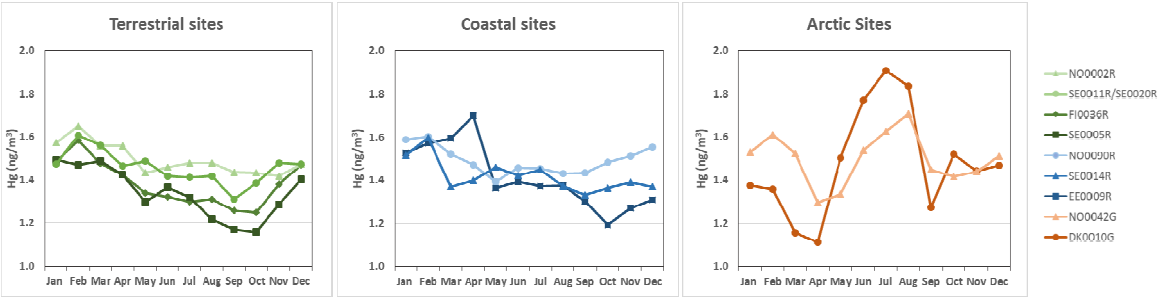

Fig. 2.7. *Average monthly mean concentrations of gaseous Hg over the five years period 2013-2016 for selected EMEP sites in different environment, ng/m^3.*

2.2. Spatial patterns of heavy metal pollution

Information on pollution levels of Pb, Cd and Hg in 2016 was prepared on the base of model calculations with the GLEMOS modelling system. Heavy metal emission data for the model are prepared by CEIP on the latitude-longitude grid (see Section 1.1). Full model-based information about heavy metal pollution levels with spatial resolution 0.1°x0.1° is allocated in the internet [*www.msceast.org*]. This section provides an overview of the main peculiarities of the heavy metal pollution levels in the EMEP region.

Heavy metal pollution levels in the EMEP countries are caused by three groups of emission sources. These are EMEP anthropogenic emissions of considered year, wind re-suspension of dust particles containing heavy metals, and emissions from sources located outside the EMEP region (non-EMEP sources). Contribution of these three groups of sources is calculated for each EMEP country on regular basis.

Spatial distribution of annual mean concentrations and total deposition of Pb, Cd and Hg over the EMEP region is highly non-uniform. Comparatively high levels of Pb air concentrations (15-30 ng/m^3) are noted for the central part of Europe (southern Poland, western Germany) and northern part of Italy (Fig. 2.8a). In the Czech Republic, Hungary, Slovakia, the western part of the United Kingdom, the northern part of France the concentrations vary within 3-15 ng/m^3. Relatively high levels (8-15 ng/m^3) also take place in the Central Asian countries (south of Kazakhstan, Turkmenistan, Uzbekistan), which is caused by high contribution of wind re-suspension of dust. Regions with elevated air concentrations of Cd are similar to those of Pb, e.g. the southern part of Poland and the western part of Germany, where the concentrations exceed 0.5 ng/m^3. Other 'hot-spots' with similar concentrations are in the Benelux countries and in a number of regions in Russia. Over most of the central European countries the levels vary from 0.1 to 0.2 ng/m^3.

Spatial distribution of annual deposition fluxes in most countries is similar to that of air concentrations. Relatively high fluxes of Pb (above 2.5 kg/km^2/y) are noted for some regions of southern part of Poland, northern Italy, the south of Kazakhstan and the west of Tajikistan (Fig. 2.8b). Over most of central, southern and south-eastern parts of Europe the deposition fluxes range from 0.6 to 2.5 kg/km^2/y, and from 0.3 to 0.6 kg/km^2/y over western and northern parts of Europe. Cadmium deposition is the highest (above 60 g/km^2/y) in southern Poland, western Germany, the

western part of Turkey, and several regions in Russia (the Central part, south Urals, south-west of Siberia). Over most part of central, eastern and southern Europe deposition fluxes of Cd vary from 20 to 60 g/km^2/y. In the western and the northern parts of Europe the levels are within 5-20 g/km^2/y. Relatively low deposition of Pb and Cd are noted for the most part of Central Asia due to low atmospheric precipitation.

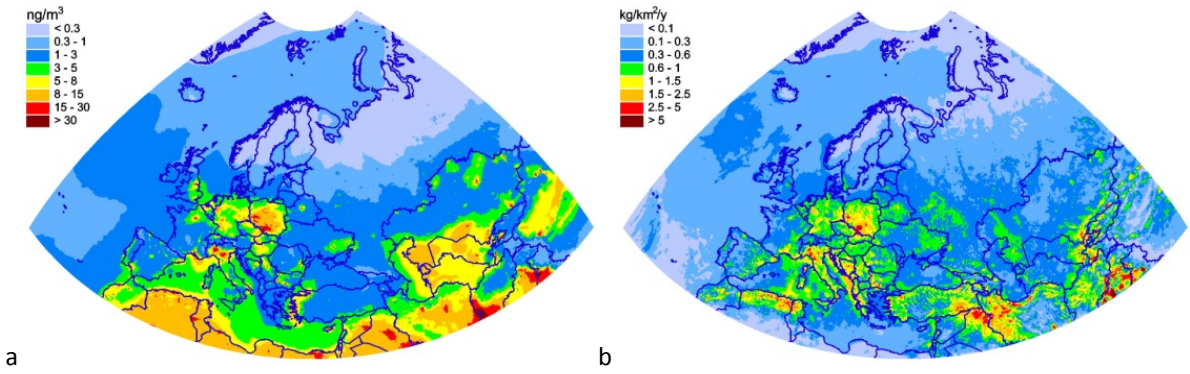

Fig. 2.8. *Mean annual air concentrations (a) and total deposition (b) of Pb in 2016*

Unlike Pb and Cd, Hg is known for long (0.5-1 year) atmospheric lifetime. Therefore, Hg can travel and disperse over global scale distances. It results in relatively smooth spatial distribution of Hg over territory of the EMEP region. Its annual mean concentrations vary from 1.4 ng/m^3 in the Arctic and Scandinavia to more than 1.8 ng/m^3 in the southern part of Europe. Elevated levels in particular areas are explained by location of strong emission sources. Areas with relatively high concentrations of Hg in the southern parts of the EMEP region are also caused by natural emissions associated with the Hg geochemical belt [*Gustin et al,* 1999]. Deposition fluxes are mostly caused by short-lived oxidized Hg forms. Relatively high deposition fluxes (30-40 g/km^2/y) in northern Italy, Poland, the central part of Russia, Balkan countries and the south-east of Europe are caused by combined effect of emissions and atmospheric precipitation.

Contributions of various groups of sources to deposition vary to high extent among the EMEP countries. For example, deposition from the EMEP anthropogenic sources of Cd contributes from 8% to 74% to total deposition (Fig. 2.9). In absolute terms the highest country-averaged deposition flux is noted for Poland (25 g/km^2/y), followed by Slovakia (20 g/km^2/y) and Slovenia (17 g/km^2/y). The results for Pb are similar to those for Cd. Contribution of anthropogenic sources ranges from 6% to 63%. The highest contribution of Pb deposition is obtained for Poland (0.8 kg/km^2/y), Slovakia (0.6 kg/km^2/y), the Czech Republic (0.5 kg/km^2/y), Bulgaria, Bosnia and Herzegovina (around 0.4 kg/km^2/y).

Contribution of secondary sources to Cd and Pb deposition varies from 26% to 80%. Therefore, these sources contribute at least a quarter of total deposition in the EMEP countries. However, it should be kept in mind that the uncertainty of estimated contribution of secondary sources is higher than that of anthropogenic sources. The highest Cd deposition flux from these sources takes place in regions, which are characterized by significant pollution in previous decades and by high extent of urbanization, such as the Netherlands and Belgium. Besides, significant relative contribution of re-suspension is noted for Iceland due to considerable input from sea salt aerosols. The highest Pb

deposition caused by wind re-suspension occurs in the Mediterranean region, namely, in Montenegro and Monaco (0.6 kg/km^2/y each), Bosnia and Herzegovina (0.5 kg/km^2/y), Italy, Albania and Croatia (0.4 kg/km^2/y each).

Contribution non-EMEP sources of Cd varies from 2% to 44%, and that of Pb - from 5% to 56%. The highest contribution, in absolute and relative terms, takes place in countries of southern and south-eastern part of the Mediterranean region. For example, deposition from non-EMEP sources of Cd is the highest in Montenegro (9 g/km^2/y), Albania (7 g/km^2/y), Turkey (6 g/km^2/y). Besides, elevated relative contribution is seen for countries in the Caucasus and Central Asia. For example, the non-EMEP contribution of Cd is 42% in Armenia, 33% in Kyrgyzstan and Georgia, around 30% in Uzbekistan and Turkmenistan. These high values in the EECCA countries is explained by emissions from non-EMEP anthropogenic sources and by re-suspension input from desert areas outside the EMEP domain.

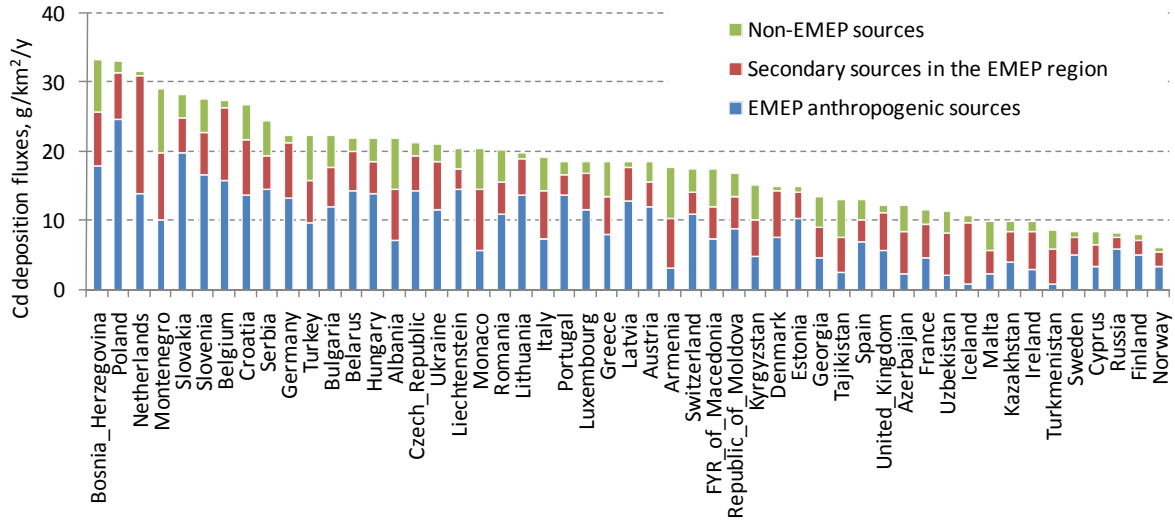

Fig. 2.9. *Country-averaged deposition fluxes of Cd from the European and Central Asian anthropogenic, secondary and non-EMEP emission sources in 2016*

Mercury deposition fluxes differ from those of Pb and Cd. Due to strong influence of intercontinental transport the contribution of non-EMEP sources to total deposition in the EMEP counties is dominating, ranging from 50% to 95%. The contribution exceeds 50% in all EMEP countries and exceeds 75% in half of them. However, it should be noted that the contribution from intercontinental transport includes also some fraction of Hg from the EMEP sources, which is emitted and entered the global Hg pool. Contribution of EMEP anthropogenic sources to country mean Hg deposition fluxes varies from 4 to 19%. The highest deposition from this sources occurs in Poland (8.3 g/km^2/y), followed by the Czech Republic (8 g/km^2/y) and Slovakia (6.9 g/km^2/y). The direct contribution of EMEP secondary (natural and re-emission) sources to deposition is small (below 1%).

2.3. Transboundary transport

Anthropogenic deposition to each country can be presented as a sum of two components: deposition from national emission sources and deposition caused by foreign emissions. Information about transboundary fluxes between the EMEP countries is prepared regularly. Since the EMEP countries report their national anthropogenic emissions, only the anthropogenic part is considered. Detailed information on source-receptor relationships is available in the Internet at [www.msceast.org]. For example, contribution of foreign sources to deposition of Pb in 2016 varies from 14% in Spain to 99% in Monaco and Liechtenstein (Fig. 2.10). High contribution of foreign sources to Cd in Monaco and Liechtenstein as well as in Iceland, Sweden, Kyrgyzstan, Lithuania is explained by small national emissions. Deposition from foreign sources exceeds deposition form national sources in 38 of 51 countries for Pb and Cd and in 40 countries for Hg.

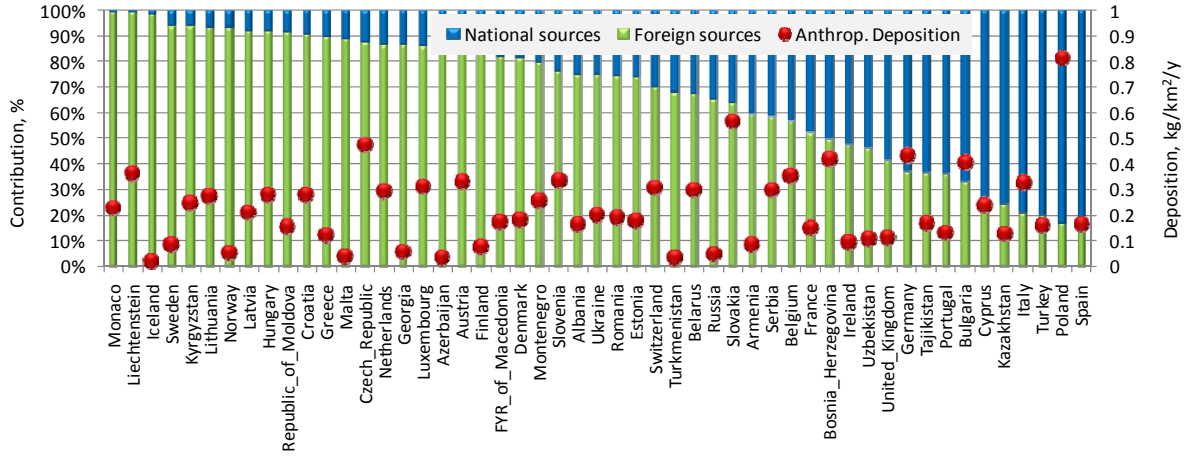

Fig. 2.10. *Relative contribution of the transboundary transport and national sources to anthropogenic Pb deposition in the European and the Central Asian countries and deposition values from anthropogenic emission sources in 2016*

Heavy metals emitted by national sources partly deposit within a country's territory and partly contribute to transboundary pollution of territories of neighbouring EMEP countries or even transported to other regions. Fractions and magnitudes of national emissions deposited to a country's own territory, to other EMEP countries and outside the EMEP countries vary considerably. Countries with large emissions make up significant absolute contribution to transboundary transport. For example, from about 700 tonnes of Pb emitted in Kazakhstan, around 233 tonnes is deposited to other EMEP countries and 204 tonnes – to areas outside the EMEP countries (Fig. 2.11). Other major counties importers of Pb are Poland, Turkey and Italy. As a rule, 60-100% of Pb and Cd emissions and 80-100% of Hg emissions are deposited outside the country's territory.

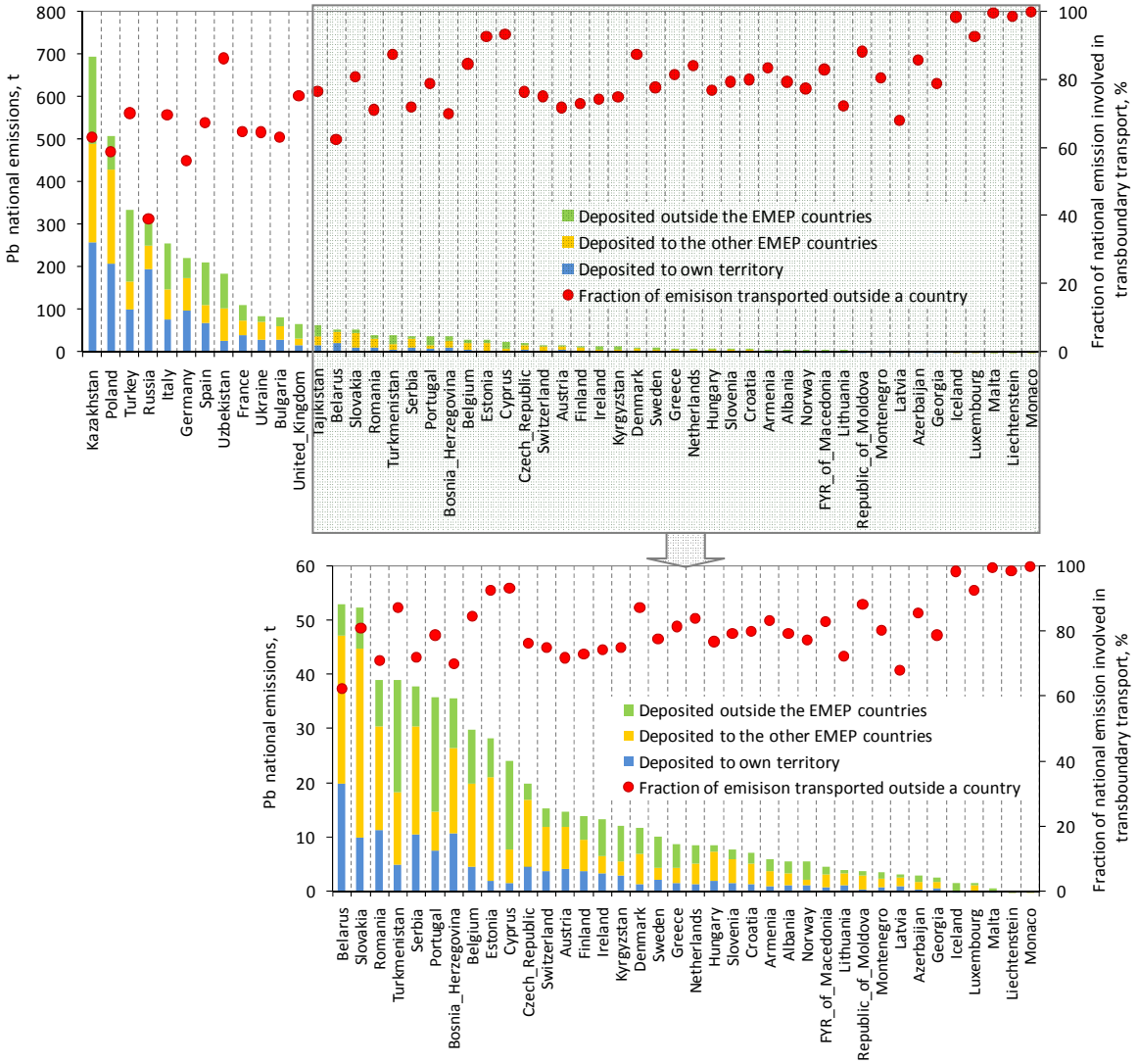

Fig. 2.11. *Distribution of Pb emitted in the EMEP countries between deposition to own territory, deposition to the other EMEP countries and deposition outside the EMEP countries in 2016. Red dots indicate relative fraction of national emissions involved into the transboundary pollution*

2.4. Pollution from different emission sectors

Information on regularly reported source-receptor relationships in the EMEP countries can be extended by analysis of transboundary transport from different emission sectors. Contributions of Cd emissions from four groups of emission source categories to deposition in the EMEP countries were simulated. These groups include Public Power (sector A), Industry (sector B), Residential Combustion (sector C) and Remaining Sectors (sum of emissions from all other source categories). Emissions in countries from particular sectors were provided by CEIP.

Country-averaged deposition fluxes from sector 'Public Power' range from 0.2 g/km^2/y (Malta) to 4.3 g/km^2/y (Belarus) (Fig. 2.12). In most of the EMEP countries (43 of 51) the contribution of foreign sources exceeds the contribution of national sources. Contribution of national sources to deposition

from this sector ranges from 0 to 96%. The highest contributions of national sources are noted for Russia (96%), Spain (92%) and Switzerland (75%). Contribution of foreign emission sources to deposition from 'Public Power' sector varies from 4 to 100%. In Georgia, Lichtenstein, Iceland and Albania all deposition from this sector is caused by transboundary transport. In 20 countries (e.g., Belarus, Croatia, Finland, Kyrgyzstan etc.) the contribution of foreign sources to deposition from sector 'Public Power' exceeds 90%.

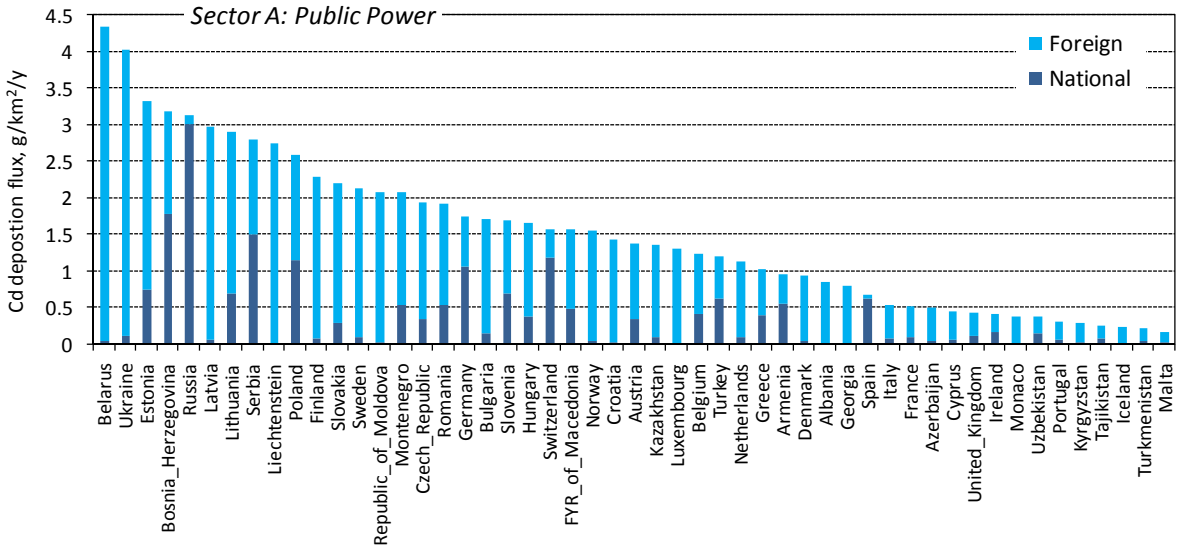

Fig. 2.12. *Country-averaged deposition fluxes of Cd from sector 'Public Power' in 2016*

The main Cd emission sector in the EMEP region is Industry, which contributes 36% to total Cd emission. Therefore, deposition fluxes caused by this sector are generally higher than those caused by other sectors. The highest country-averaged deposition occurs in Poland (around 16 g/km^2/y), followed by Portugal and Slovakia (around 11 g/km^2/y each) (Fig. 2.13). The lowest deposition takes place in Turkmenistan (0.3 g/km^2/y) and Iceland (0.4 g/km^2/y). Contribution of national sources to Cd deposition from sector 'Industry' ranges from 0 to 91%, and of foreign sources – from 9 to 100%. In 39 countries contribution of foreign sources exceeds the contribution of national sources. In 20 countries this contribution exceeds 50%, and in Iceland and Malta all 100% deposition from Industry sector are caused by transboundary transport. In some countries (e.g., Poland, Portugal, Spain, Turkey) national sources dominate over transboundary input.

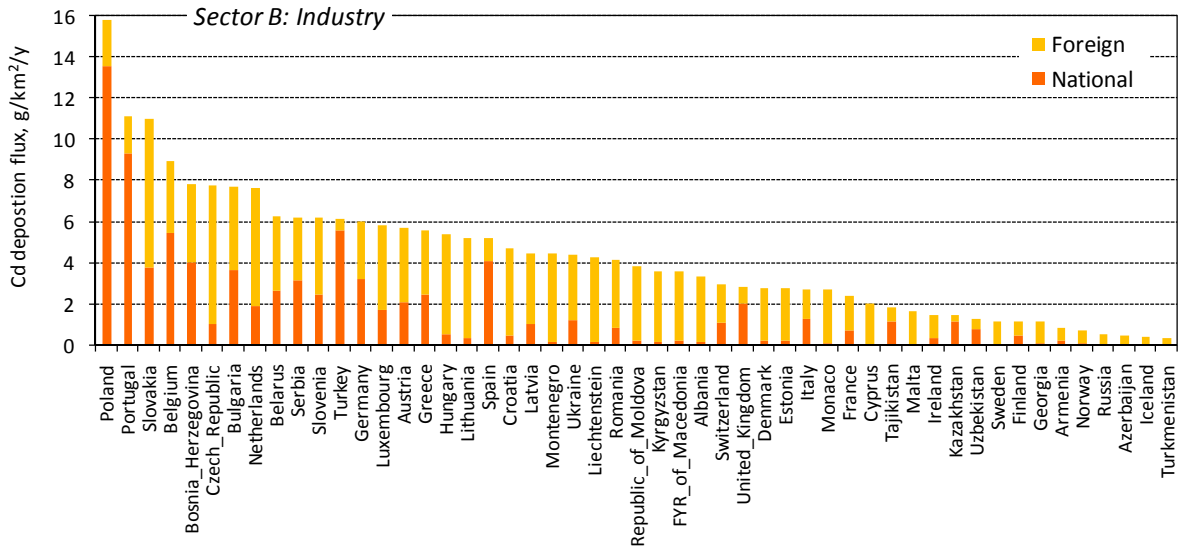

Fig. 2.13. *Country-averaged deposition fluxes of Cd from sector 'Industry' in 2016.*

The highest deposition caused by emission sector 'Residential Combustion' is noted for Slovenia (7.2 g/km^2/y), the lowest – in Turkmenistan (0.1 g/km^2/y) (Fig. 2.14). Contribution of national and foreign sources to deposition from sources of this sector varies markedly among the EMEP countries. Sources of 'Residential Combustion' sector contribute from 0 to 97% of deposition from national sources and from 3 to 100%- from foreign sources. In Turkey, Italy, Portugal and the United Kingdom the contribution of national sources exceeds 80%, whereas in some countries (e.g., Malta, Iceland, Uzbekistan) all deposition from 'Residential Combustion' comes from foreign sources. In 34 countries deposition from foreign sources exceeds deposition from national sources.

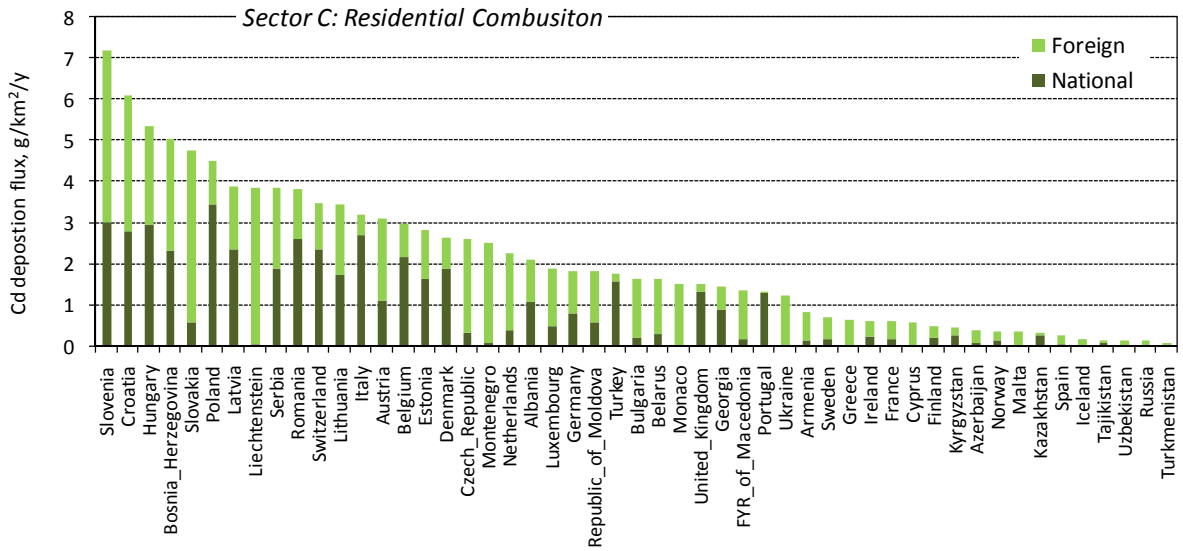

Fig. 2.14. *Country-averaged deposition fluxes of Cd from sector 'Residential Combustion' in 2016*

Emission from remaining sectors makes about 20% from total Cd emission in the EMEP countries. The highest deposition from this sector occurs in Germany (3.8 g/km^2/y), and the lowest – in Iceland (0.2 g/km^2/y) (Fig. 2.15). In 41 countries the contribution of foreign sources exceeds 50%.

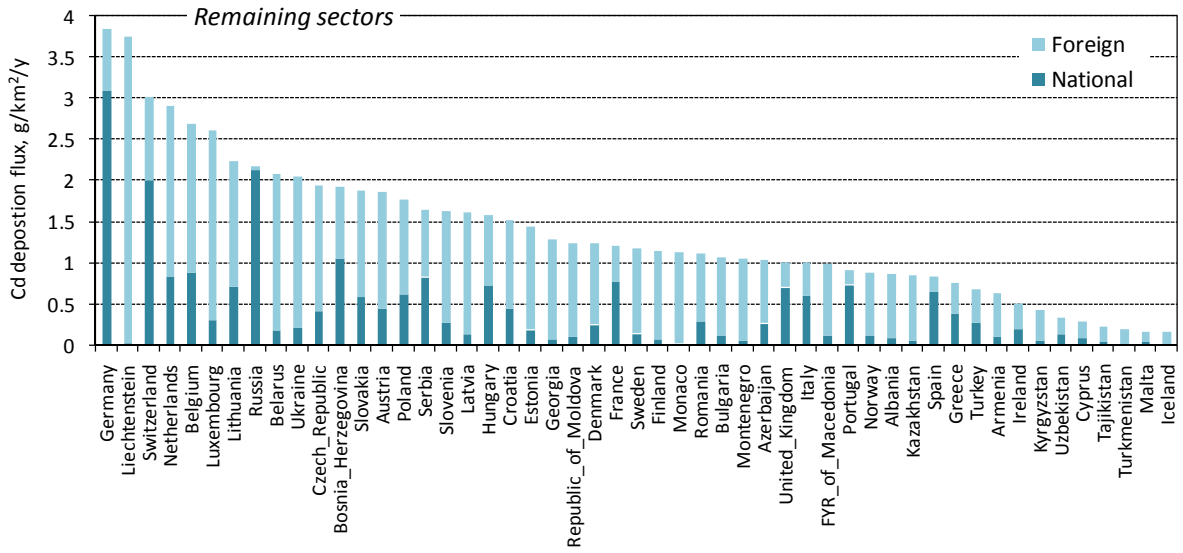

Fig. 2.15. *Country-averaged deposition fluxes of Cd from remaining sectors in 2016*

Composition of deposition in each country from viewpoint of emission sources and sectors differs largely. For example, main foreign contributors to anthropogenic deposition of Cd to the Czech Republic in 2016 are Poland (34%), Germany (19%) and Austria (7%) (Fig. 2.16a). Most of deposition (around 56%) from neighbouring countries is caused by sources of sector 'Industry'. In particular, industrial sources of Poland contribute 28% (272 kg), of Germany – 10% (91 kg) of foreign deposition (Fig. 2.16b). The second in importance is 'Residential Combustion' sector (19%) followed by 'Public Power' sector (13%).

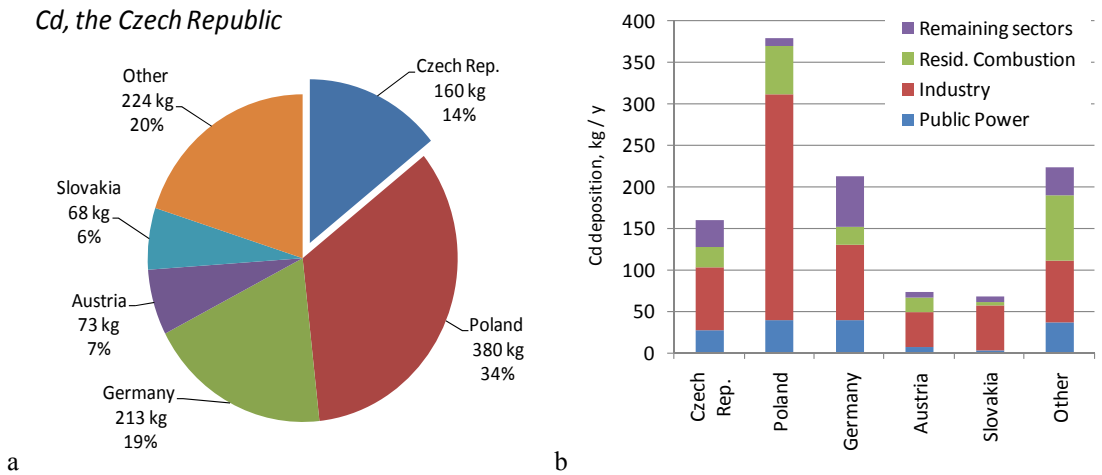

Fig. 2.16. *Main countries-sources of anthropogenic deposition to the Czech Republic (a) and their sectoral composition (b)*

Another situation takes place in Kazakhstan, which is located in the south-eastern part of the EMEP region. National sources contribute 38% to anthropogenic deposition, and the main foreign sources are Russia (48%), Uzbekistan (5%) and Turkey (3%) (Fig. 2.17a). Unlike the Czech Republic, the main foreign emission sector contributing to deposition is 'Public Power', followed by group 'Remaining sectors' in emissions of Russia(Fig. 2.17b).

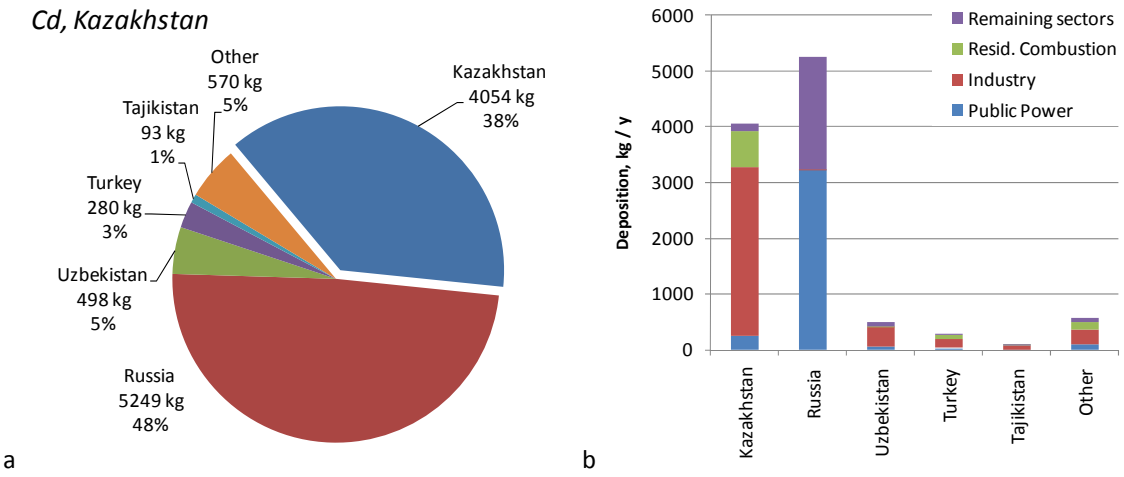

Fig. 2.17. *Main countries-sources of anthropogenic deposition to the Kazakhstan (a) and their sectoral composition (b)*

Source-receptor matrices calculated regularly for each EMEP country were supplemented by information on contributions to deposition from main emission sectors of Cd, such as 'Public Power', 'Industry' and 'Residential Combustion'. Contributions of national sources to deposition form particular emission sectors vary from zero, if this sector does not present in national emission data, to 98%. The contribution of foreign sources ranges from 3 to 100%. Fractions of deposition from emission sectors of neighbouring countries vary markedly among receptor countries. Further simulations can be carried out for other priority metals (Pb, Hg).

2.5. Ecosystem-dependent deposition

Lead, Cd and Hg are known for their harmful effects for human health and the environment. Lead and Cd affect biodiversity of soil species and microbe-mediated processes [*de Vries et al.*, 2015a]. They also reduce growth of plants. Besides, these metals tend to accumulate into plant tissues and transfer to human organisms through food chains. Mercury in water bodies can transform to the highly toxic methylated form, which accumulates in fish and affect human health through fish consumption.

For evaluation of the effects of atmospheric heavy metal deposition on human health and environment a concept of critical loads is considered under the Convention. This concept assumes that known negative effects may occur at or above certain concentration of heavy metals in soil or water. This threshold concentration is called critical level. It is assumed that this concentration is a result of a steady-state balance between input flux to soil (e.g., atmospheric deposition, weathering of rocks) and output flux from soils (e.g., leaching, biomass uptake) [*de Vries et al.*, 2015b].

Atmospheric deposition flux which leads to establishment of critical level concentration is called critical load. Exceedance of atmospheric deposition over critical load results to concentration in soil higher than critical level, which can give rise of negative effects for biota or human health.

In order to provide the Working Group on Effects with information relevant for evaluation of critical load exceedances atmospheric ecosystem-dependent deposition are calculated regularly by MSC-E. Seventeen classes of underlying surface are considered based on the MODIS land-cover data. Information on deposition of Pb, Cd and Hg to each ecosystem type in each EMEP country is available at the MSC-E website [*www.msceast.org*].

Deposition fluxes to particular land cover categories differ significantly. For example, annual Hg deposition flux to inland waters varies from 5 to 15 g/km^2/y over most part of the EMEP region (Fig. 2.18a). In some regions of northern Italy, the Balkans and Caucasus the flux reach 30 g/km^2/y. In Scandinavia the fluxes are the lowest falling below 5 g/km^2/y. However, deposition fluxes to forests are much higher than that to inland waters exceeding 15 g/km^2/y over most part of western and central Europe and more than 7 g/km^2/y in Scandinavia and central and northern Russia (Fig. 2.18b).

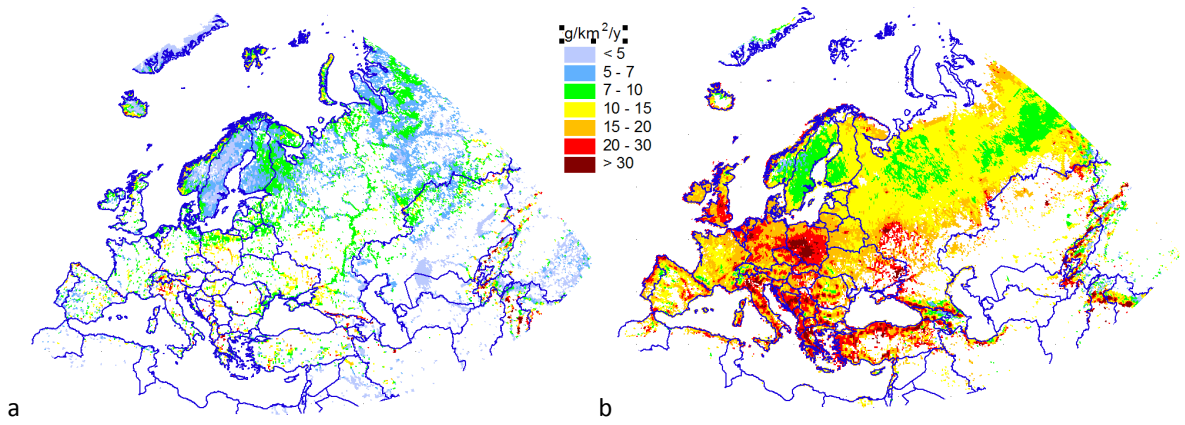

Fig. 2.18. *Annual deposition flux of Hg to inland waters (a) and forests (b) in 2016.*

Maps of critical load exceedances are resulted from comparison of ecosystem-dependent deposition maps with critical loads. According to calculations of the exceedances, negative effects of Hg and Pb deposition on human health and biota are most expected over major part of Europe [*de Wit et al*, 2015]. ***However, these results relate to 2010. In order to evaluate present-day effects of heavy metal depositions more contemporary calculations of the exceedances are needed.***

2.6. Arctic pollution

Agreement between the Convention and AMAP has been reached at the joint meeting held in Potsdam, Germany in February 2016. On the base of this agreement MSC-E continued cooperation with AMAP in the field of analysis and assessment of heavy metal pollution in the Arctic region. MSC-E has calculated atmospheric deposition to the Arctic area within the new EMEP domain, estimated contributions to deposition caused by the EMEP anthropogenic, secondary and non-EMEP sources, identified main source countries and emission sectors contributed to anthropogenic deposition in the Arctic.

Fluxes of total deposition of Pb in the considered part of Arctic range mostly from 50 to 300 g/km^2/y, and Cd – from 3 to 15 g/km^2/y (Fig. 2.19a,b). The lowest levels of Pb and Cd are noted for Greenland where they fall below 20 and 2 g/km^2/y, respectively. Besides, low Cd levels are noted in the northern Scandinavia, Franz-Josef Land and in some regions of the Arctic coast of Russian. Relatively high deposition fluxes take place over the North Atlantic, which is explained by high annual sums of atmospheric precipitation due to cyclonic activity. Besides, relatively high fluxes are noted for windward coasts (e.g., Iceland, Norway), where generation of precipitation is amplified by orographic effects. Finally, in case of Cd 'hot-spots' of elevated deposition fluxes (15-25 g/km^2/y or even more) are associated with sources of significant anthropogenic emissions located on Kola Peninsula, Archangelsk region, the Republic of Komi and Norilsk.

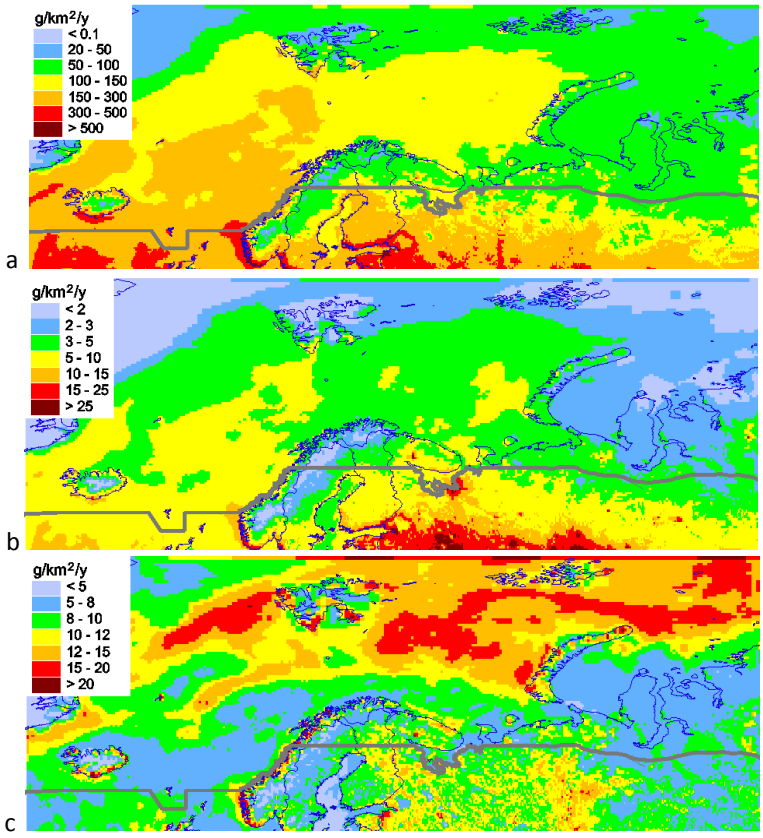

Fig. 2.19. *Total deposition fluxes of Pb (a), Cd (b) and Hg (c) to the Arctic (within EMEP domain) in 2016. Grey line denotes border of AMAP Arctic area*

Relatively high deposition fluxes along windward coasts of Scandinavian Peninsula and Iceland are also noted for Hg. However, spatial pattern of Hg deposition to the Arctic differs from that of Pb and Cd. Relatively high deposition fluxes (12-20 g/km^2/y) occur over vast areas of the Arctic Ocean (Fig. 2.19c). These fluxes are caused by the Atmospheric Mercury Depletion Events (AMDE). However, it should be also taken into account that significant part of the deposited Hg is reduced and reemitted back to the atmosphere.

The Arctic region is remote from major anthropogenic sources of Pb in the EMEP countries. The contribution of these sources to total deposition is 23%, whereas secondary emissions contribute more than half of Pb deposition to terrestrial areas of the Arctic (Fig. 2.20a). About a quarter of deposition came from emission sources located outside the EMEP domain. Structure of Cd deposition

is different (Fig. 2.20b). A number of anthropogenic emission sources are located within the Arctic area (e.g., in the Russian Arctic), It makes contribution of these sources to be higher than that of Pb (51%). Contribution of secondary sources for Cd is 36%. Considerable contribution of Pb and Cd secondary sources is explained by influence of wind suspension of marine aerosols from sea surface. It provides more than a half of deposition from secondary sources. Most of Hg deposition (93%) is caused by intercontinental transport (Fig. 2.20c). However, it should be noted that this value includes Hg which was emitted by EMEP sources and then transported outside the EMEP domain entering global Hg pool.

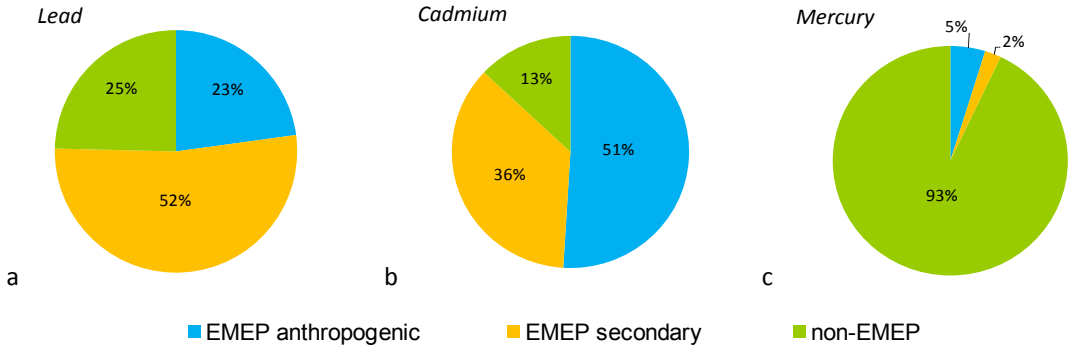

Fig. 2.20. *Average contribution of different source types to annual deposition of Pb (a), Cd (b), and Hg (c) to the European and Asian terrestrial areas of the Arctic covered by the EMEP domain*

The main source countries contributing to heavy metal deposition in the Arctic are Russia, Kazakhstan and Poland. Significant part of the Russian territory within the EMEP region relate to the Arctic region. Therefore, contribution of Russian sources to anthropogenic deposition varies from 31% (Pb) to 80% (Cd) (Fig. 2.21). The second largest source country is Kazakhstan. Although this country is located far from the Arctic region, its national emissions of Pb and Hg used for modelling are the highest among the EMEP countries, and Cd emissions are also among the highest. It should be pointed out that the source apportionment presented in Fig. 2.21 reflect average situation for the whole region, the picture can differ significantly among particular locations.

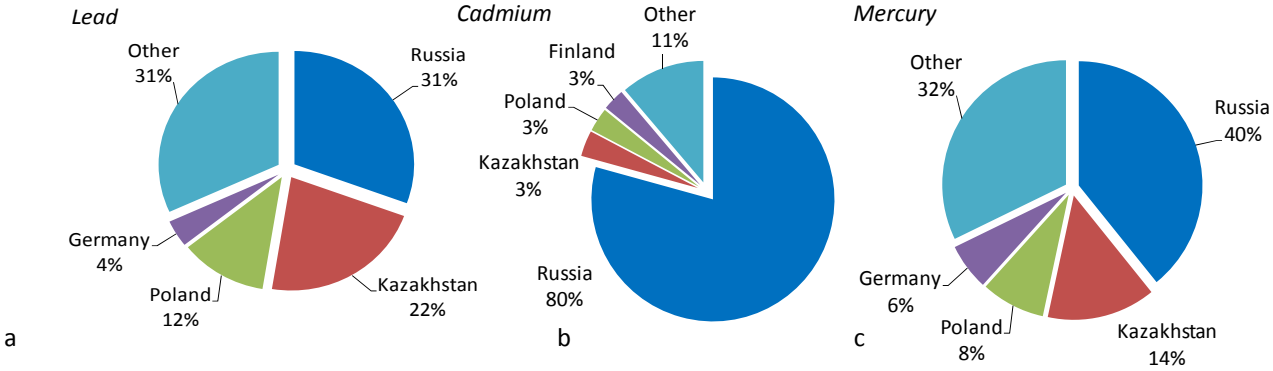

Fig. 2.21. *Contribution of main EMEP source countries to anthropogenic deposition in the terrestrial areas of Arctic within EMEP region in 2016.*

Main sector responsible for Cd pollution in the Arctic, contributing around 60% (1900 kg) to Cd deposition, is 'Public power' from Russian emissions (Fig. 2.22a). Contribution of this sector from

other EMEP countries is low (4%, 100 kg). The second largest contributor is the 'Industry' sector, which makes up 11% (around 360 kg) of total deposition. Contribution from 'Residential Combustion' is 4% (about 130 kg).

Deposition caused emission sector 'Pubic Power' are distributed unevenly over the Arctic region. The highest deposition fluxes are noted for European part of Russia (Kola Peninsula, Archangelsk region, the Republic of Komi), where the fluxes exceed 25 g/km^2/y (Fig. 2.22b). In the Asian part of the Russian Arctic, northern Scandinavia and Svalbard the deposition from this sector range from 2 to 5 g/km^2/y, or even below 2 g/km^2/y in some regions. Along the western and southern coasts of Europe and over most of the Northern Atlantic the deposition fluxes range from 3 to 10 g/km^2/y.

a

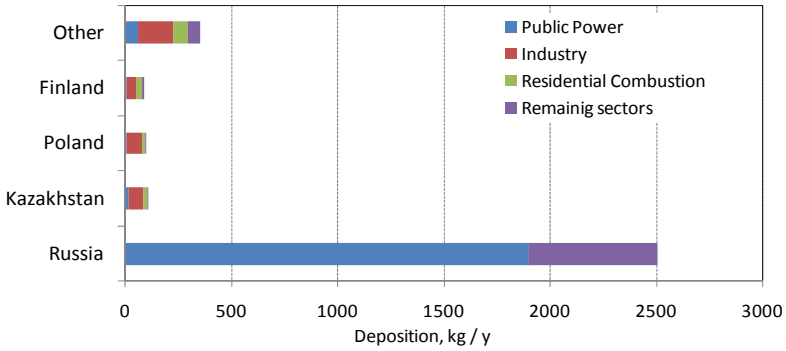

b

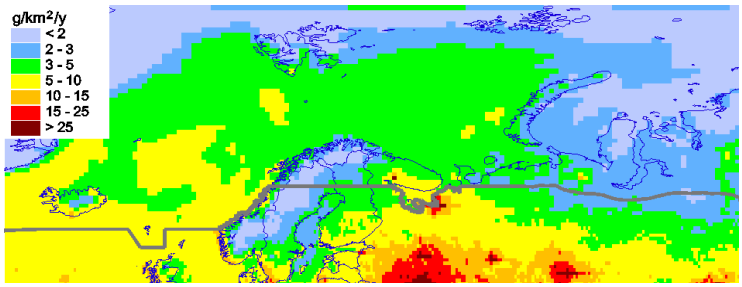

Fig. 2.22. *Cadmium deposition from sector 'Public Power' to terrestrial areas of Arctic within EMEP region from main countries-contributors in 2016*

The analysis of modelled heavy metal levels in the Arctic demonstrates that the pollution by Pb and Cd is strongly affected by secondary emission sources. Therefore, further investigation of the related processes and updating of their parameterizations are needed to improve results of the model assessment in the Arctic and to better understand the role of anthropogenic and secondary sources. Pollution of the Arctic by Hg is highly defined by *in situ* oxidation of Hg in the polar atmosphere. Further improvement of the Hg chemical scheme in the model could also improve quality of the pollution assessment for the Arctic.

Chapter 3. MODEL ASSASSMENT OF MERCURY POLLUTION

Mercury pollution is a topical issue attracting increasing attention both in the Convention and beyond. MSC-E continues its work focused on both research of various aspects of Hg pollution and improvement of the modelling tool used for the model assessment in accordance with the EMEP bi-annual workplan [ECE/EB.AIR/GE.1/2017/20-ECE/EB.AIR/WG.1/2017/13]. Recent research and development activities included detailed multi-model study of Hg pollution on a global scale as a part of the UN Environment Global Mercury Assessment 2018 and evaluation of a new chemical mechanism for Hg transformations in the atmosphere.

3.1. Multi-model study of Hg pollution on a global scale

Oleg Travnikov[3], Hélène Angot[4], Johannes Bieser[5], Mark Cohen[6], Ashu Dastoor[7], Francesco De Simone[8], Ian Hedgecock[8], Sae Yun Kwon[4], Che-Jen Lin[9], Andrei Ryjkov[7], Noelle Selin[4], Colin P. Thackray[10], and Xun Wang[9]

The current state of Hg dispersion in the global atmosphere and deposition to various terrestrial and aquatic regions was studied by an ensemble of chemical transport models as a part of the UN Environment Global Mercury Assessment 2018 (see Section 3.3.1). Four global-scale chemical transport models for Hg were involved in the study – GLEMOS (EMEP/MSC-E), GEM-MACH-Hg (Environment and Climate Change Canada, Canada), GEOS-Chem (Massachusetts Institute of Technology, USA) and ECHMERIT (CNR - Institute of Atmospheric Pollution Research, Italy). A detailed description of the models along with discussion of their differences can be found in [*Travnikov et al*., 2017]. The main results of the model assessment are briefly discussed below. More detailed information is available in [*AMAP/UNEP*, 2018].

The global distribution of Hg^0 concentration in the surface air in 2015 simulated by the model ensemble is shown in Figure 3.1a in terms of the model ensemble median. The spatial pattern is characterized by the typical latitudinal gradient with elevated concentrations (above 1.4 ng/m^3) in the temperate latitudes of the Northern Hemisphere and the lowest concentrations (below 1 ng/m^3) in the high latitudes of the Southern Hemisphere. The highest concentrations (above 2 ng/m^3) are estimated in East, South and Southeast Asia due to high levels of anthropogenic emissions as well as in equatorial Africa and South America because of active artisanal and small-scale gold mining (ASGM).

[3] Meteorological Synthesuzing Centre – East of EMEP;
[4] Massachusetts Institute of Technology, USA;
[5] Helmholtz-Zentrum Geesthacht, Germany;
[6] 1National Oceanic and Atmospheric Administration (NOAA), USA;
[7] Environment and Climate Change Canada, Canada;
[8] CNR Institute of Atmospheric Pollution Research, Italy;
[9] Lamar University, USA;
[10] Harvard University, USA.

Global distribution of Hg deposition in 2015 simulated by the model ensemble is shown in Fig. 3.1b. The deposition pattern does not reveal considerable difference in Hg deposition to the ocean in the Northern and Southern Hemispheres. Levels of Hg deposition to land vary within the continents reflecting location of anthropogenic emissions as well as the surface characteristics and climatic conditions. There are increasing north-to-south gradients of Hg deposition in North America and Eurasia with exception of desert and mountain regions in Central and East Asia. Most territory of South America is subjected to high Hg fluxes determined by ASGM emissions, except for the most southward part of the continent. In Africa, Hg deposition differs significantly from relatively low fluxes in the desert northern part to high deposition fluxes in the equatorial and southern parts of the continent.

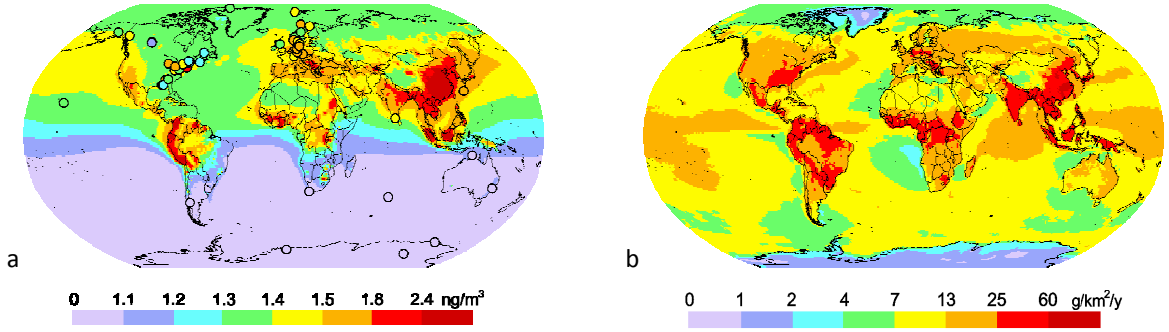

Fig. 3.1. *Global distribution of model ensemble median Hg^0 concentration in surface air (a) total (wet and dry) deposition flux (b) in 2015.*

The modelling results were evaluated against observations from global and regional monitoring networks (GMOS, EMEP, NADP/MDN, AMNet and NAtChem). The model ensemble median of Hg^0 concentration well agrees with observed values within ±20% at most of the measurement sites (symbols, Fig. 3.2a). The scattering of simulated values among the models presented by the standard deviation (whiskers, Fig. 3.2a) is relatively small and does not exceed 20%. The model-to-measurement difference is larger for wet deposition (symbols, Fig. 3.2b). The model ensemble demonstrates good correlation (r^2 = 0.7) with observations but tends to overestimate low and underestimate high deposition fluxes. Nevertheless, the deviation between the modelling results and measurements does not exceed a factor of 2 at the majority of measurement sites. The inter-model variance is also larger for wet deposition (whiskers, Fig. 3.2b) demonstrating considerable discrepancies of parameterizations of Hg oxidation chemistry, scavenging and precipitation amount between the models. A comprehensive evaluation of the participating models against variety of ground-based and aircraft measurements as well as their sensitivity to various parameters and processes can be found in a series of recent publications [*Angot et al*., 2016; *Travnikov et al*., 2017; *Bieser et al*., 2017].

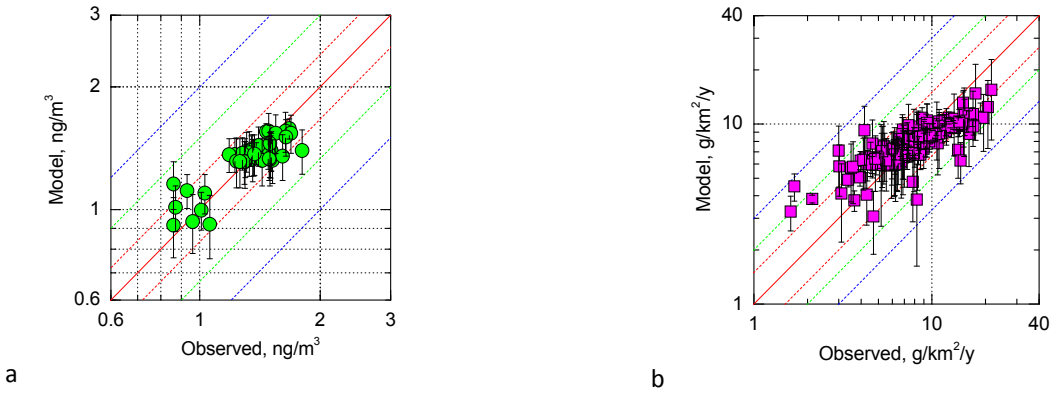

Fig. 3.2. *Comparison of simulated and observed Hg^0 concentration (a) and wet deposition flux (b) in 2015. Symbols present the model ensemble median, whiskers show the standard deviation of individual models. Lines depict different deviation levels: solid red – the 1:1 ratio; (a) dashed red – by factor 1.2; dashed green – by factor of 1.5; dashed blue – by factor of 2; (b) dashed red – by factor 1.5; dashed green – by factor of 2; dashed blue – by factor of 3.*

The analysis presented below contains information on emissions and deposition fluxes averaged over a number of geographical regions. The definition of source and receptor regions is shown in Fig. 3.3. The regions are divided into 6 continents (Europe, North, Central, and South America, Africa, Australia and New Zealand (NZ)), 5 large subcontinents (Middle East, countries of the Commonwealth of Independent States (CIS), South, East, and Southeast Asia), and 2 Polar Regions (Arctic and Antarctic). In addition, aquatic regions of the world ocean are defined in accordance with the Major Fishing Areas of the UN Food and Agriculture Organization [*FAO*, 2018].

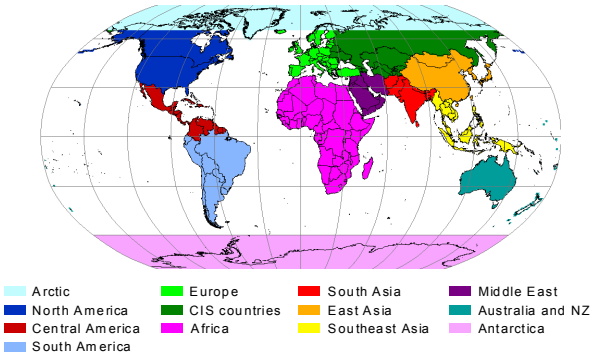

Fig. 3.3. *Source and receptor regions included in the model analysis of source apportionment of Hg deposition.*

Figure 3.4 summarizes the total Hg deposition fluxes to terrestrial and aquatic receptor regions as well as the relative contributions of direct anthropogenic and natural/secondary sources simulated by the model ensemble. Total Hg deposition fluxes are the highest in large industrial regions such as South, East, and Southeast Asia (25-30 g/km^2/y) and the lowest in remote regions such as the Arctic and Antarctica (below 6 g/km^2/y). Regions with active ASGM (Central and South America), which emit Hg in the form of Hg^0, are also subject to a relatively high total Hg deposition flux of 25 g/km^2/y.

Total Hg deposition consists of contributions from direct anthropogenic emissions as well as natural and re-emitted sources, which account for 53-81% of the total Hg deposition in various terrestrial

and aquatic regions. As illustrated in Fig. 3.4, the relative contributions of direct anthropogenic sources show a regional pattern decreasing from regions of the highest (South, East and Southeast Asia; 30-47%) to the lowest total Hg deposition flux (the Polar Regions; 20-25%). The contribution of direct anthropogenic sources to other receptors regions ranges between 25-35%. The regional pattern can be explained by the level of domestic anthropogenic emissions, which generate a substantial fraction of oxidized Hg that deposit rapidly within the source region.

Mercury deposition to various regions of the world ocean is shown in Fig. 3.4b. Average deposition flux varies from 8 g/km^2/y over the Southeast Atlantic to 14 g/km^2/y over the Western Central Pacific. Mercury deposition to the ocean is also influenced by direct anthropogenic emissions as well as natural and secondary sources. The relative contribution of direct anthropogenic sources to ocean reservoirs evaluated here varies from 19% (Southern Ocean) to 35% (Northwest Pacific) and it is slightly lower compared to direct anthropogenic contribution of terrestrial reservoirs (20-50%).

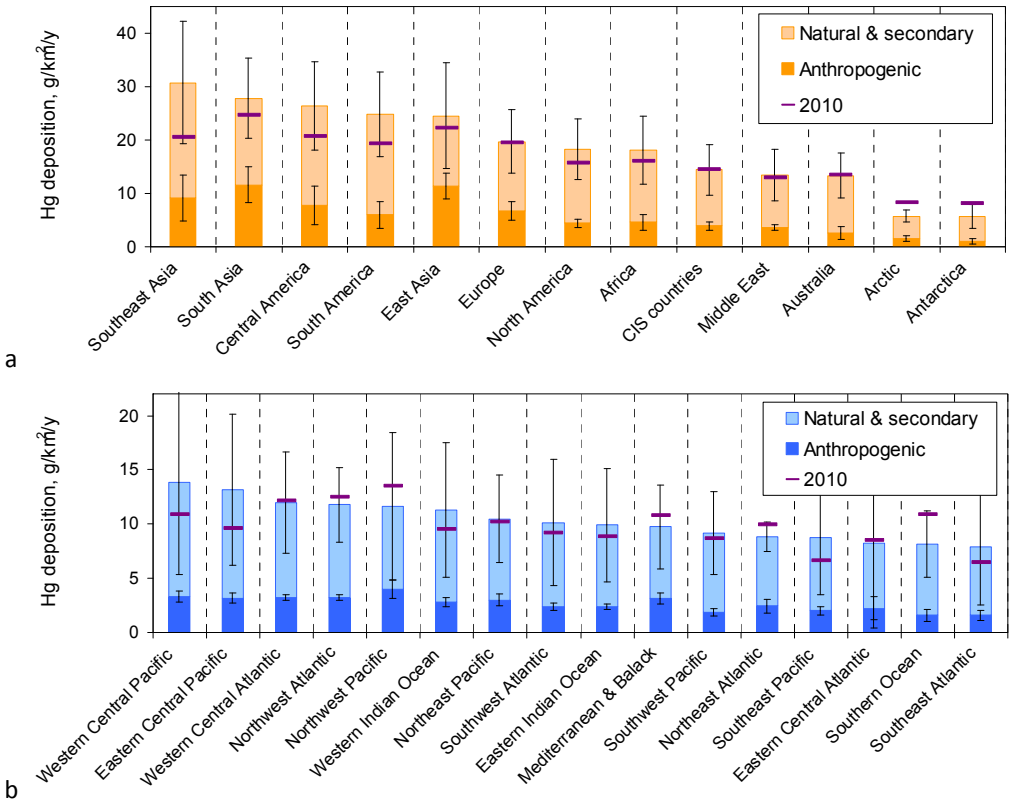

Fig. 3.4. *Total Hg deposition fluxes and the relative contributions of direct anthropogenic and natural and secondary sources to various terrestrial (a) and aquatic (b) receptor regions in 2015. Whiskers show the standard deviation of individual models for direct anthropogenic and natural/secondary sources, respectively.*

Figure 3.5 illustrates the source apportionment of Hg deposition from direct anthropogenic sources to various receptor regions. The direct anthropogenic emissions represent the mixture of domestic emissions and atmospherically transported Hg from sources located in other regions (foreign emissions). The share of foreign sources varies from 100% in Antarctic to 23% in East Asia. The largest foreign contributors are East Asia, Africa, South America, and Southeast Asia, with their contributions ranging between 10-34%, 4-24%, 3-23%, 3-11%, respectively, to various receptor regions. The largest foreign contributors are characterized by large anthropogenic emissions as well

as active ASGM, which contributes to the global transport via Hg^0 emissions. The smallest foreign contributors are the Middle East (< 2%), Australia (< 1%), and the Polar Regions (< 1%), which are characterized by the lowest anthropogenic emissions.

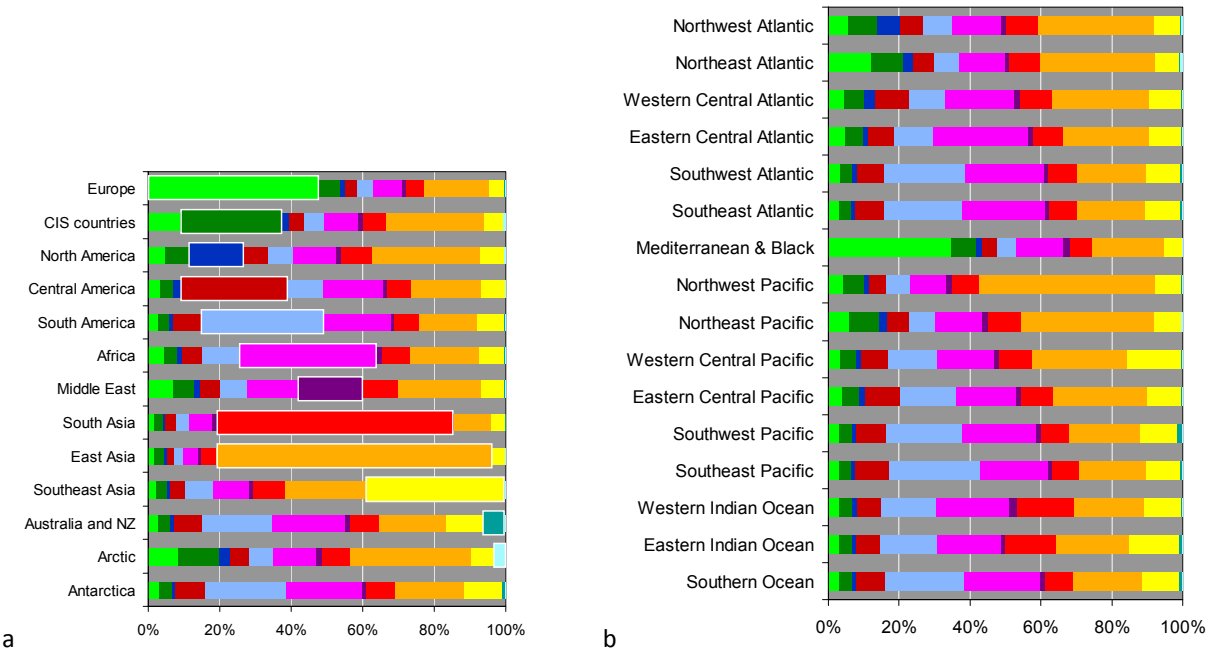

Fig. 3.5. *Model ensemble median source apportionment of Hg deposition from direct anthropogenic emissions to various terrestrial (a) and aquatic regions (b) in 2015. The colors depict source regions, which are consistent with Fig. 3.1.*

As illustrated in Figure 3.5, the share of domestic sources to various receptor regions is ranked in the order of East Asia (77%), South Asia (66%), Europe (48%), Southeast Asia (39%), Africa (38%), South America (34%), Central America (30%), CIS countries (28%), Middle East (18%), North America (15%), Australia and New Zealand (6%), Arctic (3%), and Antarctica (0%). In East and South Asia, anthropogenic Hg deposition is dominated by the contribution from domestic sources. This is due to the significant domestic anthropogenic emissions mainly from the industrial and power sectors, which emit a substantial fraction of oxidized Hg. Both domestic and foreign anthropogenic sources contribute almost equally to the total anthropogenic Hg deposition in Europe. The largest foreign contributors are ranked in the order of East Asia (18%), Africa (8%), CIS countries (6%), and South Asia (5%). Regions with active ASGM (Africa, South and Central America) also receive a relatively large fraction of anthropogenic deposition from domestic sources as well as from East Asia. Significant foreign contributors to the North American anthropogenic deposition are ranked in the order of East Asia (31%), Africa (12%), South Asia (8%), and Southeast Asia (7%). Remote regions including the Arctic and Antarctic are predominantly influenced by the long-range transport of atmospheric Hg from East Asia and Africa.

Figure 3.5 also illustrates the source apportionment of Hg deposition from direct anthropogenic sources to various ocean regions. East Asia and Africa is the largest contributors to the global ocean reservoirs, owing to their large anthropogenic emissions. The contributions from East Asia and Africa to various ocean regions range between 20-50% and 11-27%, respectively. Northwest (50%) and Northeast Pacific (38%) receive the largest contribution from the East Asian anthropogenic

emissions. Eastern Central (27%), Southeast (23%), and Southwest Atlantic (22%) receive the largest contribution from the African anthropogenic emissions. The only exceptions are the Mediterranean and Black Sea, where the contribution from the European anthropogenic emissions (20%) dominates over East Asian, African, and the South American anthropogenic emissions. A number of the ocean regions—particularly the Northwest Pacific-- receive high anthropogenic Hg deposition and demonstrate a large total capture fisheries production [*AMAP/UNEP*, 2015]. The lowest contributors to the global ocean reservoirs are the Arctic (< 2%) and Australia (< 1%), which are characterized by the lowest anthropogenic emissions.

The four global transport models were also applied for simulation of Hg deposition from different anthropogenic emissions sectors. For this purpose all the sectors of anthropogenic emissions were aggregated into four general groups: (i) power generation, (ii) industrial sources, (iii) intentional use and product waste, and (iv) ASGM. Total emissions from these four sector groups amount to 347 t/y, 874 t/y, 166 t/y and 838 t/y, respectively. Chemical speciation of Hg emissions differs considerably between different sector groups (Fig. 3.6). According to the applied inventory, emissions from power generation consist of approximately equal contributions of elemental Hg (GEM) and oxidized forms ($Hg(II)_{gas}$, $Hg(II)_{part}$). The proportion of oxidized Hg is much smaller in emissions from industrial sources (20%). One fourth of total emissions from intentional use and product waste is emitted in the oxidised forms. It is expected that Hg emitted from ASGM in elemental gaseous form. It should be noted that available estimates of Hg emissions speciation are associated with significant uncertainties.

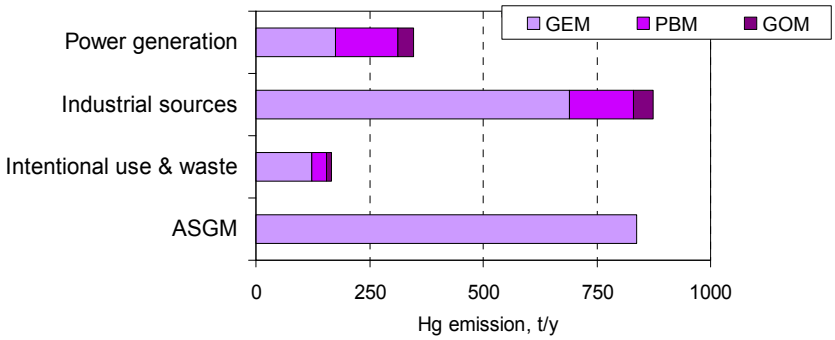

Fig. 3.6. *Chemical speciation of Hg emissions from the four groups of emission sectors*

The model simulated Hg deposition from the four emission sectors are shown in Fig. 3.7. Mercury deposition from the power generation group are largely restricted by a number of industrial regions in East and South Asia, Europe, North America, and South Africa, where the majority of large stationary combustion sources are located (Fig. 3.7a). Mercury deposition flux from power generation in these regions exceeds 2.5 g/km^2/y, whereas in other regions it falls below 1.4 g/km^2/y. The relatively short distance of Hg dispersion from this sector group is caused by substantial proportion of oxidized Hg in emissions. Emissions from the industrial sectors group are more widely distributed over the world and contain a substantial fraction of GEM (80%). Therefore, significant deposition (above 2.5 g/km^2/y) from industrial sources covers wide areas in Asia, Europe, North and South America, and Africa (Fig. 3.7b). Besides, in South and East Asia deposition from this sector group exceeds 5 and 10 g/km^2/y, respectively. The impact of the intentional use and product waste group of sectors is also mostly related to major industrial regions but its contribution is considerably

lower and commonly does not exceed 1.4 g/km^2/y except for South and East Asia (Fig. 3.7c). The majority of ASGM emission sources are located in low latitudes of the both Hemispheres. Mercury emissions from this sector in the elemental form are transported globally (Fig. 3.7d), however, most significant deposition fluxes (above 2.5 g/km^2/y) occur closer to emission sources and largely impact South America, equatorial Africa, East and Southeast Asia.

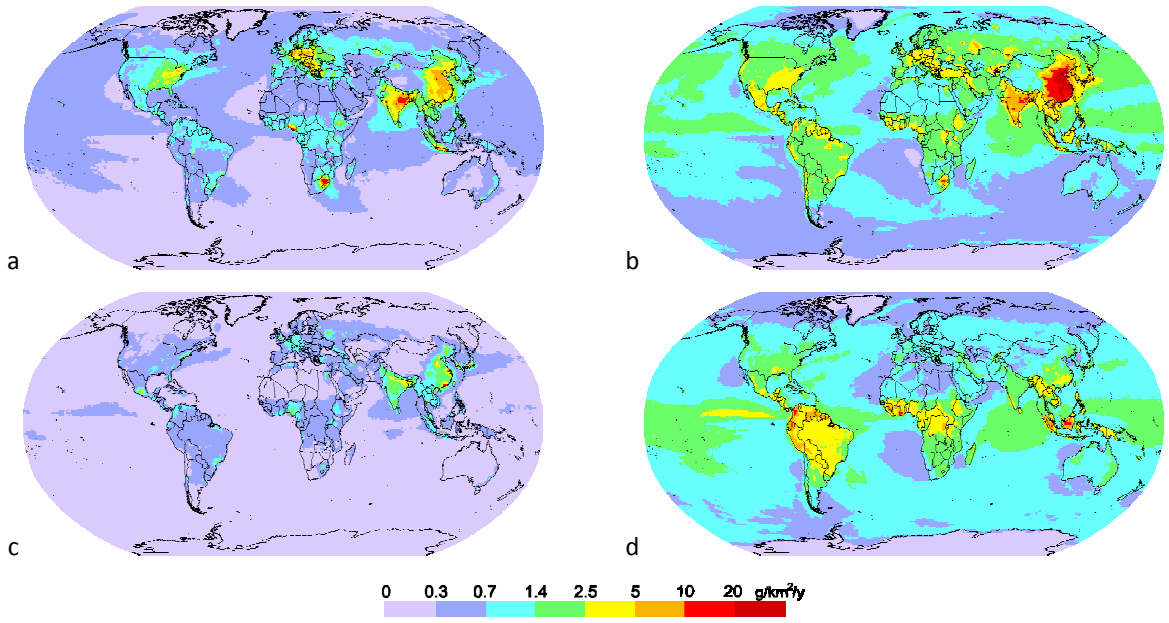

Fig. 3.7. *Global distribution Hg deposition (model ensemble median) from the four groups of emission sectors in 2015: (a) – Power generation; (b) – Industrial sources; (c) – Intentional use and product waste; (d) – ASGM.*

The multi-model assessment of Hg atmospheric dispersion and source apportionment on a global scale provides valuable information for evaluation of Hg pollution levels in the EMEP countries and improves co-operation with the UN Environment and with the Minamata Convention.

3.2. Mercury atmospheric chemistry: Testing the Br oxidation mechanism

Atmospheric chemistry plays an important role in the Hg long-range transport in the atmosphere and deposition to various ecosystems. In particular, it controls Hg transformations between the long-lived elemental gaseous form (Hg^0) and short-lived oxidized forms (Hg^{II}) that can exist both in gaseous and particulate phases. However, the nature of particular chemical reactions leading to these transformations as well as identity and phase of the products remain uncertain [*Subir et al*., 2011; 2012; *Gustin et al*., 2015; *Ariya et al*., 2015].

Numerous chemical transport models used for simulations of Hg cycling in the atmosphere during the past two decades considered Hg^0 reaction with ozone (O_3) and hydroxyl radical (OH) as the main Hg oxidation pathways in the free troposphere and demonstrated good agreement of modelling results with observations [e.g. *Christensen et al*., 2004; *Pan et al*., 2010; *Baker et al*., 2012; *Kos et al*., 2013; *Gencarelli et al*., 2014; *De Simone et al*., 2015; *Cohen et al*., 2016]. This chemical mechanism is

also included to the current EMEP operational model for Hg (GLEMOS) [*Travnikov*, 2005; *Travnikov and Ilyin*, 2009; *Travnikov et al*., 2009]. However, more recent theoretical and observational studies show that Hg^0 reactions with gaseous halogens, in particular atomic bromine (Br), should be important or even dominant pathway of Hg oxidation in the atmosphere [*Donohoue et al*., 2006; *Hynes et al*., 2009; *Goodsite et al*., 2012; *Gratz et al*., 2015; *Coburn et al*., 2016]. Besides, use of a simplified version of the Br oxidation mechanism in a chemical transport models allowed reproduction of realistic Hg levels in the atmosphere [*Holmes et al*., 2010; *Soerensen et al*., 2010; *Amos et al*., 2012]. However, since then a number of recent studies have provided some new insight into the Hg oxidation chemistry involving Br [*Dibble et al.,* 2012; 2013, 2014*; Wang et al*., 2014; *Jiao and Dibble,* 2015; 2017].

We evaluate possibility of implementation of the Br-initiated chemistry for the operational Hg modelling within EMEP. As a first step we incorporated the Br oxidation mechanism in its most recent form [*Horowitz et al*., 2017] into the GLEMOS model and performed a number of tests comparing the modelling results with observations. An experimental version the model considers five Hg chemical species in the atmosphere: Hg^0 and four Hg^{II} species ($HgBr_2$, HgBrOH, $HgBrHO_2$, $HgBrNO_2$). The oxidised species Hg^{II} are simulated both in gaseous and particulate forms using the parameterisation of gas-particle partitioning from [*Amos et al.*, 2012]. A two-step mechanism of Hg^0 oxidation by atomic Br in gas phase is the following [*Horowitz et al*., 2017]:

$$Hg^0 + X + M \rightarrow Hg^I X + M \quad \text{(R1)}$$

$$Hg^I X + M \rightarrow Hg^0 + X + M \quad \text{(R2)}$$

$$Hg^I X + Y \rightarrow Hg^0 + XY \quad \text{(R3)}$$

$$Hg^I X + Y + M \rightarrow Hg^{II} XY + M, \quad \text{(R4-R7)}$$

where X ≡ Br is the first-step Hg^0 oxidant; Y ≡ Br, OH, HO_2, NO_2 are the second-step reactants leading to reduction or further oxidation of Hg^I; and M denotes molecules of air. The reaction rate constants are given in Table 3.1. Six-hourly concentration fields of Br were archived from a GEOS-Chem simulation [*Parrella et al.,* 2012], whereas OH, HO_2, NO_2 and particulate matter (PM2.5) fields were imported from MOZART [*Emmons et al*., 2010]. We performed simulations for the period 2007-2013 using anthropogenic emissions for 2010 [*AMAP/UNEP*, 2013]. The first 6 years of the period were used for the model spin up to achieve the steady-state Hg concentrations in the troposphere. The model results are presented as annual averages for 2013.

Table 3.1. *Experimental chemical mechanism for atmospheric Hg in GLEMOS*

N	Reaction	Rate, molecule cm^{-3} s^{-1}	Reference
R1	$Hg^0 + Br + M \rightarrow HgBr + M$	1.5×10^{-32} $(T/298)^{-1.86}$ $[Hg^0][Br][M]$[(a)]	*Donohoue et al*. [2006]
R2	$HgBr + M \rightarrow Hg^0 + Br + M$	1.6×10^{-9} exp(-7801/T) [HgBr][M]	*Dibble et al*. [2012]
R3	$HgBr + Br \rightarrow Hg^0 + Br_2$	3.9×10^{-11} [HgBr][Br]	*Balabanov et al*. [2005]
R4	$HgBr + Br \xrightarrow{M} HgBr_2$	2.5×10^{-10} $(T/298)^{-0.57}$ [HgBr][Br]	*Goodsite et al.* [2004]
R5	$HgBr + OH \xrightarrow{M} HgBrOH$	2.5×10^{-10} $(T/298)^{-0.57}$ [HgBr][OH]	*Goodsite et al*. [2004]
R6	$HgBr + HO_2 \xrightarrow{M} HgBrHO_2$	$k_{HO2}([M],T)[HgBr][HO_2]$	*Jiao and Dibble* [2017]
R7	$HgBr + NO_2 \xrightarrow{M} HgBrNO_2$	$k_{NO2}([M],T)[HgBr][NO_2]$	*Jiao and Dibble* [2017]

[(a)] All concentrations in brackets are in molecule cm^{-3}; [M] is the number density of air

Figure 3.8 shows simulated global distributions of Hg^0 surface concentration and Hg wet deposition as well as their comparison with observations. A collection of data on Hg^0 air concentrations and Hg wet deposition fluxes measured at various regional and global monitoring networks in 2013 involved in the study are described in [*Travnikov et al.*, 2017]. Generally, the spatial patterns are similar to those obtained with the O_3/OH chemical mechanism [*Travnikov et al.*, 2009]. The concentration pattern demonstrates the well documented south-to-north increasing gradient and elevated concentrations in East and South Asia (Fig. 3.8a). The wet deposition pattern also shows relatively high levels over the industrial regions, in areas with intensive precipitation and over the Southern ocean, where intensive Hg oxidation takes place (Fig. 3.8b). It should be pointed out that the modelling results significantly underestimate measured Hg^0 concentrations, particularly, in remote regions of the Southern Hemisphere, where the effect of the atmospheric chemistry is the most pronounced. This is not the case for simulated wet deposition fluxes, which are comparable with the observed ones. The reasons for this contradiction are discussed below.

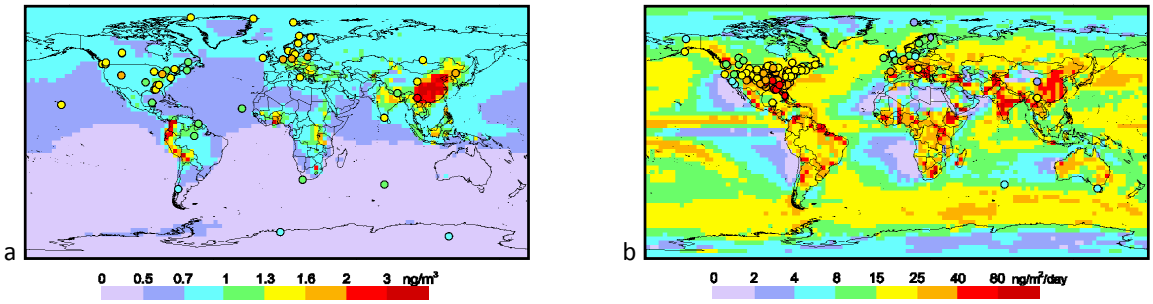

Fig. 3.8. *Spatial distributions of simulated Hg^0 surface concentration (a) and Hg wet deposition (b) in 2013. Circles show observed values in the same colour scale.*

More detailed evaluation of the modelling results against observations is illustrated in Fig. 3.9. As seen the model underestimates the observed values by 40% on average (Fig. 3.9a). The underprediction is stronger for low concentrations typical for remote regions. A few elevated values are relatively well reproduced by the model. These values relate to sites located in East Asia, which are characterised by direct effect of anthropogenic emissions. In contrast, the simulated wet deposition does not underestimate or in some cases even overestimates the measurements (Fig. 3.9a). This imbalance between too low simulated Hg^0 concentration and high wet deposition can be explained by too strong *in situ* oxidation of Hg^0 and production of Hg^{II} in the atmosphere. Indeed, if biased low Hg^0 air concentration can be additionally explained by uncertainties in emissions of this species (anthropogenic, natural or secondary), Hg wet deposition is largely formed by scavenging of Hg^{II}, which is mostly originated from Hg^0 oxidation in remote regions. So hypothetical increase of Hg emissions would shift both measured characteristics upward leading to overestimation of wet deposition. ***Thus, the analysis shows that the current mechanism of Hg^0 oxidation by atomic Br taken alone leads to too strong Hg oxidation in the atmosphere, which does not agree with available measurements.***

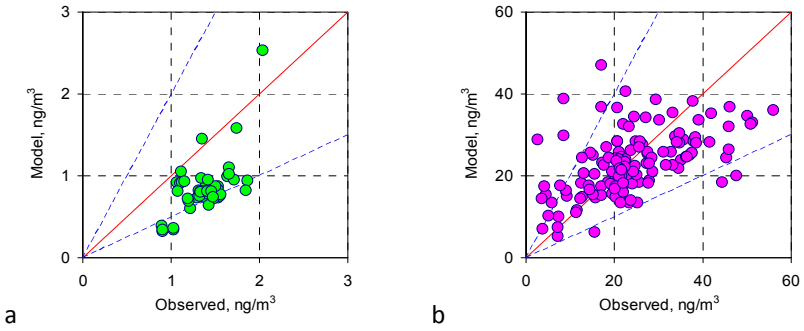

Fig. 3.9. *Comparison of simulated Hg^0 air concentration (a) and Hg wet deposition (b) with measurements in 2013.*

Some more insight to the oxidation process can be obtained from analysis of the Hg chemical budget in the atmosphere (Fig. 3.10). The simulated global atmospheric reservoir of Hg^0 is about 1600 Mg that is significantly lower than previously estimated 4000 Mg for the total atmosphere [e.g. *Travnikov et al.*, 2009; *Holmes et al.*, 2010] or 3500 Mg for the troposphere [*Horowitz et al.*, 2017].The gas-phase oxidation by atomic Br leads to transformation of 4850 Mg/y of Hg^0 to a short-lived intermediate HgBr. It corresponds to the chemical lifetime 3.9 months of Hg^0 against oxidation to HgBr. The unstable HgBr decomposes back to Hg^0 or reacts further with various atmospheric compounds (e.g. Br, OH, HO_2, NO_2) to form Hg^{II}. Decomposition of HgBr reduces 870 Mg/y of Hg^I to the elemental form. The simulated Hg^{II} species are dominated by $HgBrNO_2$, which contributes 67% of total atmospheric oxidized Hg. The second largest Hg^{II} species is $HgBrHO_2$ (20%), which is followed by $HgBr_2$ (8%) and HgBrOH (4%). Appropriate production rates vary from 20 Mg/y for HgBrOH to 2800 Mg/y for $HgBrNO_2$. So the net oxidation of Hg^0 to Hg^{II} depends on both the first-step Hg^0 reaction with Br and on the balance between decomposition and further oxidation of the HgBr intermediate.

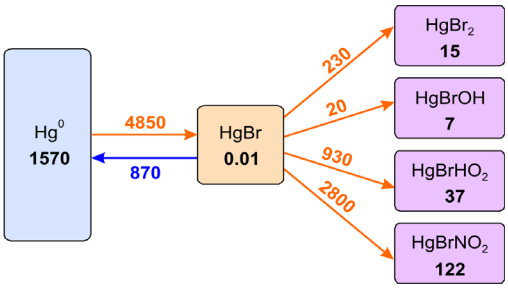

Fig. 3.10. *Global simulated budget of Hg chemical transformations in the atmosphere. The mass estimates are in Mg of Hg, the fluxes are in Mg of Hg per year.*

Figure 3.11 shows the simulated latitudinal and vertical distribution of annual zonal mean Hg^0 air concentration (standard temperature and pressure) in the atmosphere. As seen the surface concentration of Hg^0 is above 0.7 ng/m^3 in the Northern Hemisphere and drops steeply south of the equator. In the vertical, the concentration moderately decreases in the troposphere down to 0.1 ng/m^3 at the tropopause. The latitudinal pattern of Hg^0 concentration is determined by both distribution of emissions, which are mostly located in the Northern Hemisphere, and the oxidation chemistry. The figure also shows distribution of the annual mean Hg^0 oxidation rate (isolines) in reaction with Br (R1, Table 3.1). The rate depends on concentration of Br as well as on the ambient parameters such as air temperature and density. The Hg^0 oxidation has a minimum in the free troposphere over the equator due to elevated air temperatures, and two maximums – in the upper troposphere and over in the surface air of the temperate latitudes of the Southern Hemisphere – due to high concentration of Br. These extremes are reflected in the spatial pattern of Hg^0 by increased concentrations over the equator and low concentrations over the Southern Ocean.

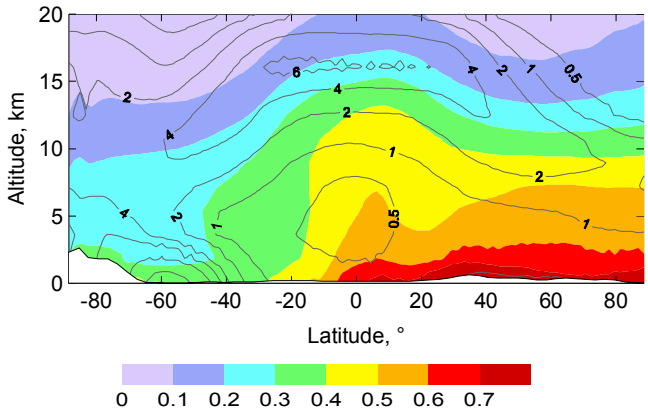

Fig. 3.11. *Annual zonal mean air concentration of Hg^0 in 2013 (colour palette, ng/m^3 STP) and rates of Hg^0 oxidation by Br (isolines, 10^6 s^{-1}) according to reaction R1 from Table 3.1.*

Formation of the Hg^{II} species is illustrated in Fig. 3.12. The figure shows distribution of average mixing ratios of $HgBr_2$, HgBrOH, $HgBrHO_2$, and $HgBrNO_2$ in the atmosphere along with production rates of these species in appropriate reactions (R4-R7, Table 3.1). The reaction rates depend on production of HgBr, concentration of appropriate oxidants (Br, OH, HO_2, NO_2), and air temperature. The dominant Hg^{II} species $HgBrNO_2$ is largely produced in the upper troposphere and next to the surface in the high latitudes of the Southern Hemisphere (Fig. 3.12d). However, intensive dry and wet deposition quickly removes this species from the surface air. In contrast, Hg^{II} produced in the upper troposphere has longer residence time that leads to its accumulation and high concentrations aloft. The second important Hg^{II} species is $HgBrHO_2$ is intensively produced at high latitudes of the Northern and Southern Hemispheres (Fig. 3.12c). These regions are also characterized by relatively high concentrations of the species in the free troposphere. Both $HgBr_2$ and HgBrOH have maximums of production rates in the upper troposphere of the tropics and near the surface at high latitudes of the Southern Hemisphere, where elevated concentrations of these species occur (Fig. 3.12a and 3.12b). There are also increased concentrations over the surface at temperate latitudes of the Northern Hemisphere, which are caused by direct anthropogenic emissions. All Hg^{II} species have small concentrations in the low troposphere of the tropics due to reduced production of HgBr in this area and high air temperature, which is damping its further oxidation to Hg^{II}.

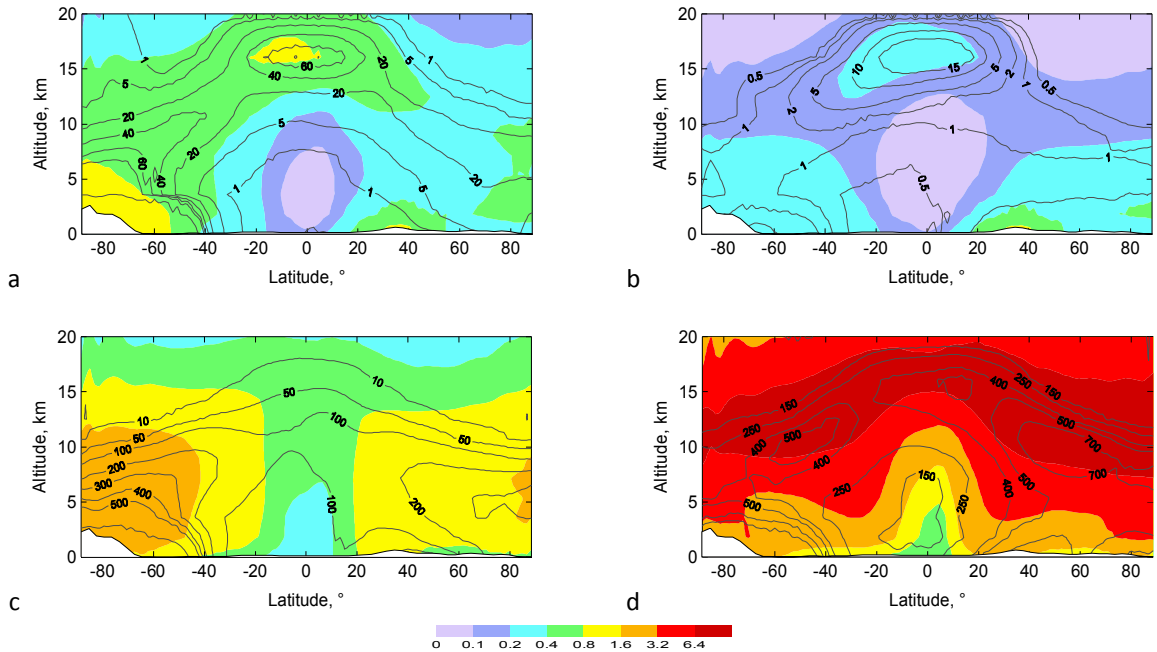

Fig. 3.12. *Annual zonal mean volume mixing ratios (colour palette, ppqv Hg) of $HgBr_2$ (a), HgBrOH (b), $HgBrHO_2$ (c), $HgBrNO_2$ (d) in 2013. Isolines show production rates (10^3 molecules cm^{-3} s^{-1}) for appropriate Hg species according to reactions R4-R7 from Table 3.1.*

Thus, use of the Br-initiated mechanism for simulations of Hg atmospheric cycle leads to strong overestimation of Hg oxidation and unrealistically low Hg^0 concentrations in the atmosphere. However, theoretical studies point out at possibility of Hg^{II} reduction mechanisms, which could take place in air, cloud water, or heterogeneously at the surface of atmospheric aerosol [*Ariya et al.*, 2015]. Besides, a number of modelling studies have successfully applied the Br oxidation mechanism along with a hypothetical reduction mechanism to reproduce observed concentrations [*Shah et al.*, 2016; *Horowitz et al.,* 2017]. But it should be noted that both nature and chemical details of the reduction reaction remain unknown. ***The next steps of implementation of the Br oxidation chemistry for the EMEP operational modelling will include evaluation of possible Hg reduction mechanisms in the atmosphere. Update and refinement of the model Hg chemical scheme should improve quality of assessment of Hg pollution of the EMEP countries.***

Chapter 4. COUNTRY-SCALE POLLUTION ASSESSMENT (POLAND)

A series of country-scale studies of heavy metal pollution in the EMEP countries has been carried out by MSC-E for long period in close co-operation with national experts [*Travnikov et al*., 2018]. This year a case study for Poland has been completed and the results of the study have been published in a special Technical Report [*Ilyin et al*., 2018]. Main results of the study are briefly discussed below.

4.1. Heavy metal pollution levels in Poland

The country-specific study for Poland was aimed at analysis of factors affecting Cd pollution levels in the country and providing the country with detailed information on Cd pollution. Assessment of Cd pollution involved emission data prepared by national experts and CEIP, measurement data from the EMEP and national monitoring networks, and atmospheric transport modelling performed by MSC-E. Results were produced with fine spatial resolution (0.1°x0.1°) and related to 2014. The work was carried out in cooperation with national experts from Poland and the Czech Republic. Detailed information about results of the study is available in [*Ilyin et al*., 2018].

Evaluation of the modelling results shows that at most stations the modelled and observed Cd air concentrations are comparable in the warm period. However, in the cold period the model underestimates the observed levels. A number of reasons of the underestimation were considered. It was found out that the main reason was low Cd emissions in the cold period from the emission sector 'Residential combustion'.

In order to improve quality of the assessment and to identify country's regions, where the emission estimates require further refinement, an emission scenario has been developed. Original national total emission of Cd in Poland is 14 t/y. For comparison, total national emission prescribed by the scenario is 17 t/y (26% higher). However, this value is within the uncertainty of annual national emissions estimated by national experts at about 70% [*Dębski et al*., 2017]. The scenario emissions of Cd from the 'Residential combustion' sector are higher than the value in the national emission data by a factor 2.6 (5.7 vs. 2.2 t/y). However, the changes vary among the country's provinces. The most substantial increase of Cd emission is noted for the southern and south-western part of Poland (Fig. 4.1).

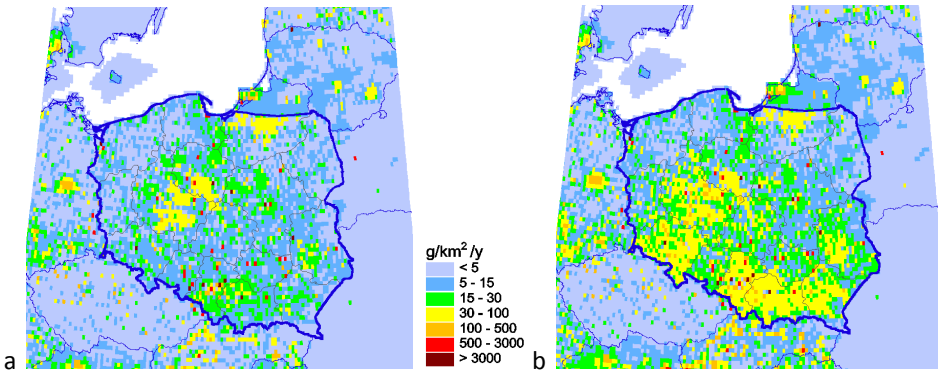

Fig. 4.1. *Original (a) and scenario (b) emissions of Cd in Poland in 2014*

The suggested emission scenario favoured significant improvement of modelling results when compared with observed levels both at Polish monitoring stations and the stations located outside the country. In particular, the comparison between modelled and measured Cd concentrations in air at the EMEP and national monitoring stations in Poland and the Czech Republic demonstrated the increase of the mean relative bias from -24% to -4% in cold period, and the increase of the spatial correlation coefficient form 0.79 to 0.83.

Thus, ***the study demonstrates that available emission data may contain significant uncertainties, which affect results of pollution assessment. Use of emission scenarios or expert (non-official) emission estimates can produce more realistic, from the viewpoint of agreement with observed values, alternative results of the assessment.*** However, this activity requires close cooperation with national experts and relevant EMEP centres and Task Forces.

Country-specific information on Cd pollution levels in Poland prepared within the study includes spatial distributions of pollution levels with fine resolution, source-receptor relationships for particular country's provinces (voevodships), pollution from various emission sectors and large point sources as well as information on pollution levels in large cities. The assessment is based on emissions data prescribed by the emission scenario.

For the country as a whole the major contributor to Cd deposition is the sector 'Industry', which makes up 43% of total anthropogenic deposition in Poland (Fig. 4.2). The second largest contributor is 'Residential Combustion' (29%). Other sectors contribute around 5% in sum, and contribution of foreign sources is about 20%.

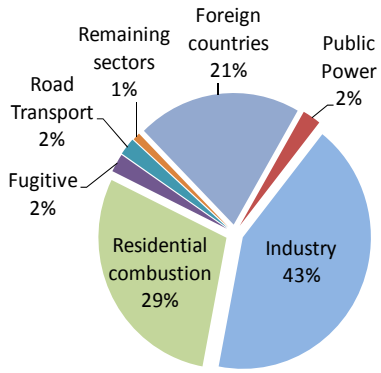

Fig. 4.2. *Contribution of the major emission sectors to deposition from anthropogenic sources in Poland*

However, the shares of emission sectors vary in the provinces of the country. In four voivodships (Opolskie, Slaskie, Malopolskie, Swietokrzyskie) the contribution of the 'Industry' sector to anthropogenic deposition exceeds 50% (Fig. 4.3). The largest contribution of 'Residential combustion' is noted for the western part of the country: Wielkopolskie (40%), Lubuskie (40%), Dolnoslaskie (36%) voivodships. The contribution of emissions from the sector 'Fugitive' is the highest in the northern and central parts: Pomorskie (8%), Mazowieckie (8%) and Kujawsko-Pomorskie (7%) voivodships. The share of the sectors 'Public Power' and 'Road Transport' varies from 2% to 4% throughout the country.

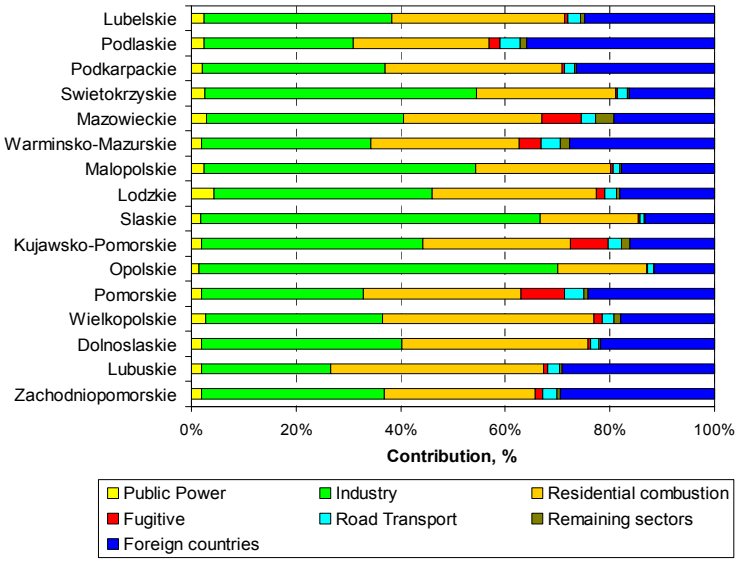

Fig. 4.3. *Contributions of main national emission sectors and foreign sources to deposition in Polish voivodships in 2014*

4.2. City pollution by heavy metals

Most of population in Europe lives in urban areas. Investigation of pollution levels in cities is currently one of priority tasks of the Convention. MSC-E has started preparatory work on evaluation of heavy metal pollution levels in cities of the EMEP region. Primary attempt to evaluate pollution levels in urban areas is carried out in the framework of country-specific case study for Poland. In this study Cd pollution levels and their seasonal variations in the selected Polish cities are analysed.

Cities can be considered as a source of pollution for ambient atmosphere as well as a receptor of pollution which comes from sources located in other parts of the country or in other countries. There are numerous studies [e.g., *Kiesewetter et al*., 2015; *Elser et al*., 2016; *Kiesewetter and Amann*, 2014] focused on differentiation of pollution levels in cities between several components such as contributions from intercontinental transport, transboundary transport, national sources and sources located in a city. The latter is called urban increment, i.e. contribution of city sources to pollution levels in the city.

The urban increment of heavy metal pollution was calculated for Polish cities by means of source-receptor calculations with fine spatial resolution (0.1°x0.1°). For this purpose, anthropogenic emissions of Cd in gridcells of the model domain, which belong to the cities, are marked as city sources. Therefore, emissions from particular cities and emissions from other territory of Poland are distinguished in national polish emission data. As a result, for each selected city contribution of the city's sources and contribution of other anthropogenic sources (national and foreign) are calculated. Similar approach is used also by other researches [e.g. *Thunis et al*., 2016, *Guo et al*., 2016]. In this study contribution of urban sources was assessed for 23 Polish cities (Fig. 4.4).

Although the model has not been designed to simulate urban-scale pollution levels, the calculated concentrations reasonably agree with the observed values. The model successfully reproduces spatial pattern (correlation coefficient 0.71) and magnitude (relative bias -8%) of the observed

concentrations of Cd measured at urban locations (Fig. 4.5). In 60% of stations the difference between modelled and observed values lies within a factor of 2. At some stations the model underestimates the observed levels, and in one city – overestimates by more than a factor of 2. These discrepancies could be caused by both uncertainties of emissions in cities and uncertainties of model parameterizations which do not take fully into account peculiarities of dispersion of pollution levels over urban territories. As seen, at most of the stations the main contribution to pollution levels is made by anthropogenic emissions. Seasonal variability of the observed concentrations was also reproduced by the model.

Fig. 4.4. *Location of the selected Polish cities*

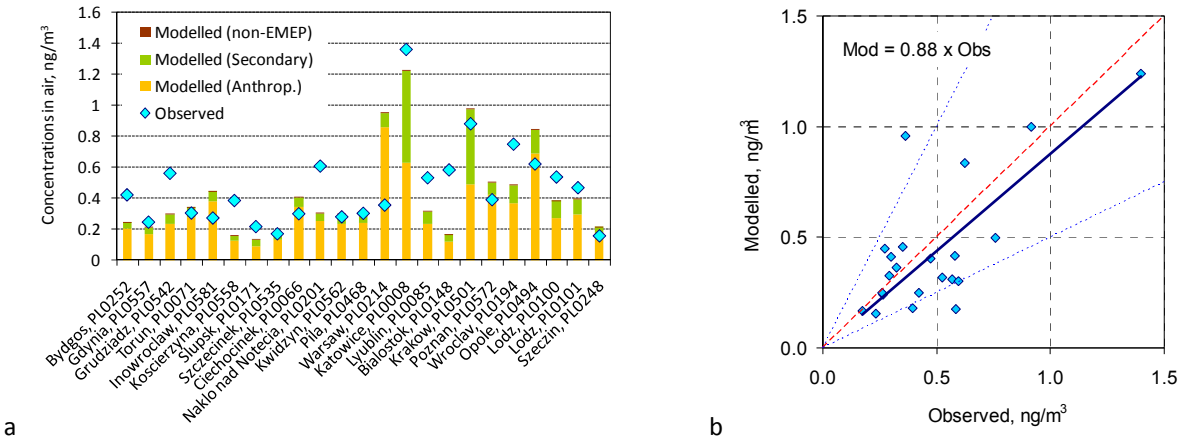

Fig. 4.5. *Annual mean modelled and observed concentrations of Cd at urban background stations in selected Polish cities depicted as bar charts for particular stations (a) and as scatter plot (b). Red dashed line in (b) indicates 1:1 ratio, and dashed blue lines indicate a two-fold difference between modelled and observed values.*

Calculated annual mean concentrations of Cd in air caused by contribution of anthropogenic sources located outside city area (external sources) and city sources (urban increment) to annual mean air concentrations of Cd are shown in Fig. 4.6 for various Polish cities. In large cities such as Warsaw, Krakow, Gdansk, Katowice, Poznan the city sources contribute significant faction (20–70%) of anthropogenic concentrations. In other considered cities the urban increment is relatively small making up from 1-2% to about 10-15%.

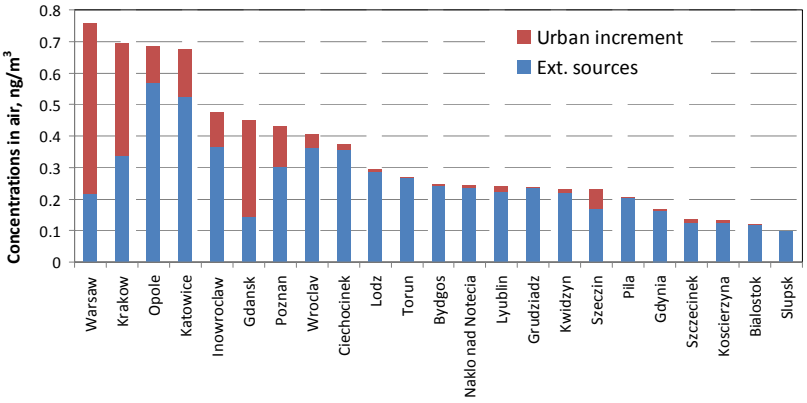

Fig. 4.6. *Calculated concentrations of Cd in air caused by anthropogenic sources outside city (external) and by city sources (urban increment).*

Verification of these results is hampered by very limited information. Therefore, information on PM2.5 and PM10 contributions from urban sources is also taken into account, because their emission sources and atmospheric behaviour resembles those of Cd. Detailed modelling study of PM pollution levels in Warsaw is presented in [*Holnicki et al*., 2017a]. It is shown that contribution of city emission sources is dominating and ranging from 62% to 70% for PM2.5 and from 76% to 78% for PM10. Besides, analysis of population-weighted exposure demonstrated that contribution of local sources of PM2.5, PM10 and Cd amounted to about 50%, 40% and 90%, respectively [*Holnicki et al*., 2017b]. In work [*Pastuszka et al*., 2009] it was shown that wintertime concentrations of Cd on fine particles (PM2.5) in the center of the Zabrze city (Upper Silesia) is about 60% higher than the concentrations at the urban background level. For Cd on coarse particles (PM10) the difference is 90%. Urban increments of PM10 during short-term episodes in cities Krakow, Zabrze, Jelenia Gora and Warsaw, calculated on the base of observed values at regional background and traffic stations, varies from about 20% to 60% [*Reizer and Juda-Rezler*, 2016]. These values of the urban increment are comparable with the values obtained in the current study.

Evaluation of model-based urban increments for large cities in Europe, including Poland, was carried out using the SHERPA tool [*Thunis et al*., 2017]. Contribution of intercontinental and transboundary transport of PM2.5 as well as external and internal emissions of Polish cities was considered.

Results of the comparison of the urban increments estimated by the SHERPA tool and calculated in this study are presented in Fig. 4.7. Since two different pollutants are considered, fractions of urban increment are compared instead of absolute values of the concentrations. For large cities (Warsaw, Katowice, Krakow, Poznan, Gdansk, Szeczin) the fractions of concentrations caused by city sources of Cd are comparable with

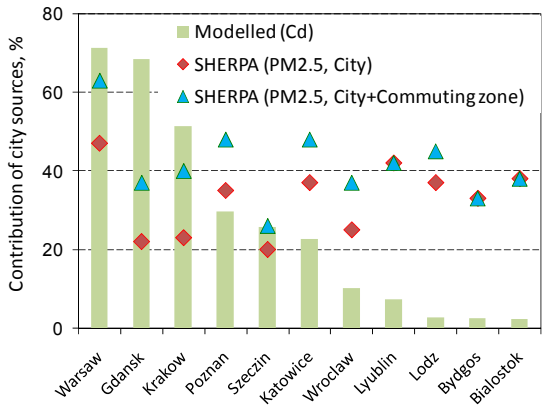

Fig. 4.7. *Contribution of city sources to mean annual cadmium air concentrations (this study) and PM2.5 derived from the results of SHERPA project*

those of PM2.5. For some cities the difference between the results of the current and SHERPA studies is significant. For example, the urban increment of Cd concentrations for cities Lodz, Lyublin, Bydgos and Bialostok vary from 2 to 7%, while the increment of PM2.5 is 30-45%. This discrepancy can be caused by differences between spatial distributions of Cd and PM emissions. Besides, the calculations of urban increments are based on different models – GLEMOS in this study and CHIMERE [*Menut et al*., 2014] in SHERPA study. Differences in the model formulations also give rise to discrepancies in final results. Nevertheless, in spite of the mentioned reasons, values of the urban increments based on this study and the SHERPA tool are comparable by the order of magnitude for most of considered cities.

An alternative way to estimate the urban increment is based on comparison of measured concentrations in a city and at rural station located near the city [*Lenschow et al*., 2001]. This approach was used for evaluation of seasonal variability of urban increments of Cd air concentrations in cities of north-western Poland located nearby (within 100-km distance) rural station PL0077A (Fig. 4.8). Besides, for comparison purposes similar analysis was performed for concentrations of PM10 measured at the same stations.

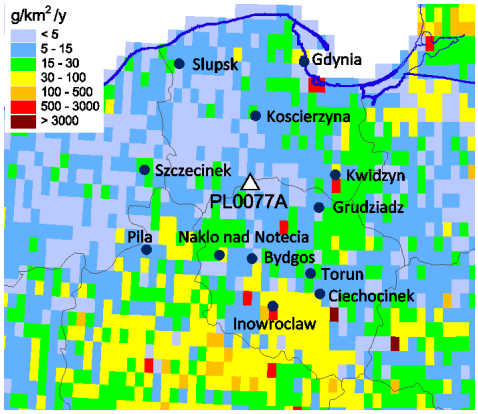

Fig. 4.8. *Emission flux of Cd with resolution 0.1°x0.1° and location of regional background (white triangle) and urban-background (dark circles) measurement stations.*

Seasonal variability of monthly mean modelled and measurement-based urban increments are compared (Fig. 4.9). Since the absolute magnitudes of the Cd and PM10 increments differ significantly, they were normalized by the corresponding maximum monthly-mean values. Observed seasonal changes of the normalized urban increments of Cd are well reproduced by the model at a number of stations, for example, at Bydgos, Ciechocinek, Naklo nad Notecia, Koscierzyna and Kwidzyn. At these stations minimum of the urban increment is noted for warm period, while the maximum – for cold period. Similar seasonal behaviour is also exhibited by urban increment of PM10 concentrations. At the same time, at other stations (e.g., Grudziadz) no distinct seasonal variability of modelled urban increment is noted, while the increments based on observations undergo seasonal changes.

The obtained discrepancies in seasonal changes of the modelled and measured increments may be caused by uncertainties/inconsistencies in emission data. For instance, seasonal variability of Cd concentrations is significantly affected by emissions from the sector 'Residential combustion'. Emissions from this sector are much higher in cold period and smaller in warm period. However, for some cities where the measurement stations are located, emission values from this sector in the corresponding grid cells are minor or even absent in the used emissions inventory (Fig. 4.10).

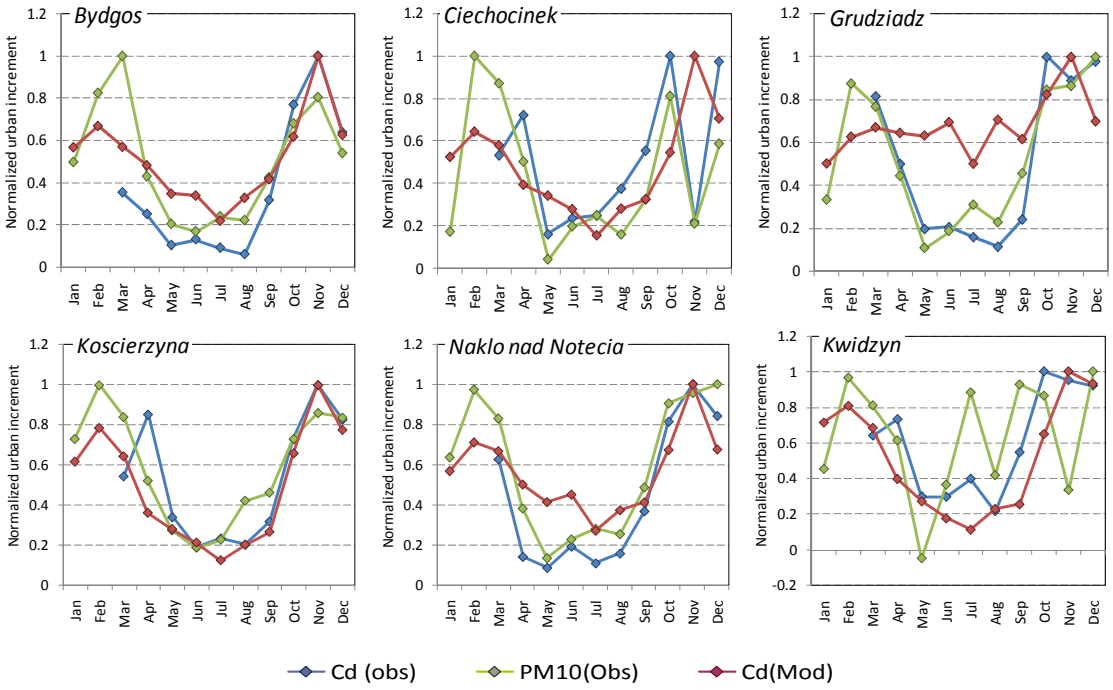

Fig. 4.9. *Seasonal changes of normalized Cd urban increments obtained on the base of modelling results as well as Cd and PM10 urban increments derived from measurements*

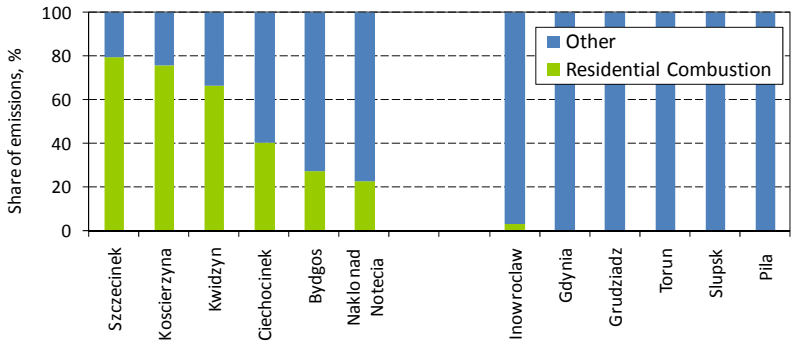

Fig. 4.10. *Fractions of emissions from residential combustion and sum of other sectors in grid cells where cities are located. Left part of the bar chart: stations where seasonal variability of urban increment reproduced; right part: stations where seasonal variability of urban increment not reproduced by the model.*

Thus, the suggested method of direct fine resolution modelling allows matching modelled and observed air concentrations of Cd in Polish cities with sufficient quality. Comparison of the urban increments calculated in the current study with results of other studies, based on modelling or observations, revealed reasonable agreement of the applied methods for large cities. As a rule, larger cities are characterized by higher contribution of emissions from urban sources to Cd and PM pollution compared to smaller cities. At the same time, contribution of sources located outside urban areas is substantial even in large cities.

5. COOPERATION AND DISSEMINATION OF INFORMATION

Co-operation is an important component of research and operational pollution assessment performed by MSC-E to support countries with information on heavy metal pollution levels in Europe and other regions. In this context MSC-E closely collaborates with Parties to the Convention and its Subsidiary Bodies and exchanges information with various international organizations.

5.1. Subsidiary bodies of the Convention

Co-operation with Subsidiary bodies of the Convention includes collaborative work with the Task Force on Measurements and Modelling (TFMM), the Task Force on Emissions Inventories and Projections (TFEIP), and the Working Group on Effects (WGE).

5.1.1. Task Force on Measurements and Modelling

MSC-E continued cooperation with TFMM. The Centre took part in the TFMM meeting held in May, 2018 in Geneva, Switzerland. TFMM participants were informed about the results of the country-specific case study of Cd pollution in Poland. Besides, the main outcomes of the case study activities gained during past years were overviewed.

It was shown that the main reason of the discrepancies between modelled and observed Cd levels in Poland was underestimation of emissions from the sector 'Residential combustion' (Section 4.1). It was demonstrated that the model could be used as a tool to evaluate national emission data and help to understand the directions to improve the emissions in cooperation with national experts and relevant Task Forces and EMEP Centres. Besides, it was suggested to use emission scenarios or expert estimates to produce an alternative assessment of pollution levels along with the assessments based on official data.

One of thematic session of the recent TFMM meeting was focused on the long range transport and urban air pollution. MSC-E presented results on evaluation of Cd pollution levels in cities of Poland (Section 4.2). In particular, source apportionment of Cd air concentrations in the cities and their seasonal variations were investigated. The results of the study were compared with available data on urban increments for particulate matter.

Plans of further country-specific activities were discussed. Further possible candidates to the study were proposed including Germany and the United Kingdom. In addition, cooperation of the Centre with WGE in the field of evaluation of Hg atmospheric inputs to surface water bodies and catchment areas of Scandinavia is expected.

5.1.2. Task Force on Emission Inventories and Projections

Emissions data are the key information required for pollution assessment. The basic information on anthropogenic emissions is provided by Parties to the Convention and processed by CEIP with methodological support and quality assurance by the Task Force on Emission Inventories and Projections (TFEIP). The EMEP modelling Centres utilize emissions data for pollution assessment and gather important bottom-up information on quality of the data. To contribute to the improvement of emissions data MSC-E participated in the recent Workshop on verification of emission estimates organized back-to-back with the annual TFEIP meeting in April 2018 in Sofia, Bulgaria.

MSC-E presented its approach to preparation of additional emission parameters required for modelling, which include sector-specific seasonal variation, vertical distribution and chemical composition of heavy metal and POP emissions (see Section 1.2 for details). Besides the Centre provided examples of the model application for evaluation of quality and revealing of potential uncertainties of emissions data. The presented analysis was performed in the framework of country-scale case studies for Poland and Spain. In particular, it was shown that data on Cd emissions from 'Residential Combustion' (Section 4.1) and B(a)P emissions from 'Field burning in agriculture' can contain significant uncertainties in Poland and Spain, respectively.

Formulating recommendations for the emissions community the Centre noted that ***information on the chemical composition of Hg and POP emissions required update and refinement, which could be done in co-operation with other international bodies (e.g. UN Environment, Minamata and Stockholm Conventions). Besides, the model evaluation of national emissions can be applied on a regular basis as a part of the emissions review process. It is particularly relevant on a country scale, where variety of national data can be involved.***

5.1.3. Working Group on Effects

In the framework of co-operation with WGE MSC-E took part in the 31th Task Force meeting of the International Cooperative Programme on Effects of Air Pollution on Natural Vegetation and Crops (ICP-Vegetation) held in Dessau, Germany. Under supervision of ICP-Vegetation surveys of concentrations of heavy metals in mosses are carried out. The most recent survey took place in 2015. Information on Pb, Cd and Hg concentrations in moss was provided to MSC-E.

Information about concentrations in mosses is useful for evaluation of the atmospheric modelling results. Mosses have no roots and obtain their nutrients from the atmosphere. Hence, concentrations of pollutants in moss tissues depend on atmospheric deposition. Unlike regular station-based measurements carried out at the EMEP monitoring network, measurements in mosses are characterized by higher spatial density. Besides, these measurements are often organized in countries where EMEP network is scarce, e.g. in the EECCA countries and Russia (Fig. 5.1).

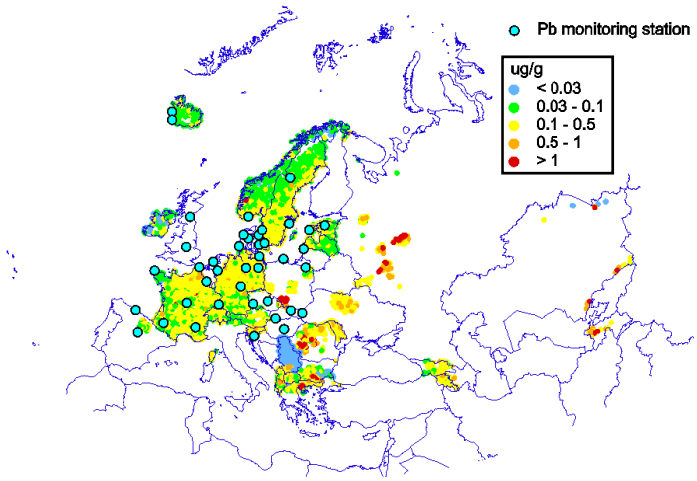

Fig. 5.1. *Concentrations of Cd in mosses in 2015 and location of the EMEP heavy metal monitoring stations.*

Heavy metal concentrations in mosses cannot be compared directly with modelled deposition. However, spatial distributions and long-term trends of concentrations in mosses and total deposition can be compared. For example, spatial pattern of concentrations in mosses is similar to that of total deposition of Cd in the Scandinavia region (Fig. 5.2). Both fields demonstrate higher levels in the southern part and lower levels in the northern part of the region. Spatial correlation between two fields is significant (0.64). In the whole region, the correlation between the modelled deposition and concentration in mosses exceeds 0.5 in 6 countries for Pb, and in 5 countries for Cd.

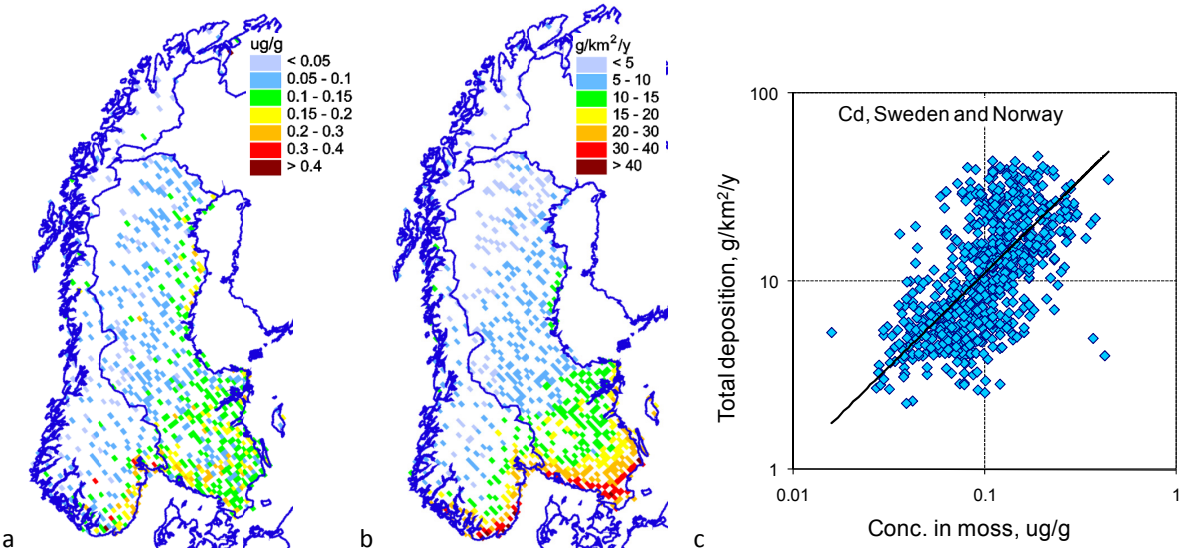

Fig. 5.2. *Cd concentrations in mosses (a), deposition flux (b), and comparison of both parameters (c) for Scandinavia in 2015.*

Comparison of normalized country-averaged deposition and concentrations in mosses demonstrates that spatial gradients of Pb and Cd pollution levels between the countries were generally reproduced by the model. Relatively high concentrations in mosses and total deposition of Pb and Cd are noted for Poland, Slovenia, Armenia, Georgia, and the Czech Republic (Fig. 5.3). Relatively low levels occur in Ireland, Iceland, Estonia, Latvia, and Norway. This comparison allows identifying regions where difference between the considered normalized parameters is substantial. For example, concentrations in mosses of Pb is high compared to mean deposition fluxes in Bulgaria. On other

hand, deposition of Pb in Slovakia is much higher than concentrations in mosses. These discrepancies may be caused by uncertainties of emission data used in the modelling or approaches of measurements in mosses, and need additional research.

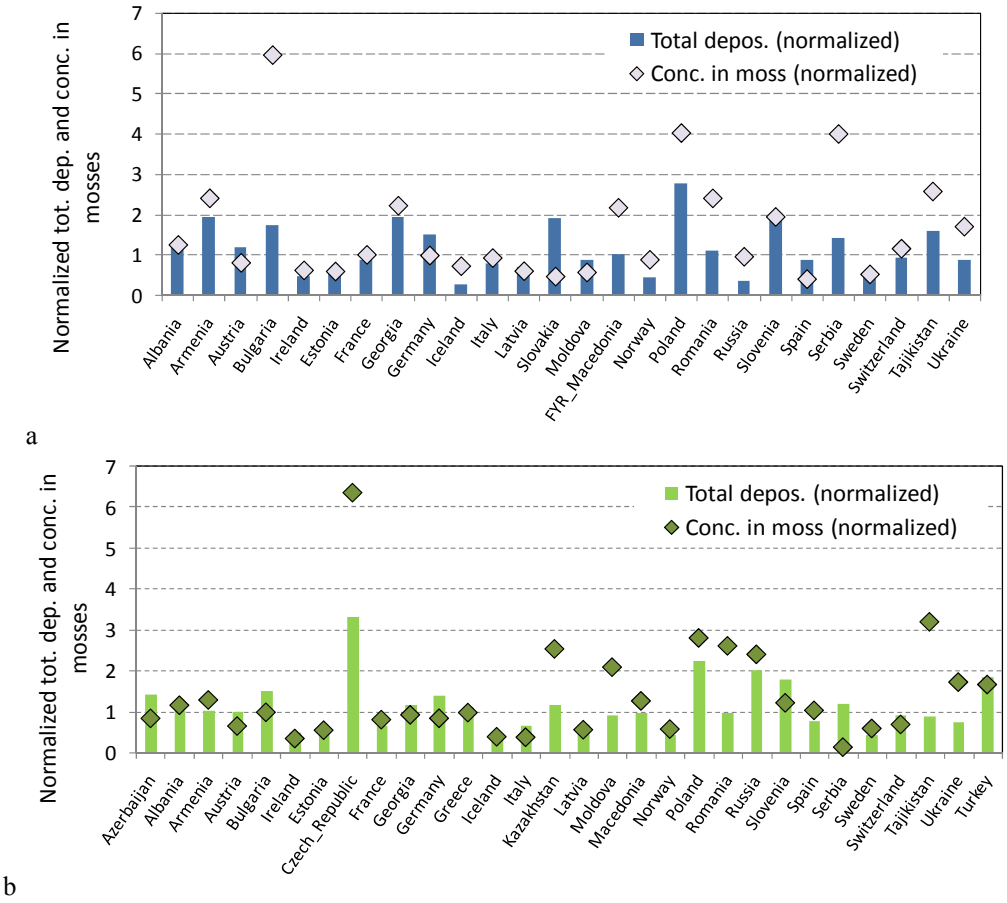

Fig. 5.3. *Normalized country-averaged total deposition and concentrations in mosses of Pb (a) and Cd (b) in 2015.*

Long-term changes of heavy metal deposition during the period 1990-2015 were compared with the changes of concentration in mosses. Relative reduction of Pb deposition over the period varies within 80-90%, which is comparable with the corresponding reduction of concentrations in mosses (Fig. 5.4a). For Cd the reduction is somewhat lower: 30-70% for concentrations in mosses and 25-70% for total deposition (Fig. 5.4b). Relative reduction of both Hg deposition and concentration in mosses is 4-40% over the period 1995-2015.

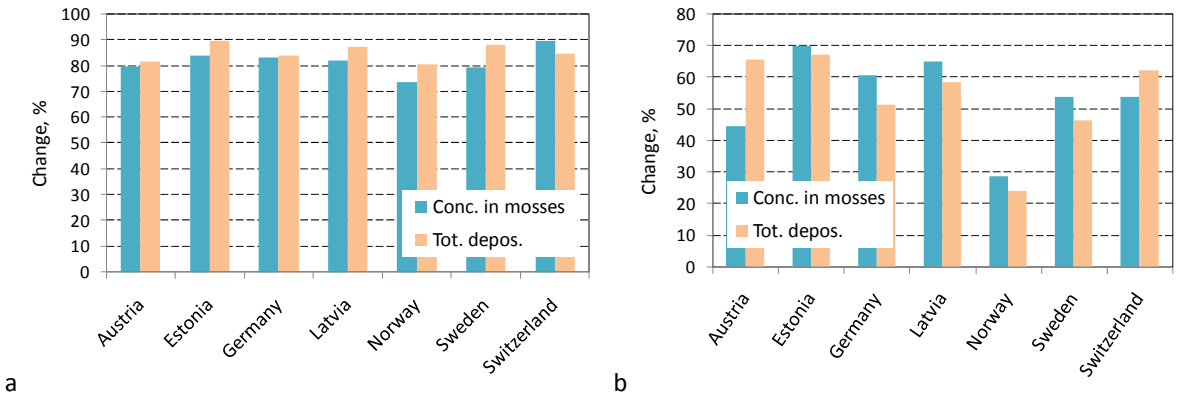

Fig. 5.4. *Relative change [(1990-2015)/1990 x 100%] of country-averaged concentrations in mosses and total deposition of Pb (a) and Cd (b) over the period 1990-2015.*

Measurement data on concentrations of heavy metals in mosses is valuable type of information for the analysis of heavy metal pollution in the EMEP region and for the evaluation of the model performance. Comparison of country-averaged values of the concentrations and deposition demonstrates that the model capable of reproducing spatial gradients and long-term pollution changes. However, comparison of deposition and levels in mosses at smaller spatial scales reveals higher discrepancies in spatial patterns of these two parameters. Most likely it is explained by the fact that concentrations in mosses depend not only on atmospheric deposition but on a number of other environmental factors. Further research of these factors is needed in cooperation with the experts of WGE for improvement of interpretation of the biomonitoring results as well as for the model evaluation.

5.2. International organizations

5.2.1. UN Environment and Minamata Convention

MSC-E continuously co-operates with the United Nations Environment Programme (UN Environment) on assessment of Hg pollution. Mercury is a global pollutant that causes growing public concern about the dangerous effects on human health and biota. To support the international negotiation process aimed at Hg pollution reduction UN Environment coordinated preparation of a series of Global Mercury Assessments (GMA) [*UNEP*, 2002; *AMAP/UNEP*, 2008; *AMAP/UNEP*, 2013; *AMAP/UNEP*, 2015]. MSC-E has been involved in all the assessments sharing information on Hg pollution and coordinating activities on global scale modelling.

Currently, MSC-E takes part in the new Global Mercury Assessment 2018 (GMA 2018). The Centre is responsible for the part of GMA 2018 focused on assessment of Hg fate and transport in the atmosphere and coordinates activities of international group of experts on modelling of Hg pollution on global and regional scales. The expert group includes modelling teams from different scientific institutions of Europe and North America: Helmholtz-Zentrum Geesthacht (HZG, Germany), Institute of Atmospheric Pollution Research (CNR-IIA, Italy), Massachusetts Institute of Technology (MIT, USA), Environment and Climate Change Canada (ECCC, Canada), National Oceanic and Atmospheric Administration (NOAA, USA), and Lamar University (LU, USA). The work consists of both review of recent studies on model assessment of Hg pollution and new model estimates of Hg intercontinental transport involving an updated global inventory of Hg anthropogenic emissions. The major results of the multi-model assessment of Hg pollution on a global scale are summarized in Section 2.1 of the current report. The MSC-E co-ordination work for GMA 2018 is funded by the Arctic Monitoring and Assessment Programme (AMAP) as a part of a bi-lateral contract.

In addition, MSC-E participated in the first meeting of the Conference of the Parties to the Minamata Convention on Mercury (COP1) held in September 2017 in Geneva, Switzerland. MSC-E contributed to discussions at the thematic session focused on various aspects of atmospheric Hg pollution. In

particular, approaches used within CLRTAP to assess Hg atmospheric pollution in the EMEP region were overviewed including evaluation of national emissions by countries, assessment of pollution levels by means of monitoring and modelling, and evaluation of the effects on human health and biota. The experience gained within CLRTAP in the field of assessment and abatement of Hg pollution could be shared with the Minamata Convention. Further collaboration between these two Conventions is appreciated.

Co-operation with UN Environment and the Minamata Convention broaden dissemination of scientific and policy oriented information generated within the Convention. Besides, it improves pollution assessment within EMEP by possibility to evaluate and refine the modelling tools and involve variety of additional input data (emission inventories and observations).

5.2.2. Helsinki Commission

MSC-E performs regular evaluation of airborne pollution load of heavy metals to the Baltic Sea in the framework of cooperation with the Helsinki Commission. This work is carried out in accordance with the Memorandum of Understanding between the Baltic Marine Environment Protection Commission (HELCOM) and the United Nations Economic Commission for Europe (UN ECE) and is based on the long-term EMEP/HELCOM contract.

This year activity was focused on the evaluation of Pb, Cd and Hg pollution of the Baltic Sea. In particular, long-term variations of heavy metal deposition fluxes to the Baltic Sea were estimated for the period 1990-2015. Source apportionment of deposition and verification of modelling results against measurements was performed for 2015. Results of the assessment are summarized in the Joint report of the EMEP Centres for HELCOM [*Bartnicki et al*., 2017] and also presented in several indicator fact sheets, published on the HELCOM website [*http://www.helcom.fi*].

Declines of Pb, Cd and Hg anthropogenic emissions in the HELCOM countries from 1990 to 2015 were 87%, 40% and 46%, respectively. Poland, Russia and Germany were the major contributors to heavy metal emissions among the HELCOM countries in 2015. Their share to total emission of the HELCOM countries exceeded 90%.

Analysis of the results of the model simulations revealed significant decrease of atmospheric deposition of Cd, Pb, and Hg to the Baltic Sea over the period 1990-2015. The largest decease is noted for deposition of Pb (80%), followed by Cd (63%) and Hg (34%) (Fig. 5.5a). The decrease of deposition varies substantially among different sub-basins of the Baltic Sea. The largest decrease of Cd deposition occurred in the Bothnian Bay and the Gulf of Finland (76% and 74%, respectively). The most significant changes of Hg deposition took place in the Sound and the Kattegat (60% and 41%). In case of Pb the largest changes of deposition were estimated for the Bothnian Bay and the Gulf of Finland (86% and 85%). The decrease of heavy metal deposition was stronger in the first decade of the considered period, while after 2000 it became smaller or almost levelled off.

Deposition of Pb, Cd and Hg to the Baltic Sea in 2015 was lower than those in 2014. In particular, Pb deposition decreased by 33%, Cd deposition by 39%, and Hg deposition by 12%. These changes can

be explained by the influence of inter-annual variability of meteorological conditions, in particular, the atmospheric transport pathways.

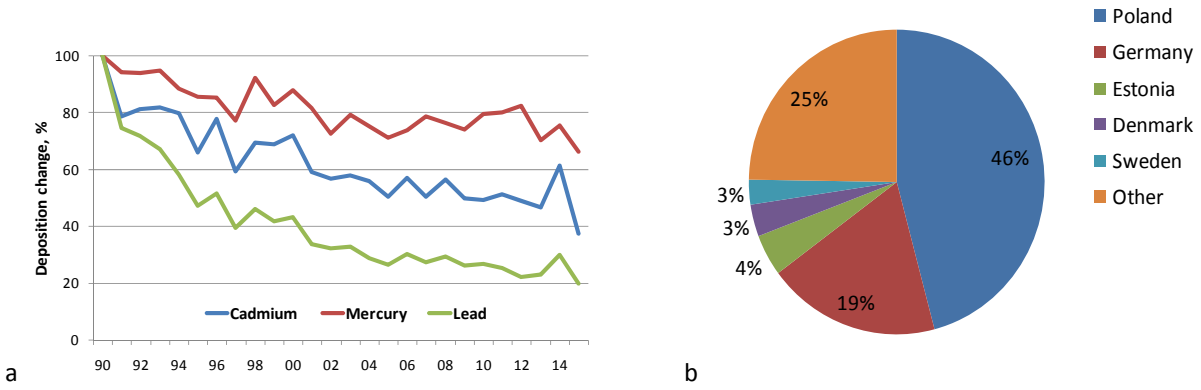

Fig. 5.5. *Relative changes of annual atmospheric deposition of Cd, Pb, and Hg to the Baltic Sea in the period 1990-2015 (a) and contribution of emission sources from the EMEP countries to total anthropogenic deposition of Pb to the Baltic Sea in 2015 (b)*

Model calculations revealed distinct spatial gradients of atmospheric deposition fluxes to the Baltic Sea in 2015 [*Bartnicki et al*., 2017]. Higher deposition levels took place in the southern and western parts of the sea, while the northern part is characterised by the lowest fluxes.

Anthropogenic emission sources of the HELCOM countries contributed about 36%, 30%, and 14% to annual deposition of Cd, Pb, and Hg, respectively, over the Baltic Sea in 2015. Among the HELCOM countries Poland, Russia, and Germany are the main contributors of anthropogenic deposition to the Baltic Sea (Fig. 5.5b). Along with anthropogenic emissions significant contribution (more than 50%) to heavy metal deposition to the Baltic Sea was made by wind re-suspension (Cd and Pb), natural emission and re-emission (Hg) as well as by long-term transport from sources located outside the HELCOM countries.

MAIN CHALLENGES AND DIRECTIONS OF FUTURE RESEARCH

The Status Report summarizes EMEP activities in the field of heavy metal pollution assessment in 2018. It includes information on spatial patterns of Pb, Cd and Hg pollution levels and transboundary transport, research and development activities on improvement of the modelling tool, cooperation with national experts of the EMEP countries, CLRTAP Subsidiary Bodies, and international organizations. Main challenges of heavy metal pollution assessment and directions of future research are overviewed below.

- Emissions data reported by countries still contain significant uncertainties, particularly, in terms of completeness and sectoral composition. The dispersion modelling supplemented by monitoring data can be used as an independent tool for evaluation of reported emissions. The evaluation is particularly relevant when performed on a country scale with involvement of detailed national data. Besides, the model evaluation of national emissions can be applied on a regular basis as a part of the emissions review process.

- The country-scale case studies demonstrated high effectiveness in evaluation of various aspects of heavy metal pollution. They provide valuable information on pollution assessment with fine spatial resolution, detailed source apportionment of pollution levels, evaluation of national emissions etc. The studies will be continued for a number of countries (e.g. Germany, the UK, Norway) with particular focus on Hg pollution and the link with adverse effects on human health and biota.

- The problem of the limited coverage of the EMEP region with measurements of heavy metals remains unresolved. Monitoring sites, which perform heavy metal measurements, are mostly located in Central, Western, and Northern Europe, whereas observations in Eastern Europe and Central Asia are scarce. The problem can be partly resolved by involvement of data from other networks or using data of biomonitoring (e.g. measurements in mosses). However, the latter require thorough interpretation when used for model evaluation.

- Recent studies revealed possible important role of vegetation uptake for Hg atmospheric cycle and deposition. Further improvement of understanding of Hg deposition processes and development of model parameterization require more measurements of Hg air-vegetation exchange that could be reflected in the revised EMEP monitoring strategy.

- Mercury pollution of the EMEP countries attracts particular attention within the Convention. Therefore, update and improvement of modelling approaches for Hg pollution assessment is among the priority tasks. The Hg chemical scheme of the GLEMOS model will be revised including further testing of the Br oxidation mechanism and evaluation of possible reduction pathways. Besides, evaluation of Hg pollution over long periods requires consideration of cycling and accumulation in different environmental media. The multi-media approach for Hg simulations in GLEMOS will be further developed.

- Another important issue of human exposure to airborne contaminants is pollution of cities. A tentative approach of assessment of the city pollution by heavy metals using the direct fine

resolution modelling with source apportionment demonstrated promising performance when compared with urban observations and other assessment methods. Thorough testing and evaluation of the approach will be continued for other countries and pollutants.

- Evaluation of adverse effects of heavy metal pollution on human health and ecosystems is of high importance. Long-term co-operation between EMEP and WGE led to successful application of the critical loads approach for risk assessment of heavy metal pollution within the EMEP region. However, the estimates of critical load exeedances for heavy metals are outdated. Additional efforts on development of the effect assessment are needed (e.g. for Hg pollution of aquatic ecosystems) in close co-operation between the monitoring, modelling and effect communities.

References

Aas W, Nizzetto P.B. and Breivik K. [2018]. Heavy metals and POP measurements 2016, Norwegian Institute for Air Research. EMEP/CCC-Report 3/2018

AMAP/UNEP [2008] Technical Background Report to the Global Mercury Assessment. Arctic Monitoring and Assessment Programme / UNEP Chemicals Branch. 159 pp. http://www.unep.org/chemicalsandwaste/LinkClick.aspx?fileticket=gwLbyNhGtn8%3d&tabid=3593&language=en-US. Accessed on June 28, 2016.

AMAP/UNEP [2013] Technical Background Report for the Global Mercury Assessment 2013a. Arctic Monitoring and Assessment Programme, Oslo, Norway / UNEP Chemicals Branch, Geneva, Switzerland, vi + 263 pp., available at: http://www.amap.no/documents/download/1265 (last access: 10 April 2018).

AMAP/UNEP [2015] Global Mercury Modelling: Update of Modelling Results in the Global Mercury Assessment 2013. Arctic Monitoring and Assessment Programme, Oslo, Norway/UNEP Chemicals Branch, Geneva, Switzerland. iv + 32 pp.

AMAP/UNEP [2018] Technical Background Report for the Global Mercury Assessment 2018, in press.

Amos H.M., Jacob D.J., Holmes C.D., Fisher J.A., Wang Q., Yantosca R.M., Corbitt E.S., Galarneau E., Rutter A.P., Gustin M.S., Steffen A., Schauer J.J., Graydon J.A., Louis V.L.St., Talbot R.W., Edgerton E.S., Zhang Y., and Sunderland E.M. [2012] Gas-particle partitioning of atmospheric Hg(II) and its effect on global mercury deposition, *Atmos. Chem. Phys*., 12, 591–603, doi:10.5194/acp-12-591-2012.

Angot H., Dastoor A., De Simone F., Gårdfeldt K., Gencarelli C.N., Hedgecock I.M., Langer S., Magand O., Mastromonaco M.N., Nordstrøm C., Pfaffhuber K.A., Pirrone N., Ryjkov A., Selin N.E., Skov H., Song S., Sprovieri F., Steffen A., Toyota K., Travnikov O., Yang X., and Dommergue A. [2016] Chemical cycling and deposition of atmospheric mercury in polar regions: review of recent measurements and comparison with models, *Atmos. Chem. Phys*., 16, 10735-10763, doi:10.5194/acp-16-10735-2016.

Ariya P.A., Amyot M., Dastoor A., Deeds D., Feinberg A., Kos G., Poulain A., Ryjkov A., Semeniuk K., Subir M. & Toyota K. [2015] Mercury Physicochemical and Biogeochemical Transformation in the Atmosphere and at Atmospheric Interfaces: A Review and Future Directions, Chemical Reviews 115(10), 3760-3802.

Baker K.R. and Bash J.O. [2012] Regional Scale Photochemical Model Evaluation of Total Mercury Wet Deposition and Speciated Ambient Mercury, *Atmos. Environ*., 49, 151–162.

Balabanov N., Shepler B., Peterson K. [2005] Accurate global potential energy surface and reaction dynamics for the ground state of HgBr2, *J. Phys. Chem*. A, 109, 8765—8773.

Bartnicki J., A. Gusev, W. Aas, M. Gauss and J. E. Jonson [2017] *Atmospheric Supply of* Nitrogen, Cadmium, Mercury, Lead, and PCDD/Fs to the Baltic Sea in 2015 Summary Report for HELCOM MSC-W, Technical Report 2/2017.

Bieser J., Aulinger A., Matthias V., Quante M., and Builtjes P. [2011]. SMOKE for Europe – adaptation, modification and evaluation of a comprehensive emission model for Europe. *Geosci. Model Dev.,* 4, 47–68.

Bieser J., Slemr F., Ambrose J., Brenninkmeijer C., Brooks S., Dastoor A., DeSimone F., Ebinghaus R., Gencarelli C.N., Geyer B., Gratz L.E., Hedgecock I.M., Jaffe D., Kelley P., Lin C.-J., Jaegle L., Matthias V., Ryjkov A., Selin N.E., Song S., Travnikov O., Weigelt A., Luke W., Ren X., Zahn A., Yang X., Zhu Y., and Pirrone N. [2017] Multi-model study of mercury dispersion in the atmosphere: vertical and interhemispheric distribution of mercury species, *Atmos. Chem. Phys*., 17, 6925-6955, doi: 10.5194/acp-17-6925-2017.

CCC [2018]. EMEP laboratory intercomparison. EMEP35. https://www.nilu.no/projects/ccc/intercomparison/index.html. Accessed in 27.06.2018.

Christensen J.H., Brandt J., Frohn L.M. and Skov H. [2004] Modelling of Mercury in the Arctic with the Danish Eulerian Hemispheric Model, *Atmos. Chem. Phys*., 4, 2251–2257, doi:10.5194/acp-4-2251-2004.

Coburn S., B. Dix, E. Edgerton, C. D Holmes, D. Kinnison, Q. Liang, A. Ter Schure, S. Wang, and R. Volkamer [2016] Mercury oxidation from bromine chemistry in the free troposphere over the southeastern US, *Atmospheric Chemistry and Physics*, 16(6), 3743–3760, doi:10.5194/acp-16-3743-2016.

Cohen M.D., Draxler R.R., Artz R.S., Gustin M., Han Y.-J., Holsen T.M., Jaffe D., Kelley P., Lei H., Loughner C., Luke W., Lyman S., Niemi D. Pacyna J.M., Pilote M., Poissant L., Ratte D., Ren X., Steenhouisen F., Tordon R. and Wilson S. [2016] Modelling the global atmospheric transport and deposition of mercury to the Great Lakes, Elementa: Science of the Anthropocene, 4, 000118, doi:10.12952journal.elementa.999118, 2016.

De Simone F., Cinnirella S., Gencarelli C.N., Yang X., Hedgecock I.M., and Pirrone N. [2015] Model study of global mercury deposition from biomass burning, *Environ. Sci. Technol*., 49, 6712–6721.

De Vries W, Groenenberg J.E. and Posch M. [2015b]. Mass balance approaches to assess critical loads and target loads of metals for terrestrial and aquatic ecosystems. pp. 207-222. In: Critical loads and dynamic risk assessments. Nitrogen, acidity in terrestrial and aquatic ecosystems. Edited by W. de Vries, J-P. Hettelingh and M. Posch. *Envitornmental pollution* 25, Springer.

De Vries W., Posch M., Sverdrup H.U., Larssen T., de Wet H.A., Bobbink R. and Hettelingh J-P. [2015a]. Geochemical indicators for use in the computation of critical loads and dynamic risk assessment. pp 15-58. In: Critical loads and dynamic risk assessments. Nitrogen, acidity in terrestrial and aquatic ecosystems. Edited by W. de Vries, J-P. Hettelingh and M. Posch. *Envitornmental pollution* 25, Springer.

De Wit H.A., Hettelingh J-P., and Harmens H. [2015]. Trends in ecosystem and health responses to long-range transported atmospheric pollutants. Norwegian Institute for Water Research, 92p.

Dębski B., Olecka A., Bebkiewicz K., Chłopek Z., Kargulewicz I., Kubica K., Rutkowski J., Zasina D., Zimakowska–Laskowska M. and Żaczek M. [2017] Poland's Informative Inventory Report 2017. Submission under the UN ECE Convention on Long-range Transboundary Air Pollution and the DIRECTIVE (EU) 2016/2284. IOS-PIB/KOBiZE, Warsaw, March 2017.

Dębski B., Olecka A., Bebkiewicz K., Chłopek Z., Kargulewicz I., Kubica K., Rutkowski J., Zasina D., Zimakowska–Laskowska M. and Żaczek M. [2017] Poland's Informative Inventory Report 2017. Submission under the UN ECE Convention on Long-range Transboundary Air Pollution and the DIRECTIVE (EU) 2016/2284. IOS-PIB/KOBiZE, Warsaw, March 2017.

Denier van der Gon H., Hendriks C., Kuenen J., Segers A. and Visschedijk A. [2011] TNO Report. Description of current temporal emission patterns and sensitivity of predicted AQ for temporal emission patterns. EU FP7 MACC deliverable report D_D-EMIS_1.3. 22 p.

Dibble T.S., M.J. Zelie and H. Mao [2012] Thermodynamics of reactions of ClHg and BrHg radicals with atmospherically abundant free radicals. *Atmospheric Chemistry and Physics*, 12:10271-10279.

Dibble T.S., M.J. Zelie and H. Mao [2013] Corrigendum to "Thermodynamics of reactions of ClHg and BrHg radicals with atmospherically abundant free radicals" published in Atmospheric Chemistry and Physics, 12:10271-10279, 2012. *Atmospheric Chemistry and Physics*, 13:9211-9212.

Dibble T.S., M.J. Zelie and Y. Jiao [2014] Quantum chemistry guide to PTRMS studies of as yet undetected products of the bromine atom initiated oxidation of gaseous elemental mercury. *Journal of Physical Chemistry* A, 118:7847-7854

Donohoue D., Bauer D., Cossairt B., and Hynes A. [2006] Temperature and pressure dependent rate coefficients for the reaction of Hg with Br and the reaction of Br with Br: A pulsed laser photolysispulsed laser induced fluorescence study, *J. Phys. Chem*. A, 110, 6623–6632, doi:10.1021/jp054688j.

Elser M., Bozzetti C., El-Haddad I., Maasikmets M., Teinemaa E., Richter R., Wolf R., Slowik J.G., Baltensperger U. and Prévôt A.S.H. [2016] Urban increments of gaseous and aerosol pollutants and their sources using mobile aerosol mass spectrometry measurements. *Atmos. Chem. Phys*., 16, 7117–7134.

Emmons L.K., Walters S., Hess P.G., Lamarque J.-F., Pfister G.G., Fillmore D., Granier C., Guenther A., Kinnison D., Laepple T., Orlando J., Tie X., Tyndall G., Wiedinmyer C., Baughcum S.L., and Kloster S. [2010] Description and evaluation of the Model for Ozone and Related chemical Tracers, version 4 (MOZART-4), *Geosci. Model Dev*., 3, 43–67, doi:10.5194/gmd-3-43-2010.

FAO [2018] Search Geographical Information. FAO Major Fishing Areas. UN Food and Agriculture Organization (www.fao.org/fishery/area/search/en).

Gencarelli C.N., De Simone F., Hedgecock I.M., Sprovieri F., and Pirrone N. [2014] Development and Application of a Regional-Scale Atmospheric Mercury Model Based on WRF/Chem: A Mediterranean Area Investigation. *Environ. Sci. Pollut.* R., 21, 4095–4109.

Goodsite M.E., Plane J.M. C. and Skov H. [2012] Correction to A Theoretical Study of the Oxidation of Hg^0 to HgBr2 in the Troposphere, *Environ. Sci. Technol*., 46, 5262, doi:10.1021/es301201c.

Goodsite M.E., Plane J.M.C. and Skov H. [2004] A Theoretical Study of the Oxidation of Hg0 to HgBr2 in the Troposphere, *Environ. Sci. Technol*., 38, 1772–1776.

Gratz L.E., Ambrose J.L., Jaffe D.A., Shah V., Jaegle L., Stutz J., Festa J., Spolaor M., Tsai C., Selin N.E., Song S., Zhou X., Weinheimer A.J., Knapp D.J., Montzka D.D., Flocke F.M., Campos T.L., Apel E., Hornbrook R., Blake N.J., Hall S., Tyndall G.S., Reeves M., Stechman D., and Stell M. [2015] Oxidation of mercury by bromine in the subtropical Pacific free troposphere, *Geophysical Research Letters*, 42, 10.1002/2015gl066645.

Guo J., He J., Liu H., Miao Y., Liu H. and Zhai P. [2016] Impact of various emission control schemes on air quality using WRF-Chem APEC China 2014. *Atmospheric Environment*, 140, 311-219.

Gusev A., I. Ilyin, L.Mantseva, O.Rozovskaya, V. Shatalov, O. Travnikov [2006] Progress in further development of MSCE-HM and MSCE-POP models (implementation of the model review recommendations) EMEP/MSC-E Technical Report 4/2006.

Gusev A., O.Rozovskaya, V. Shatalov [2007] Modelling POP long-range transport and contamination levels by MSCE-POP model. EMEP/MSC-E Technical Report 1/2007.

Gustin M. S., Lindberg S., Marsik F., Casimir A., Ebinghaus R., Edwards G., Hubble-Fitzgerald C., Kemp R., Kock H., Leonard T., London J., Majewski M., Montecinos C., Owens J., Pilote M., Poissant L., Rasmussen P., Schaedlich F., Schneeberger D., Schroeder W., Sommar J., Turner R., Vette A., Wallschlaeger D., Xiao Z., and Zhang H. [1999] Nevada STORMS project: Measurement of mercury emissions from naturally enriched surfaces. *J. Geophys. Res*. 104(D17), 21831-21844.

Gustin M.S., H.M. Amos, J. Huang, M.B. Miller, and K. Heidecorn [2015] Measuring and modelling mercury in the atmosphere: a critical review, *Atmospheric Chemistry and Physics*, 15(10), 5697–5713, doi:10.5194/acp-15-5697-2015.

HMCR [2018]. Hydrometeorological Centre of Russia. The main peculiarities of atmospheric circulation and weather in the northern hemisphere. https://meteoinfo.ru/circulation-review. Accessed on June 18, 2018.

Holmes, C. D., Jacob, D. J., Corbitt, E. S., Mao, J., Yang, X., Talbot, R., and Slemr, F. [2010] Global atmospheric model for mercury including oxidation by bromine atoms, *Atmos. Chem. Phys*., 10, 12037–12057, doi:10.5194/acp-10-12037-2010.

Holnicki P., Kałuszko A., Nahorski Z., Stankiewicz K. and Trapp W. [2017a] Air quality modelling for Warsaw agglomeration. *Archives of Environmental Protection*, Vol. 43 no. 1 pp. 48–64.

Holnicki P., Tainio M. , Kałuszko A. and Nahorski Z. [2017b] Burden of Mortality and Disease Attributable to Multiple Air Pollutants in Warsaw, Poland. Int. *J. Environ. Res. Public Health*, 14, 1359.

Horowitz H.M., D.J. Jacob, Y. Zhang, T.S. Dibble, F. Slemr, H.M. Amos, J.A. Schmidt, E.S. Corbitt, E.A. Marais and E.M. Sunderland [2017] A new mechanism for atmospheric mercury redox chemistry: Implications for the global mercury budget. *Atmospheric Chemistry and Physics Discussions*, 1-33, 10.5194/acp-2016-1165.

Hynes, A. J., Donohoue, D. L., Goodsite, M. E., and Hedgecock, I. M. [2009] Our Current Understanding of Major Chemical and Physical Processes Affecting Mercury Dynamics in the Atmosphere and At the Air-Water/Terrestrial Interfaces, in: Mercury Fate and Transport in the Global Atmosphere, edited by: Pirrone, N., and Mason, R., *Springer Science Business Media*, LLC, 427–457.

IIR Belarus [2016] Belarusian emission inventory data. Informative Inventory Report to CLRTAP/EMEP 2016. 42 p.

IIR Belgium [2017] Informative Inventory Report about Belgium's annual submission of air emission data reported in February 2017 under the Convention on Long Range Transboundary Air Pollution CLRTAP. VMM, AWAC, IBGE-BIM, IRCEL-CELINE, LNE. 190 p.

IIR Finland [2017] Air Pollutant Emissions in Finland 1990 – 2015. Informative Inventory Report to the secretariat of the UNECE Convention on long-range transboundary air pollution. Part 5 Annexes. Finish Environmental Institute.

IIR Sweden [2017] Informative Inventory Report Sweden 2017. Submitted under the Convention on Long-Range Transboundary Air Pollution. Swedish Environmental Protection Agency Report 2017. 272 p.

Ilyin et al. [2018] Detailed assessment of heavy metal and POP pollution in the EMEP countries, PART II: Poland" Joint MSC-E & IER-NRI & EGAR & CHMI Report Technical Report 5/2018.

Ilyin I., O.Rozovskaya, O.Travnikov, W. Aas [2017] Assessment of heavy metal transboundary pollution on regional and national scales, transition to the new EMEP grid. EMEP Status Report 2/2017.

Jiao Y. and Dibble T.S. [2017] First kinetic study of the atmospherically important reactions BrHg + NO2 and BrHg + HOO, *Phys. Chem. Chem. Phys*., 19, 1826–1838, doi:10.1039/c6cp06276h.

Jiao Y. and T.S. Dibble [2015] Quality structures, vibrational frequencies, and thermochemistry of the products of reaction of BrHg• with NO2, HO2, ClO, BrO, and IO. Journal *of Physical Chemistry* A, 119:10502-10510.

Jiskra, M, Sonke, JE, Obrist, D, Bieser, J, Ebinghaus, R, Myhre CL, Pfaffhuber, KA, Wangberg, I, Kyllonen, K, Worthy, D, Martin, LG, Labuschagne, C, Mkololo, T, Ramonet, M, Magand, O, Dommergue, O. [2018]. A vegetation control on seasonal variations in global atmospheric mercury concentrations. Nature Geoscience, 11, 244-250.

Kain J.S. [2004] The Kain-Fritsch convective parameterization: An update*. J. Appl. Meteor*., 43 , 170–181.

Kiesewetter G. and Amann M. [2014]. Urban PM2.5 levels under the EU Clean Air Policy Package. TSAP Report #12 Version 1.0. International Institute for Applied Systems Analysis IIASA.

Kiesewetter G., Borken-Kleefeld J., Schöpp W., Heyes C., Thunis P., Bessagnet B., Terrenoire E., Fagerli H., Nyiri A., and Amann M. [2015] Modelling street level PM10 concentrations across Europe: source apportionment and possible futures. *Atmos. Chem. Phys*., 15, 1539–1553.

Kohv N., Heintalu H., Mandel E. and Link A. [2017] Estonian Informative Inventory Report 1990-2015 Submitted under the Convention on Long-Range Transboundary Air Pollution. Environment Agency, Tallinn 2017, 286 p.

Kos G., Ryzhkov A., Dastoor A., Narayan J., Steffen A., Ariya P. A., and Zhang L. [2013] Evaluation of discrepancy between measured and modelled oxidized mercury species, *Atmos. Chem. Phys*., 13, 4839–4863, doi:10.5194/acp-13-4839-2013.

Lenschow P., Abraham H.-J., Kutzner K., Lutz M., Preu J.-D. and Reichenbacher W. [2001] Some ideas about the sources of PM10. Atmospheric Environment 35 Supplement No. 1 23–33.

Menut L. et al. [2014] CHIMERE 2013: a model for regional atmospheric composition modelling, *Geosci. Model Dev*., 6, 981-1028

Nielsen O-K., Plejdrup M.S., Winther M., Mikkelsen M.H., Nielsen M., Fauser P., Albrektsen R., Hjelgaard K.H., Bruun H.G. and Thomsen M. [2017] ANNUAL DANISH INFORMATIVE INVENTORY REPORT TO UNECE. Emission inventories from the base year of the protocols to year 2015. Aarhus University, Department of Environmental Science., 475 p.

Pacyna J.M., Scholtz M.T. and Y.-F. Li [1995] Global Budgets of Trace Metal Sources, Environmental Reviews, 3, 145-159.

Pan L., Lin C.-J., Carmichael G.R., Streets D.G., Tang Y., Woo J.-H., Shetty S. K., Chu H.-W., Ho T. C., and Friedli H. R. [2010] Study of Atmospheric Mercury Budget in East Asia Using STEM-Hg Modelling System, *Sci. Total Environ*., 408, 3277–3291.

Papadopoulos C. and Charalambous C. [2016] Cyprus Informative Inventory Report 2014. Ministry of Labour, Welfare and Social Insurance. Department of Labour Inspection. Nicosia, March 2016. 211 p.

Parrella J.P., Jacob D.J., Liang Q., Zhang Y., Mickley L.J., Miller B., Evans M.J., Yang X., Pyle J.A., Theys N., and Van Roozendael M. [2012] Tropospheric bromine chemistry: implications for present and pre-industrial ozone and mercury, *Atmos. Chem. Phys*., 12, 6723–6740, doi:10.5194/acp-12-6723-2012.

Pastuszka J. S., Rogula-Kozłowska W. and Zajusz-Zubek E. [2009] Characterization of PM10 and PM2.5 and associated heavy metals at the crossroads and urban background site in Zabrze, Upper Silesia, Poland, during the smog episodes. *Environ Monit Assess* (2010) 168:613–627.

Poljanac M., Marković B., Švedek I., Hublin A., Magdić D., Abrashi A., Jelavić V., Zovko N. and Z. Mužek [2018] Republic of Croatia 2017 Informative Inventory Report (1990 – 2015). Submission to the Convention on Long-range Transboundary Air Pollution and National Emission Ceilings Directive (NECD 2016/2284/EU). Croatian Agency for Environment and Nature. 421 p.

Reizer M. and Juda-Rezler K. [2016] Explaining the high PM10 concentrations observed in Polish urban areas. *Air Qual Atmos Health* 9:517–531.

Ringuet J. (ed.) [2017] Inventaire des émissions de polluants atmosphériques en France au titre de la convention sur la pollution atmosphérique transfrontalière à longue distance et de la directive européenne concernant la réduction des émissions nationales de certains polluants atmosphériques. CITEPA, Mars 2017. 286 p.

Shah V., Jaeglé L., Gratz L.E., Ambrose J.L., Jaffe D.A., Selin N.E., Song S., Campos T.L., Flocke F.M., Reeves M., Stechman D., Stell M., Festa J., Stutz J., Weinheimer A.J., Knapp D.J., Montzka D.D., Tyndall G.S., Apel E.C., Hornbrook R.S., Hills A.J., Riemer D.D., Blake N.J., Cantrell C.A., and Mauldin III R.L. [2016] Origin of oxidized mercury in the summertime free troposphere over the southeastern US, *Atmos. Chem. Phys*., 16, 1511–1530, doi:10.5194/acp-16-1511-2016.

Skamarock W.C., Klemp J.B., Dudhia J., Gill D.O., Barker D.M., Duda M.G., Huang X-Y., Wang W. and Powers J.G. [2008]. A Description of the Advanced Research WRF Version 3. NCAR/TN–475+STR NCAR TECHNICAL NOTE

Skrebele A., Ratniece V., Rubene L., Cakars I., Siņics L., Klāvs G., Gračkova L., Bērziņa L., Frolova O., Lazdiņš A., Bārdule A., Griķe I., Maslova L., Gancone A., Lavrinoviča I., Braņicka I., Ozoliņa I., Černovska L., Kadiķis K. and Rustanovičs N. [2017] Latvia's Informative Inventory Report 1990 - 2015. Submitted under the Convention on Long-Range Transboundary Air Pollution. Latvian Environment, Geology and Meteorology Centre.

Slemr F., Angot H., Dommergue A., Magand M., Barret M., Weigelt A., Ebinghaus R., Brunke E.-G., Pfaffhuber K.A., Edwards G., Howard D., Powell J., Keywood M., Wang F.. [2015] Comparison of mercury concentration measured at several sites in the Southern Hemisphere. *Atmospheric Chemistry and Physics*, 15, 3125-3133.

Soerensen A.L., Sunderland E.M., Holmes C.D., Jacob D.J., Yantosca R.M., Skov H., Christensen J.H., Strode S.A., and Mason R.P. [2010] An improved global model for air-sea exchange of mercury: high concentrations over the north Atlantic, *Environ. Sci. Technol*., 44, 8574–8580.

Sprovieri F., Pirrone N., Bencardino M., DAmore F., Carbone F., Cinnirella S., Mannarino V., Landis M., Ebinghaus R., Weigelt A., Brunke E.-G., Labuschagne C., Martin L., Munthe J., Wangberg I., Artaxo P., Morais F., Cairns W., Barbante C., Dieguez M.C., Garcia P.E., Dommergue A., Angot H., Magand O., Skov H., Horvat M., Kotnik J., Read K.A., Neves L.M., Gawlik B.M., Sena F., Mashyanov N., Obolkin V. A., Wip D., Feng X., Zhang H., Fu X., Ramachandran R., Cossa D., Knoery J., Marusczak N., Nerentorp M. and Norstrom C. [2016] Atmospheric Mercury Concentrations observed at ground-based monitoring sites globally distributed in the framework of the GMOS network, *Atmos. Chem. Phys. Discuss*., doi:10.5194/acp-2016-466.

Subir M., Ariya P.A., and Dastoor A.P. [2011] A review of uncertainties in atmospheric modelling of mercury chemistry I. Uncertainties in existing kinetic parameters – Fundamental limitations and the importance of heterogeneous chemistry, *Atmos. Environ*., 45, 5664–5676, doi:10.1016/j.atmosenv.2011.04.046.

Temme C., Blanchard P., Steffen A., Banic C., Beauchamp S., Poissant L., Tordon R., Weins B.. [2007] Trend, seasonal and multi-variate analysis of total gaseous mercury data from the Canadian Atmospheric Mercury Network (CAMNet). *Atmospheric Environment*, 41, 5423-5441.

Thunis P., Degraeuwe B., Pisoni E., Ferrari F. and Clappier A. [2016] On the design and assessment of regional air quality pans: The SHERPA approach. *Journal of Environmental Management*, 183, 952-958.

Thunis P., Degraeuwe B., Pisoni E., Trombetti M., Peduzzi E., Belis C.A., Wilson J. and Vignati E. [2017] Urban PM2.5 Atlas - Air Quality in European cities. EUR 28804 EN, Publications Office of the European Union, Luxembourg, 2017. ISBN 978-92-79-73875-3. doi 10.2760/851626, JRC108595.

Tista M., Mareckova K. and R.Wankmueller [2017] Methodologies applied to the CEIP GNFR gap-filling 2017. Part I: Heavy Metals (Pb, Cd, Hg). Technical report CEIP 01/2017.

Travnikov O. [2005] Contribution of the intercontinental atmospheric transport to mercury pollution in the Northern Hemisphere. *Atmos. Environ*., 39, 7541–7548.

Travnikov O. and Ilyin I. [2009] The EMEP/MSC-E Mercury Modelling System, in: Mercury Fate and Transport in the Global Atmosphere: Emissions, Measurements, and Models, edited by: Pirrone, N. and Mason, R. P., Springer, 571–587.

Travnikov O., A.Gusev, I.Ilyin [2018] "Detailed assessment of heavy metal and POP pollution in the EMEP countries, PART I: An overview of case studies". EMEP/MSC-E Technical Report 4/2018.

Travnikov O., Angot H., Artaxo P., Bencardino M., Bieser J., D'Amore F., Dastoor A., De Simone F., Diéguez M. D. C., Dommergue A., Ebinghaus R., Feng X. B., Gencarelli C. N., Hedgecock I. M., Magand O., Martin L., Matthias V., Mashyanov N., Pirrone N., Ramachandran R., Read K. A., Ryjkov A., Selin N. E., Sena F., Song S., Sprovieri F., Wip D., Wängberg I., and Yang X. [2017] Multi-model study of mercury dispersion in the atmosphere: atmospheric processes and model evaluation, *Atmos. Chem. Phys*., 17, 5271-5295, doi:10.5194/acp-17-5271-2017.

Travnikov O., Jonson J.E., Andersen A.S., Gauss M., Gusev A., Rozovskaya O., Simpson D., Sokovyh V., Valiyaveetil S., and Wind P. [2009] Development of the EMEP global modelling framework: Progress report, EMEP/MSC-E Technical Report 7/2009, Meteorological Synthesizing Centre – East of EMEP, Moscow, 44 pp., available at: http://www.msceast.org/index.php/publications/reports (last access: 19 June 2018).

UNECE [2009] EMEP monitoring strategy. ECE/EB.AIR/GE.1/2009/15.

UNEP [2002] Global Mercury Assessment 2002. UNEP Chemicals. 258 pp. http://www.unep.org/chemicalsandwaste/Portals/9/Mercury/Documents/final-assessment-report-25nov02.pdf. Accessed on June 28, 2016.

Wakeling D., Passant N.R., Murrells T.P., Pang Y., Thistlethwaite G., Walker ., Brown P., Del Vento ., Hunter R., Wiltshire J., Broomfield M., Watterson., Pearson B., Rushton K., Hobson M., Smith H. and Misselbrook T. [2017] UK Informative Inventory Report (1990 to 2015). Ricardo Energy & Environment. 254 p.

Wang F. Saiz-Lopez A., Mahajan A.S., Gómez Martín J.C., Armstrong D., Lemes M., Hay T., and Prados-Roman C. [2014] Enhanced production of oxidised mercury over the tropical Pacific Ocean: A key missing oxidation pathway. *Atmos. Chem. Phys*. 14, 1323–1335.

WMO [2016] Annual Bulletin on the Climate in WMO Region VI - Europe and Middle East - 2016 . Ed. by Deutscher Wetterdienst. Responsible Mächel H. https://www.dwd.de/DE/leistungen/ravibulletinjahr/bulletin_2016.pdf?__blob=publicationFile&v=7. Accessed on June 18, 2018.

Annex A

EVALUATION OF MODELLING RESULTS VS. OBSERVATIONS

Calculated mean annual concentrations in air and annual sums of wet deposition of Pb, Cd and Hg were evaluated via comparison with the corresponding values measured at the EMEP monitoring network. The agreement between modelled and observed values is influenced by uncertainties of model parameterizations, emissions and monitoring data.

Since description of various environmental processes considered in the model is based on a number of assumptions, any model is capable of describing pollution levels only approximately. Analysis of the model uncertainties undertaken some time ago [*Travnikov and Ilyin*, 2005] demonstrated that intrinsic model uncertainty (i.e. uncertainty of the model as such, without effect of emission data) of modelled deposition of heavy metals was amounted to ±30-40% for Europe as a whole. Intrinsic uncertainty for air concentrations of particulate metals (Pb, Cd) is around ±40%, and Hg - around ±20%.

Uncertainty estimates of the heavy metal emission data are available for several EMEP countries. Table A.1 contains results of the uncertainty analysis carried out by national emission experts. The presented uncertainty values are related to total emission values in the countries. As seen, in some counties the uncertainties of Pb emissions reach almost 500%, of Cd – almost 450% and Hg – around 180%. Even median values of the uncertainties are significant: 100% for Pb, about 80% for Cd and around 70% for Hg. These high uncertainties may affect the modelling results and interpretation of evaluation of calculated concentrations and deposition against measurement data.

Table A.1. *Uncertainties (%) of the national total values of heavy emission data used in calculations for 2016*

2015	Pb	Cd	Hg	Reference
Belarus	192	266	111	*IIR Belarus* [2016]
Belgium	106	81	32	*IIR Belgium* [2017]
Croatia	140	291	78	*Poljanac et al.* [2017]
Cyprus	95	81	13	*Papadopoulos and Charalambous* [2016]
Denmark	488	449	103	*Nielsen et al.* [2017]
Estonia	184	134	182	*Kohv et al*. [2017]
Finland	29	29	19	*IIR Finland* [2017]
France	163	39	34	*Ringuet* [2017]
Latvia	60	70	68	*Skrebele at al*. [2017]
Poland	67	69	68	*Dębski et al*. [2017]
Sweden	23	37	70	*IIR Sweden* [2017]
United Kingdom	29	-30 to >50	-30 to 50	*Wakeling et al*. [2017]

Quality of Pb and Cd monitoring data is regularly evaluated via laboratory intercomparison tests. According to the most recent results, related to measurements in 2016, almost all laboratories managed to predict theoretical values of Cd and Pb concentrations in precipitation with satisfactory accuracy (within ±25%) [*CCC,* 2018]. However, these tests characterize only uncertainty of analytical methods applied in country's laboratories. Uncertainties arisen at other steps of monitoring (e.g.,

sampling, transportation, storing etc.) are not taken into account. Therefore, full uncertainty is most likely higher than the uncertainty estimated via considered tests.

This fact is indirectly confirmed when real measurement data are analyzed. Almost at every station there are some samples which values are flagged as 'invalid'. These samples are not included in the process of comparison of modelled and measured values. If more than half of samples have flag 'invalid', annual mean values are not considered in the comparison procedure. For example, measurements of heavy metals in precipitation at Portugal stations, and Cd in precipitation at French stations in 2016 are not used because of this reason. Besides, concentrations of Pb and Cd in air measured at Estonian station EE9 are ignored because their annual mean values are several times higher than the values in the previous year.

Modelled air concentrations and wet deposition of Pb in 2016 were somewhat higher than the corresponding observed levels. For concentrations in air mean relative bias is 23%, and for wet deposition – almost 8% (Table. A.2). At most of the stations the bias between modelled and observed annual mean concentrations in air is within ±30% (Fig. A1a). Good agreement is noted for wet deposition fluxes in the United Kingdom, most of stations in Germany, the Czech Republic, France (Fig. A1b). At some of the stations (DK12, SE5, NO90, ES17) the overestimation of the observed air concentrations by the model may be linked with overestimated contribution of wind re-suspension. Overestimation of wet deposition fluxes due to the same reason is noted for some stations in Germany, Slovenia, and Poland. Nevertheless, at most of the stations, e.g. in Germany, the United Kingdom, France, the Czech Republic, the usage of re-suspension favoured improvement of agreement between modelled and observed values. Therefore, further work on improvement of parameterization of this process can facilitate better modelling results for the EMEP countries. At some stations (e.g., DE3 for concentrations in air, PL5, SK4 and SK7 for wet deposition) even the anthropogenic component of the modelled value considerably exceeds the observed value. It can be explained by the uncertainties of the emissions in the vicinity of these stations. Hence, further work on the emission data is needed. There are countries (e.g., Slovakia, the Netherlands) where good agreement for wet deposition for some stations is accompanied by large discrepancies for other stations. This situation results in relatively low correlation between annual wet deposition fluxes (0.47) compared to that for concentrations in air (0.88).

Table A2. *Main statistical indicators of agreement between annual modelled and measured levels of air concentrations and wet deposition fluxes in 2016*

	Pb		Cd		Hg	
	C_{air}	Wet Dep	C_{air}	Wet Dep	C_{air}	Wet Dep
Mean relative bias, %	23.1	7.8	31	-45	6	68.2
Correlation coefficient	0.88	0.47	0.79	0.55	-0.74	0.73
NRMSE	0.44	0.64	0.73	0.48	0.10	0.95
F2, %	78	70	78	64	100	76
F3, %	90	91	88	81	100	94
N	40	43	40	36	8	17

C_{air} – concentration in air
Wet Dep – wet deposition flux
NRMSE – Normalized Root Mean Square Error
F2 – fraction of values fitting to factor of 2 difference
F3 – fraction of values fitting to factor of 3 difference
N – number of model-observation pairs

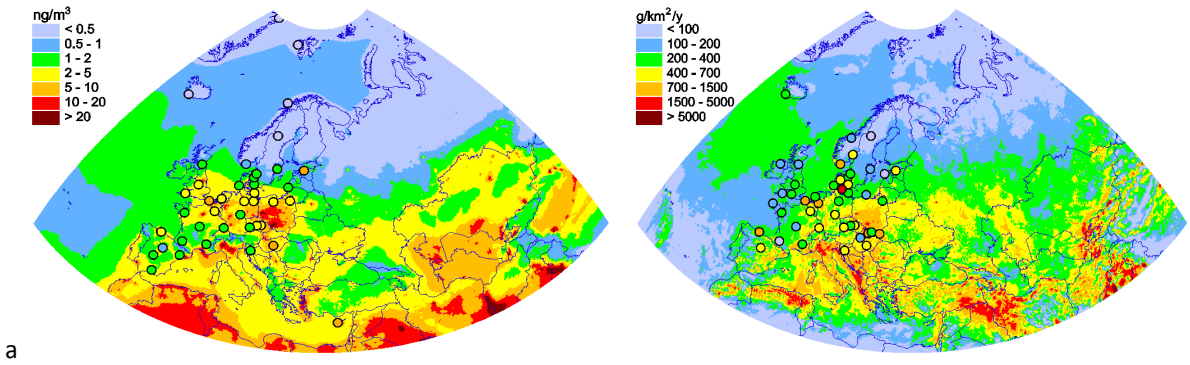

Fig. A1. *Spatial distribution of modelled and observed Pb concentrations in air (a) and wet deposition fluxes (b) in 2016*

Model performance for Cd in air is similar to that of Pb. There are some overestimation (about 30%) of mean observed values by the model and significant (0.79) spatial correlation between modelled and measured air concentrations (Table A.2). At most of stations the difference between modelled and observed concentrations in air is within a factor of two (Fig. A.2a). At some stations (e.g., BE14, NL8, GB17) high contribution of wind re-suspension produces the overestimation of the observed Cd concentrations in air. Similar to Pb, anthropogenic component of Cd concentrations in air at station DK12 and DE3 is higher than the observed concentration. Most likely it can be connected with uncertainties of anthropogenic emissions in the vicinity of these stations. Modelled wet deposition fluxes of Cd are lower than the observed ones by 45% on average. Large (2-fold and more) deviations of modelled values from observed ones can be explained by uncertainties of national emission data or monitoring issues. Understanding of the reasons requires further investigation. Satisfactory agreement between modelled and observed annual wet deposition fluxes is noted for stations in the United Kingdom, most of stations in Germany, some stations in Poland, Sweden, Slovakia and the Netherlands (Fig. A.2b).

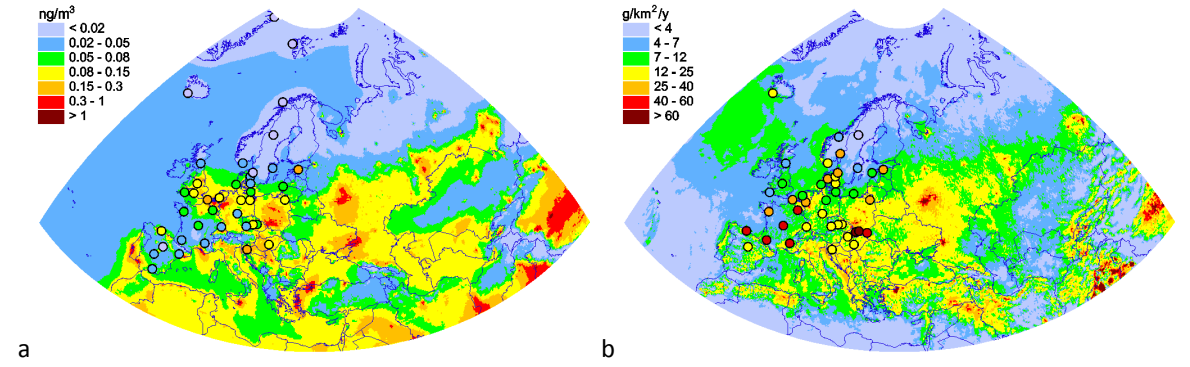

Fig. A.2. *Spatial distribution of modelled and observed Cd concentrations in air (a) and wet deposition fluxes (b) in 2016*

Mercury concentrations in air are distributed relatively smoothly over the EMEP region. Therefore, both modelled and measured values are within the range 1.3-1.6 ng/m^3 (Fig. A.3a). The difference between calculated and observed concentrations does not exceed ±15%. Taken into account low variability of Hg concentrations and low number of stations, negative spatial correlation between

modelled and observed values is not representative for characterizing the model performance. The model overestimates wet deposition fluxes of Hg by 68% on average. Significant uncertainties affecting modelling of Hg concentrations and deposition are connected with poor information about Hg speciation of anthropogenic emissions. Mercury is emitted as relatively inert and long-lived elemental form as well as in short-lived gaseous reactive and particulate Hg forms. Information about fractions of these three forms is not available in the official emission data. This information is derived from the expert estimates. Another source of uncertainties is atmospheric chemistry of Hg. Elemental form of Hg is oxidized and converted to reactive gaseous or particulate form, but rates and products of this process are not well established yet. In spite of general overestimation of the observed levels, at many stations (e.g. BE14, DE2, DE9, ES8, NL91, GB17, GB48) the agreement between modelled and observed values is within ±50% (Fig. A.3b).

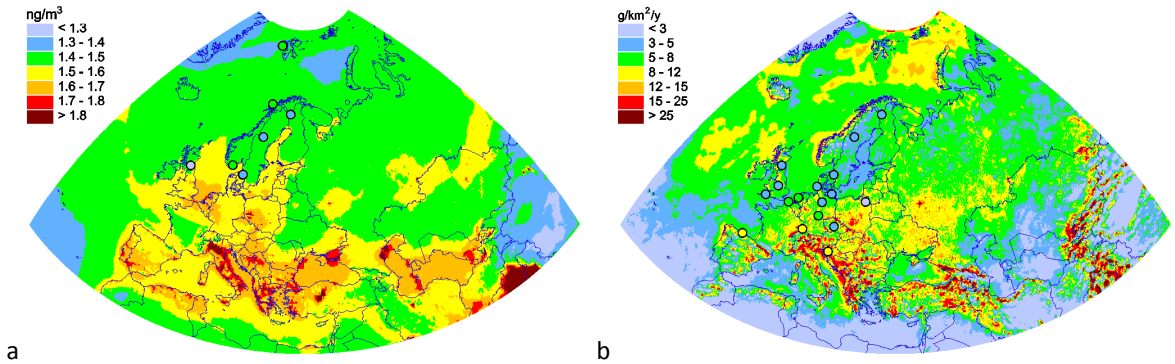

a b

Fig. A.3. *Spatial distribution of modelled and observed Hg concentrations in air (a) and wet deposition fluxes (b) in 2016*

Discrepancies between modelled and observed concentrations can be explained by various reasons including intrinsic uncertainties of model parameterizations, emission data and sometimes quality of measurements. Transition to the finer spatial resolution resulted to higher detalization of pollution level patterns in the EMEP countries. At the same time, it is in line with the outcome of country-specific studies stating that improvement of the model performance due to refinement of the grid can be achieved if quality of input data is also improved. The performed comparison demonstrated that further work is needed on anthropogenic and secondary emissions in the EMEP region.